AD A 281 631

AD A 281 631

LPEE GROWTH & CHARACTERIZATION OF $In_xGa_{1-x}As_ySb_{1-y}$ LATTICE MATCHED TO GaSb AND InAs FOR PHOTODETECTORS

FINAL REPORT

for period September 15, 1989 to October 31, 1993

by

SHANTHI N. IYER AND ALI ABUL FADL

U. S. ARMY RESEARCH OFFICE

GRANT NO. DAAL-03-89-C-0115

DEPARTMENT OF ELECTRICAL ENGINEERING
NORTH CAROLINA A & T STATE UNIVERSITY
GREENSBORO NC 27411

APPROVED FOR PUBLIC RELEASE;
DISTRIBUTION UNLIMITED

MASTER COPY KEEP THIS COPY FOR REPRODUCTION PURPOSES

REPORT DOCUMENTATION PAGE

Form Approved
OMB No. 0704-0188

Public reporting burden for this collection of information is estimated to average 1 hour per response, including the time for reviewing instructions, searching existing data sources, gathering and maintaining the data needed, and completing and reviewing the collection of information. Send comments regarding this burden estimate or any other aspect of this collection of information, including suggestions for reducing this burden, to Washington Headquarters Services, Directorate for Information Operations and Reports, 1215 Jefferson Davis Highway, Suite 1204, Arlington, VA 22202-4302, and to the Office of Management and Budget, Paperwork Reduction Project (0704-0188), Washington, DC 20503

1. AGENCY USE ONLY (Leave blank)	2. REPORT DATE	3. REPORT TYPE AND DATES COVERED

4. TITLE AND SUBTITLE
LPEE Growth & Characterization of InxGA1-xAsYSb1-y LATTICE Matched To GaSb And InAs for Photodetectors

5. FUNDING NUMBERS
DAAL03-89-G-0115

6. AUTHOR(S)
S. Iyer, A. Abul-Fadl

7. PERFORMING ORGANIZATION NAME(S) AND ADDRESS(ES)
North Carolina A&T State University
Department of Electrical Engineering
Greensboro, NC 27411

8. PERFORMING ORGANIZATION REPORT NUMBER

9. SPONSORING/MONITORING AGENCY NAME(S) AND ADDRESS(ES)
U.S. Army Research Office
P. O. Box 12211
Research Triangle Park, NC 27709-2211

10. SPONSORING/MONITORING AGENCY REPORT NUMBER

11. SUPPLEMENTARY NOTES
The views, opinions and/or findings contained in this report are those of the author(s) and should not be construed as an official Department of the Army position, policy, or decision, unless so designated by other documentation.

12a. DISTRIBUTION/AVAILABILITY STATEMENT
Approved for public release; distribution unlimited.

12b. DISTRIBUTION CODE

13. ABSTRACT *(Maximum 200 words)*

The optical characteristics of LPEE grown undoped and doped GaSb and GaInAsSb epilayers of different compositions were the subject of detailed investigations. The temperature and intensity dependences of the low temperature photoluminescence (PL) spectra of these alloys were studied as a function of the alloy compositions to determine the nature of the recombination processes.

In Te-doped GaSb epilayers, the PL spectra become increasingly complicated due to the presence of additional transitions associated with deeper acceptor levels. A systematic and quantitative evaluation of the effects of compensation in GaSb has been examined as a function of Te concentration in the layers and growth temperature, under both low and high excitation conditions. Photoreflectance spectroscopy has been assembled for the characterization of semiconductor band structure and surface.

Electrical transport characteristics of Au-n-GaSb Schottky diodes were investigated on the LPEE grown epilayers as a function of the growth temperature of the grown layers. Well behaved p-n homojunctions with forward onset voltage of 0.5V were fabricated on LPEE grown GaSb layers by Zn diffusion in an open tube configuration. The room temperature electrical characteristics of these junctions were studied in detail.

Ion implantation technique was used as an alternate technique for doping GaSb. Dependence of lattice disorder and their recovery by rapid thermal annealing on the atomic weight and dosages of the implanted species were studied by Rutherford backscattering/channeling technique.

14. SUBJECT TERMS	15. NUMBER OF PAGES
LPEE, LPE, GaInAsSb, Gasb, Photoluminescence, Ion Implantation, Schottky Barriers, PN-Junction	105
	16. PRICE CODE

17. SECURITY CLASSIFICATION OF REPORT	18. SECURITY CLASSIFICATION OF THIS PAGE	19. SECURITY CLASSIFICATION OF ABSTRACT	20. LIMITATION OF ABSTRACT
UNCLASSIFIED	UNCLASSIFIED	UNCLASSIFIED	UL

NSN 7540-01-280-5500

Standard Form 298 (Rev 2-89)
Prescribed by ANSI Std 239-18
298-102

TABLE OF CONTENTS

ABSTRACT

During the period of this research grant, the optical characteristics of LPEE grown undoped and doped GaSb and GaInAsSb epilayers of compositions corresponding to the room temperature photoluminescence peak wavelength of 1.7 μm to 2.32 μm were the subject of detailed investigations. The variations in the low temperature Fourier transform photoluminescence (PL) spectra of these alloys as a function of the alloy compositions have been examined . The nature of the recombination processes has been identified from the temperature and intensity dependence of the PL spectra. A systematic trend in the low temperature PL spectra is observed with the change in the alloy composition. GaSb and GaInAsSb with compositions close to GaSb exhibit several bound exciton peaks which have been attributed to different neutral acceptors.

In Te-doped GaSb epilayers, the PL spectra become increasingly complicated due to the presence of additional transitions associated with deeper acceptor levels. Considerable change in the PL spectra with the excitation intensity is also observed. A systematic and quantitative evaluation of the effects of compensation in GaSb has been examined as a function of Te concentration in the layers and growth temperature, under both low and high excitation conditions.

Another optical characterization technique, photoreflectance (PR) spectroscopy has been assembled for the characterization of semiconductor band structure and surface. However no PR signals were detected on GaSb layers and will be the focus of future research efforts.

Electrical transport characteristics of Au-n-GaSb Schottky diodes were investigated on the LPEE grown epilayers as a function of the growth temperature of the grown layers. Well behaved p-n homojunctions with forward onset voltage of 0.5V were fabricated on LPEE grown GaSb layers by Zn diffusion in an open tube configuration. The room temperature electrical characteristics of these junctions were studied in detail.

Ion implantation technique was used as an alternate technique for doping GaSb. Dependence of lattice disorder and their recovery by rapid thermal annealing on the atomic weight and dosages of the implanted species were studied by Rutherford backscattering/channeling technique. Te implanted samples showed the best recovery with the value of χ_{min} as low as 11%.

Grant# DAAL-03-89-C-0115, funded for $255,000 from 9 /15/89-10/31/93
Project Title: LPEE GROWTH & CHARACTERIZATION OF $In_xGa_{1-x}As_ySb_{1-y}$ LATTICE MATCHED TO GaSb AND InAs FOR PHOTODETECTORS

This is a final technical report describing the research activities of the above USARO grant. The three year grant period began on Nov 15, 1989 and was extended on a no-cost basis for a little more than a year up to Oct. 31, 1993. This program involved the effort of two faculty members, nine MSEE students and six undergraduate students. Three of the graduate students were minority students and one graduate student was a female.

During this period, close collaborations were established with Dr. Mitchel's group at Wright Laboratories, WPAFB, Dr. Nalin Parikh's group at University of North Carolina, Chapel Hill, Dr. McGuire's group at Microelectronics Center of North Carolina, Research Triangle Park and Dr. K.K. Bajaj's group, Emory University . These collaborations were extremely fruitful and permitted rapid advances outlined in this report. During this entire grant period , the suggestions from the two technical monitors Dr. Trew and Dr. LittleJohn were extremely helpful.

The tasks proposed in the original proposal were modified throughout the grant period depending on the progress made in various focussed areas of interest, availability and accessibility of the equipments. The major thrusts in the research work during this period could be broadly classified into three categories:

1. Optical Characterization of LPEE grown GaSb and GaInAsSb alloy systems
   (a) Low temperature photoluminescence studies of undoped GaSb and GaInAsSb alloys.
   (b) Variation in the low temperature photoluminescence (PL) spectra with Te concentration in GaSb and GaInAsSb alloys.
   (c) Photoreflectance.
2. Schottky barrier and PN junction on LPEE grown GaSb
3. Ion implantation and annealing in GaSb

The following sections review the various technical accomplishments. A few of the above work have already been published and hence will not be elaborated in the text of the report and the original reprint/ manuscript of the paper submitted to the journals are attached in the Appendix of this report.

I INTRODUCTION

The recent research research interest in both the binary semiconductor compound GaSb and (In,Ga)(As, Sb) stems from the need for developing lasers and photodetectors operating at wavelengths of 1.55μm to couple the optical fiber communication sytems This alloy covers the spectral range from 1.24μm to 4.3μm and is ideally suited for this application. Furthermore, the theoretically predicted high carrier mobility in GaSb makes it an attractive candidate for microwave devices.

GaInAsSb quaternary alloys have usually been grown by liquid phase epitaxy with only a few reports in the literature of growth by molecular beam epitaxy (MBE) [1,2] and metal-organic chemical vapor deposition(MOCVD)[3,4]. A notable feature of this alloy system is the presence of a large miscibility gap covering almost the entire composition range at typical growth temperatures. Hence, the compositions grown by the near equilibrium techniques, e.g. LPE and LPEE is limited to a very narrow range 1.7-2.32μm towards the GaSb corner of the phase diagram [5-13]. However, other techniques, namely, MBE and MOCVD have been successful in penetrating the miscibility gap due to their nonequilibrium nature of the growth process. The extent to which this miscibility gap is penetrated depends on the particular technique. Molecular beam epitaxy(MBE) has been successful in penetrating the miscibility gap only a little. The longest wavelength so far reported on this system by this technique is 2.5μm[1]. Organometallic vapor phase epitaxy (MOVPE) [3,4,14] technique has been successfully used for the growth of these layers throughout the miscibility gap, however evidence of compositional clustering has been reported [3] for layers in the miscibility gap. The extent to which this affects the performance of GaInAsSb based optical devices is presently unknown.

However LPE and LPEE, still attractive growth techniques for optoelectronic applications and in applications wherever the grown layers have to be rather thick. Further as it is inexpensive, it is an efficient tool for basic research on novel material systems where there exists problems with other growth techniques either due to the toxicity of the gases used or the reproducibility.

In LPEE technique, the growth is induced and sustained by an external parameter, namely, the current density, and is carried out at a constant furnace temperature. Hence the interface stability [15], surface morphology[16] and the compositional uniformity[17,18] of the layers grown by this technique have shown to be considerably improved over the conventional LPE technique. *With the financial support from USARO, LPEE technique has been used to fabricate pn junctions on GaSb for the first time.*

II. LPEE GROWTH

The first phase of the work involved the determination of the necessary growth conditions for the growth of GaSb and GaInAsSb epilayers on (100) GaSb by liquid phase electroepitaxial (LPEE) technique, and to determine the extent to which the miscibility gap can be penetrated by this technique.

The multiple well horizontal slider boat system was built. The body of the boat consists of two high purity graphites which are insulated from each other by quartz spacers, and a graphite slider as shown in Fig.2.1 . The latter consists of a dummy well containing the GaSb melt for the back contact, a boron nitride substrate recess to hold the substrate and two rectangular strips of boron-nitride. The purpose of boron nitride is to insulate the slider from the top part of the graphite thus ensuring that the current passes only through the melt-substrate interface, when the substrate is slid underneath the melt. A quartz rod which is interlocked with the graphite plunger serves as a push rod to drive the melt back and forth, in order to make and break the electrical contact, respectively with the substrate. The boat has been designed for multilayer growth on the substrate of small size (6mm x 6mm). The temperature profile on the boat was typically 1°C over 6 cm length of the boat. We have grown layers of GaSb and GaInAsSb in the composition range corresponding to a wavelength range of 1.689μm to 2.32μm. The details of the growth conditions are summarized in Ref.12. The surface morphology is found to be very sensitive to various factors. These include the saturation period prior to the growth and the temperature uniformity inside the furnace. With a few additional refinements in the growth system and growth procedure, layers of good surface morphology could be achieved with good reproducibility. X-ray rocking curves carried out on these layers at AT&T Bell Labs, Murray Hills, and Wright Patterson Laboratory, Dayton, indicated a full width half maxima (FWHM) typically in the range of 30 - 55 arcsec. The smallest half width we have obtained so far is 16 arcsec.

Compositional analysis of the samples were carried out using energy dispersive x-ray analysis attached to an ISI SS-40 scanning electron microscope available in Mechanical Engineering department. The details of the analysis along with the list of all the samples grown by this technique have already been published [11,12] (see Appendix-A).

III. OPTICAL CHARACTERIZATION OF UNDOPED GaSb AND GaInAsSb

A. LOW TEMPERATURE PL STUDIES OF GaSb and GaInAsSb

The PL spectra of the layers were examined up to a low temperature of 4.5K. Our PL set-up has a closed cycle refrigerator system which goes only up to a temperature of 10K. In GaSb and GaInAsSb, excitons have been found to provide the prominent radiative decay mechanisms and information on these can be obtained only at lower temperatures of 4.5K. Hence, 4.5K PL measurements were carried out at Wright Laboratory, WPAFB in collaboration with Dr. Mitchel and Dr. Hegde.

Low temperature PL study of GaSb is well documented in the literature. For a reference we compared our PL spectra of LPEE grown GaSb with corresponding LPE data in the literature. No major differences were noticed between the two spectra. Normally, GaSb PL spectra are characterized by four bound excitons (BE) and recombination at the neutral acceptor level (BA) with its weak longitudinal optical (LO) phonon replica[19-21]. This acceptor level has been attributed to native lattice defects which is a combination of Ga vacancy and a Ga atom on Sb site [22-24]. It is present in GaSb layers grown by all the techniques.

The PL spectra of the quaternary layers exhibit similar features to those described for GaSb, however fewer near band edge structures are seen. The samples of three different compositions of GaInAsSb labelled as α,β,γ were studied. The room temperature PL peak wavelengths of band edge related peaks of these samples ranged from 1.7 μm to 2.28 μm. 4.5K PL spectral characteristics of the quaternary layers have been summarized in references 12 and 13. The peak energy position and full width at half maxima (FWHM) of each peak has been determined by a quantitative fit to the experimental PL spectra using sum of the Gaussian line distributions. The FWHM of the bound excitons for the quaternary alloys were in the range of 4-7meV in β and γ layers at 4K. These are the smallest line-widths reported for GaInAsSb on GaSb reported so far.A definite trend in the overall PL spectra is seen with the shift in the composition towards InAs. The overall integrated intensity remains the same for GaSb, α and β layers, but decreases by almost a factor of five to ten for γ samples. Free exciton is seen only for α-23 sample, as a weak band centered at 764.96 meV on the high energy side of the spectrum. This is seen in both GaSb and quaternary layers only under the highest excitation level used. With the shift in the composition towards lower energy gap, the highest energy transition line identified as BE_1 becomes dominant. The other bound excitons and donor to acceptor transitions become weaker. For γ sample, the donor to acceptor transition line is detectable only under high magnification. This is consistent with the experimental observations [4,25] on the layers grown by other nonequilibrium techniques where only one peak is seen for layers with compositions closer to or inside the miscibility gap region.

The identity of all the above transitions were further confirmed from the PL intensity dependence of the incident laser intensity. The temperature dependence of the PL integrated intensity and band gap energies were also investigated in detail. With increase in temperature, the overall integrated emission intensity of the quaternary PL spectra gradually decreases, indicating the presence of non-radiative mechanisms of decay with low activation energies.

The temperature dependence of the band gap energies were fitted using the well-known

Varshni's [26] equation. In GaInAsSb layers the band to band transition was estimated from the binding energy of BE_4. For GaSb the values of the empirical constants used to fit the Varshni's equation were in excellent agreement with the values reported by Camassel et al. [27]. However, they were considerably larger for layers with compositions closer to GaSb which may be an indicative of the presence of high degree of disorder in these layers. In the temperature range of 100-300K, the linear portion of the plot exhibited a slope of ≈ -0.31 meV/K for the quaternary layers which compared well with the value of -0.35 meV/K for GaSb[23].

Line shape analysis was also carried out. For GaSb and quaternary samples all the PL peaks could be well fitted by sum of Gaussian line distributions at low temperatures. With rise in temperature the PL spectra become increasingly asymmetrical, and the asymmetry sets in around 25-35K range indicating the dominance of band to band transitions. The PL spectral shape of band to band transitions were analyzed using the simple model of von Roosbroeck-Shockley equation. A good fit was obtained at higher energies, however at lower energies a good fit was obtained if exponential band edge was assumed.

At higher temperatures, the emission spectra are narrower than the analytical spectra on the high energy side of the emission spectra, as self absorption due to higher photon energy within the epilayer has not been taken into account. The value of E_g determined from this analysis was found to be kT/2 less than the PL peak energy suggesting the k-conservative nature of the recombination processes.

It may be noted that these low temperature PL data represent the first results on GaInAsSb alloy system. The details of the results presented in this section has been published in Phys. Rev. B [12] and J. Appl.Phys. [13] (see Appendices A & B).

B. LOW TEMPERATURE PL STUDIES OF TE-DOPED GASB

Group VI elements namely, S, Se and Te are normally used for n-doping of GaSb. However, the group VI elements exhibit high vapor pressure and segregation coefficient. Amongst these Te appears to be the most suitable one for layers grown by any technique. Optical characteristics namely the photoluminescence characteristics of the melt grown Te-doped GaSb single crystal has been extensively studied[28-32]. Te is known to form a shallow donor level and in addition has been reported to introduce deep impurity levels [28-32] which are acceptor like and close to the native residual acceptors in undoped GaSb. Accordingly, this has led to some confusion in the identity of these levels. Most of the PL characteristics that have been reported are generally at two low temperature ranges, 12K-18K and 70-85K, respectively. Typically [28-30], recombination involving neutral residual acceptors A (34meV)[28-30], ionized residual acceptors A^- (70-120meV) [29,30], deep acceptors (65-100meV) [28,29] and another deep acceptor level [29] (130 meV, the origin of which is not yet clearly understood) have been reported. A line corresponding to the recombination level at 65 meV has also been reported in the luminescence spectra of other III-V compound materials GaInSb [33,34] and GaAlSb [35] which has been attributed to the donor-residual acceptor complex formation ($V_{Ga}Ga_{Sb}Te_{Sb}$). The dominance of any of these transitions was found to depend on the Te doping level and the incident excitation level. For the doped epilayers one has to take into consideration the influence of the growth technique and the growth parameters on the doping level. In the case of LPE grown epilayers, it has been well established that the equilibrium concentration of the intrinsic defect, namely Ga antisite defect is strongly dependent on the growth temperature and this intrinsic defect is generally considered to be the origin of the dominant residual acceptor A observed in undoped GaSb [36,37,24]. Hence the background acceptor doping is found to be a function of the growth temperature [36].

There are only a few reports [38,39] on LPE grown Te-doped GaSb layers. Wu et al.[39] have grown Te- doped layers of concentrations in the 10^{17} range and their emphasis has been on the relative dominance of band edge transitions with respect to the residual acceptor transition at 777.5meV. The low energy transitions were unresolved. Again both these reports have been in the 16-19K temperature range where most of the band edge transitions become weak. Less information.[40] is available on Te doped GaInAsSb epilayers. Wu et al.[40] reported a Burstein Moss shift in the PL peaks and broadening of the spectra with increase in carrier concentration.

We have attempted to carry out a systematic and quantitative evaluation of the effects of Te compensation in GaSb as a function of the Te doping and incident excitation levels. In order to distinguish between the effect of the growth temperature and Te compensation, Te doped layers of varying concentrations have been grown at two different growth temperatures of 476 and 539°C. We have also gathered limited data on Te-doped GaInAsSb.

B.1. EXPERIMENTAL DETAILS

Te doped layers were grown on Te doped (100) GaSb single crystal. The melt consisted of Ga melt with GaSb as the source. Due to the high segregation coefficient associated with Te , it was added in the form of single crystal Te doped GaSb to the source. The carrier concentration at each of the growth temperature was varied by appropriately replacing undoped GaSb source in the melt by Te doped GaSb from 0 to 100%. However, at a given temperature due to the

solid solubility limitation the carrier concentration in the layer can be varied utmost only by an order of magnitude. The carrier concentrations in these layers were determined by forming Schottky barriers with gold. These concentrations were also verified using secondary ion mass spectroscopy (SIMS) technique. Te implanted GaSb of dosages of $10^{15}/cm^2$ were used as the standard . For Te the limit of the detection was found to be $10^{16}/cm^3$. In the case of the quaternary only an estimate of the Te concentration could be made. The samples grown at 476 and 539°C were denoted by L and H respectively, at the beginning of the sample name. The energy positions and the line widths at half maximum (FWHM) of each peak have been determined by a quantitative fit to the experimental PL spectra using a sum of Gaussian line distributions. Due to the complicated nature of the experimental spectra, the dominant peaks were fit first with the additional peaks added as necessary.

B.2. Te -DOPED GaSb

The PL spectra of the Te -doped layers grown at 530°C and 474°C at incident levels of 1, 16 and 0.7,19W/cm^2, respectively for different Te concentrations are shown in Figs. 3.1-3.4, respectively. Table 3.1 summarizes the various PL transitions and these are compared to the lines reported in literature on undoped GaSb by all of the major growth techniques[41] and our results on LPEE grown GaSb at 580°C[12,13].

The spectra of the doped layers exhibit numerous transitions in addition to the ones observed in undoped layers as listed in Tables 3.2-3.5. Due to the Te compensation in the layer, transitions due to the various deep acceptors occurring in the range 745-748 meV(C), 731-737 meV (D), 721-725 meV (E)and the second ionization level of the acceptor level (A^-) at 703-10 meV are observed. These are in addition to the transitions at 777 meV and 760 meV due to the residual acceptor levels at 34 meV and 51 meV above the valence band acceptor level, respectively observed in undoped layers. The transition line at 745 meV has been attributed to the LO optical phonon replica of A by Wu et al. [39] as it is energetically at the same peak position as A-LO in undoped GaSb. However, the high intensity observed for this transition particularly in high temperature grown layers rules out the possibility of identifying this transition as optical phonon replica. The D peak is dominant in layers grown at lower temperature. A similar transition has also been observed by Lebedev and Stel'nikova [28] in the doped GaSb single crystal with Te doping level in mid 10^{16} range and has been attributed to transition from the conduction band to an acceptor bound to a Te complex with Ga antisite defect of the type $V_{Ga}Ga_{Sb}Te_{Sb}$ lattice defect. The E peak at 726 meV is seen in all the layers was also observed in undoped LPE [39] and MBE [41] grown epilayers and in Te -doped layers with $10^{17}/cm^3$ doping range [29,39], respectively. Kastalskii et al. [30] attributed this transition to the second ionization level of the residual acceptor, A^- and we attribute to a deep acceptor. The transition at 703-710 meV is coincidental to the second ionization level of the residual acceptor [42-44] and is observed in all the layers though somewhat weak.

Other additional transition lines present are at 770-4meV, 714-717meV and 690-7 meV. The intensity of the transition at 771 meV deceases with increase in carrier concentration and is located about 5-10 meV below the transition corresponding to residual acceptor level. We attribute this emission to the radiative transitions from donor levels to the acceptor. The activation energy of this level is 5 meV for layers in the 10^{16} range and increases to 8-10 meV

for the layers with 10^{17} range.This value is consistent with the activation energy of Te reported in literature by Kyuregyan et al. [29] but differs considerably from that reported by Chen et al .[38]. The weak peak at 714 meV is energetically shifted by about 29 meV from C acceptor level and is also 10 times smaller consistently and hence we attribute this to its phonon replica. Another weak peak at 694 meV is also shifted by about 29 meV from the E peak, however, its intensity remains constant and has been observed in both doped [29,30] and undoped GaSb layers. In doped layers this peak has been attributed to a Te complex with Ga vacancy by Kyuregyan et al. [29] and could be a combination of deep acceptor and a phonon replica.

Figure 3.5 shows a typical variation of the low temperature PL spectra of Te-doped binary layer with the incident intensity level. Spectral distributions undergo considerable change with excitation intensity, in accordance with the previous reports in literature [29,30] on GaSb crystals. At high intensity, the spectra is dominated by the high energy transitions, namely the excitonic and shallow level acceptor transitions. The Table 3.1 lists all the bound excitonic peaks that have been observed in different Te -doped layers and it does not represent lines observed in a single epilayer. Typically in each layer one or two bound excitonic transitions are observed. The transition A corresponding to the native acceptor level at 34 meV from the valence band, which is a dominant PL feature in undoped GaSb continues to be so in low temperature grown layers (see Fig. 3.4). However, this transition becomes weak in H series sample and the deeper acceptor transitions identified as B and C become prominent (see Fig. 3.2). A Burstein shift of 2-4 meV with intensity is observed in L -series samples for all the peaks except A'.

On decreasing the excitation intensity by an order of magnitude , these excitonic transitions either become weak or disappear and the low energy transitions become dominant. The shallow acceptors become very weak for low temperature grown layers (Fig. 3.3) and is not observed in high temperature grown layers (Fig. 3.1). The transitions D and C corresponding to the deep acceptor levels become dominant in L and H series samples, respectively.

Figures 3.1-3.4 show also the variations of the low temperature PL spectra with Te concentration in L and H- layers. Lebedev and Stel'nikova [28] have reported a systematic change in the dominance of the peak from native acceptor (A) in undoped to the Te-related acceptor level (D) at intermediate doping concentrations of mid 10^{16} range, and, finally, to the deep level of the doubly ionizable acceptor (A^-) at the highest Te concentration of $1x10^{17}/cm^3$. In our study (Tables 3.1-3.5) we do not observe the dominance of A^- however, the intensity of the high energy and low energy emission bands correspondingly decrease and increase with carrier concentration. The overall spectra broadens and shifts towards the higher energy with the increasing carrier concentration. However, for carrier concentration of $6x10^{17}/cm^3$, the high energy transitions in the region 780-791 meV overlap and form a high energy shoulder in the spectra and the intensity increases with carrier concentration. It should be noted that this observation has been made on quite a few samples exceeding $3x10^{17}/cm^3$, though the spectra of only one sample HE6 has been shown.

To explain the experimental observations one has to consider the shift in the position of the equilibrium Fermi level in conjunction with the changes in the quasi Fermi level under nonequilibrium conditions. The position of the equilibrium Fermi level is determined by the doping level. The lowest n-doping that could be achieved is determined by the growth temperature- decreasing with the growth temperature, while the highest doping is limited by solid solubility of Te in the melt which increases with the growth temperature. The relative shift

of the electron and hole quasi Fermi levels depends on the doping level and incident excitation level. Hence, considerable variation in the spectra occurs with respect to the growth temperature, intensity and the doping levels due to the variations in the occupancy of the different impurity levels.

At low excitation levels for the heavily doped samples (H-series) , the hole quasi Fermi level (F_p) will not shift significantly from the equilibrium Fermi level which lies close to the conduction band and the shallow impurity centers will be effectively shielded by the high density of free carriers. Consequently transitions to deeper acceptor levels are observed leading to lower energy transitions. In the case of low doped samples (L-series) as the equilibrium Fermi level lie relatively lower in the energy gap, transitions due to the shallow acceptors A are observed though weak. Hence a dominant low energy emission band is observed followed by a high energy emission band of lower intensity. With increased doping level the intensity of the high energy transitions decrease, which is accompanied by a Moss Burstein shift of the PL peak by 2-3 meV towards higher energy. The Moss Burstein shift occurs primarily due to the shift in the Fermi level with the carrier concentration, hence the PL peak position should also shift by the same amount as Fermi level, ie proportional to $n^{2/3}$. For a carrier concentration change of 5 times the Burstein shift is 1.4 meV close to the observed data. As the density of states at the bottom of the conduction band in GaSb is small, Moss Burstein shift is observed at a relatively lower carrier concentrations.

With increasing laser intensity, the hole quasi Fermi level will move down in the forbidden gap and the nonequilibrium holes will be readily captured by the acceptors, which become neutral. Hence, there is an increased probability of the recombination of the nonequilibrium carriers due to the decrease in the repulsive coulomb barrier leading to the dominance of high energy transitions. Therefore for the low doped samples, the PL spectra exhibits two bands, a weak low energy band with the high energy band dominated by residual acceptor transition. The Moss Burstein shift is observed in the low energy band with increasing doping level. For heavily doped samples, since the equilibrium Fermi level is high, the shallow residual acceptor still remains screened and a somewhat deeper acceptor level labelled as B is dominant. With increasing carrier concentration the intensity of the lower energy band in L series samples increase and the high energy band decreases in H-series due to the shift in F_n. However, for carrier concentration exceeding $3x10^{17}/cm^3$, the limit where the GaSb becomes degenerate, the high energy transitions starts to dominate forming a broad shoulder while the low intensity spectra do not appear to vary significantly. This is consistent with the observations of Wu et al.[40], and they have attributed this increase as evidence of semiconductor band shrinkage. In such a case there could be significant contribution of high energy PL transitions lines reflected from the back side of the substrate, thereby increasing the intensity of high energy transitions.

Variation of output integrated intensity with the excitation intensity exhibited slopes of 0.7-1.1 range in the log-log plots for all the acceptors identified, further confirming that these are impurity-related transitions.

B.3. Te-DOPED QUATERNARY

Doping in the quaternary layer of composition $Ga_{0.912}In_{0.088}As_{0.056}Sb_{0.944}$ was examined which we have referred earlier as β composition. The doped layer exhibit many additional transitions

as in doped binary and the PL transitions are listed in Table 3.6. The Te concentration in this layer was determined using SIMS data. The undoped PL characteristics examined previously were used as a reference in identifying prospective Te-related levels. There is a considerable difference in the highest PL peak energy of undoped and Te doped GaInAsSb layers probably due to the fact that undoped layer was not lattice matched to GaSb. The highest energy transition at 681 meV dominant at higher intensity levels exhibit show many of the characteristics of the excitonic transitions.Firstly, no shift in the peak positions were noticed in the intensity range investigated and integrated intensity of this transition exhibited a power dependence of $P^{1.01}$. This value is close to the power dependence of $P^{1.22}$ that we have observed for a similar transition in undoped quaternary layer. Secondly, the intensity of this peak remains high with increase in temperature up to 40K and thereafter decreases sharply. The temperature dependence of the integrated intensity , as shown in Fig. 3.6, can be well described using the three level Boltzmann distribution for excitonic transitions developed by Bimberg et. al.[45]

$$I_T/I_o = 1 / \{1+C_1 \exp(-\Delta E_1/kT)+C_2\exp(-\Delta E_2/kT)\}, \qquad (1)$$

where I_T/I_O represents the normalized integrated intensity at 4.5K, ΔE_1 and ΔE_2 represent the effective mass donor binding energy and dissociation energy of the bound exciton, respectively, C_1 and C_2 are constants and are functions of the density of states. The values of C_1 and C_2 were determined to be approximately 1.01 and 2064 in excellent agreement with the undoped GaSb layers. However, the values of ΔE_1 and ΔE_2 were found to be around 2.1 meV and 27 meV, respectively, considerably higher than 1.1 and 10 meV computed in undoped LPEE GaSb layers [12]. The exact reason for this discrepancy is not clear at this point.

The other low energy transitions that are observed in the PL spectra are at 661meV identified as A , 653, 634, 614, 595 and 577 meV identified as UI. The weak transition at 661 meV is shifted by 22 meV from the highest energy transition as in undoped quaternary layer. If it is assumed that the first peak at 681meV has the same binding energy of 15.7 meV as in undoped layer, then the binding energy of this peak at 661meV will be 37.7 meV, in excellent agreement with the previous reports of 34-38 meV in GaSb and our reports on GaInAsSb. We therefore suggest that this transition be associated with the recombination of a free electron with a bound hole.

The dependence of the PL spectral variations of doped quaternary layers on incident excitation level is similiar to the undoped layer as shown in Fig. 3.7. On lowering the incident excitation level, the overall spectra is dominated by low energy transitions consistent with the observation in the GaSb layers. The peak at 661 meV is not present at this intensity level and many additional low energy peaks are observed. This further confirms our assignment of this peak as band to acceptor transition. We will not attempt to identify the other peaks due to the limited data present.

In summary, the major PL features found in our study can be described using the proposed band diagram in Fig. 3.8. We observe a doubly ionizable native residual acceptor (A/A^-) with shallow and deep levels at 34 meV and 97 meV, respectively, another native acceptor level for GaSb (B) is seen at 54 meV, and three Te-related acceptor levels (C, D and E) are found at 68meV, 80 meV and 86meV, respectively. The relative dominance of each of these transitions is dependent on the degree of Te compensation in the layers and incident excitation intensity.

C. PHOTOREFLECTANCE

The experimental arrangement for photoreflectance is shown schematically in Fig. 3.9. Light from a 100 W tungsten-halogen source was dispersed through a monochromator and was focused on the sample by means of two lenses. The reflected light was focused onto a silicon detector. An Argon-ion (4880Å) laser was used as a pump beam and neutral density filters were used to reduce the laser power to about 100mW/cm^2. A beam expander was utilized to increase the laser spot size. The laser was focused onto the same spot as the monochromatic light on the sample, typical spot size was 10 mm x 1.0 mm. By chopping the laser beam at 200 Hz, the crystal's reflectivity is modulated periodically, and the signal was detected using the conventional lock-in techniques. To avoid self-modulation by the probe due to the variation in lamp-source intensity with wavelength, the dc component of the reflected signal was monitored and held constant by means of a variable neutral density filter placed in the optical path between the monochromator and the sample. The filter was driven by a stepper motor which was controlled electronically by the Compumotor Velocity and Acceleration card. This normalization procedure automatically corrects for any fluctuations in the reflected intensity due to the changes in the light intensity and variations on the surface of the sample. Two filters placed in front of the detector prevented the scattered laser from entering the detector.

Fig. 3.10 shows the PR spectra of a GaAs/AlGaAs HEMT structure obtained at Wright Laboratory, and in our laboratory. The resolution needs to be considerably improved. PR spectra was also obtained on semi-insulating GaAs samples indicating that the system is operational. However, no PR spectra were obtained in GaSb and GaInAsSb samples . This was also verified at Wright Patterson Laboratory. The system needs to be considerably modified.

IV GaSb SCHOTTKY DIODES

D.1 INTRODUCTION

The metal/n-GaSb Schottky barrier rectifying contacts are of interest from both the fundamental point of view and also due to its potential for device applications such as metal-semiconductor photodetectors. The characteristics of these devices are expected to be somewhat better than the n-InGaAs due to its comparably high mobility, and higher Schottky barrier height and hole to electron impact ionization ratio at the same band gap ranges. Its high hole-to-electron mobility ratio is promising for complementary circuit applications. Further these diodes allow capacitance based measurements to be made, and hence the evaluation of the concentration of the grown epilayers. In particular, it becomes very important for the LPE and LPEE grown epilayers where the lack of semi-insulating GaSb substrates do not permit the use of Hall characterization techniques for the electrical characterization of the samples.

The formation of near ideal Schottky contact on GaSb has proven to be somewhat more difficult than that of GaAs and Si due to the severe oxidation problem of the GaSb surface which leads to inhomogeneous interface structure. The number of reports on GaSb [46-49] has been somewhat limited as compared to other III-V semiconductors namely, GaAs [50] and InP [51] which has been the subject of extensive investigations. Most of the studies have been carried out on Schottky diodes fabricated from the bulk GaSb substrates or LPE grown GaSb layers with carrier concentration in the low 10^{17} range. There are few reports on MBE grown layers[46,52]. A range of metals deposited by evaporation have been investigated [47]. The available electrical data show that the barrier heights show a weak dependence on the metal work function , generally falling in a fairly small band of values between 0.4 and 0.65eV [47,48]. This suggests a pinning of Fermi level at the surface in the lower half of the band gap due to either the midgap neutrality level pinning or the defect limited pinning . The rational [53] behind the former is that there exists an intrinsic midgap neutrality level whose position relates to the average energy of sp^3 hybrid orbital. Another school of thought[54-56] proposes that the mechanism of Fermi level pinning in Schottky diodes is the result of an action of some dominant lattice defects at the crystal surface. However, the pinning doesn't appear to be very pronounced for Ga and Sb Schottky diodes [47,48], where the Schottky barriers tend to be somewhat different from other metals. The ideality factors are higher as compared with those of other Schottky diodes fabricated from Si or GaAs. The cause has commonly been attributed to generation recombination currents resulting from high surface state densities and to the presence of the interfacial layer due to the severe oxidation problem associated with GaSb [49]. Typically n has been in the range of 1.15 to 2.5 [46-48,52]. The lowest ideality factor has been obtained on Al Schottky diode, with n in the range of 1.16-1.35 suggesting the complexity of the interface with other metals.

In general, the barrier height seems to depend on the ideality factor of the Schottky diode, the lower the value of n, the lower the barrier height [49]. This was also confirmed by soft x-ray photoemission spectroscopy. This phenomenon is known as "2/3 Eg rule". The barrier heights determined from I-V and C-V were not found to be consistent and differs significantly [49,48]. Again only Al contact seems to give consistent results [49,52] . Due to the large barrier height in n-GaSb, the transport mechanism at room temperature in a typical Au-n-GaSb Schottky barrier is dominated by generation recombination current arising from a midgap center while at high

temperature the conventional thermionic emission prevails [47] The electron trap contributing to this generation recombination current was found to be like a DX-center[47]. the effect of different surface treatments prior to the metal deposition. They found that sulphur treatment improves significantly the I-V characteristics of the diode.

In this work we have investigated the electrical transport characteristics of the Au-GaSb(Te doped) Schottky barrier which was accomplished by electroplating. I-V and C-V measurements were performed on the Schottky diode to determine the carrier concentration and barrier height, and also the quality of these grown layers at the two different growth temperatures.

D.2 EXPERIMENTAL

The LPEE grown Te-doped GaSb samples were initially cleaned using organic solvents, soaked in HCl for 2 minutes, rinsed in DI water and propanol, and then blown dry in N_2. The patterns of 220μm circular dots were defined using standard photolithography technique. The photoresist served as electroplating mask and the layers were etched in buffered HF for 30 seconds to minimize oxidation. Electroplated Au and Au-In were used for Schottky contact to the epilayer and the ohmic contact to the Te -doped substrate, respectively. Figures 4.1(a) and (b) show the structure of the Au/n-GaSb Schottky diode and the top view of the finished device.

Effect of surface treatments prior to the deposition of metal as mentioned by Polyakov et al. [47] were also attempted. The surface of the samples turned dark , after 10 minutes soaking in $(NH_4)_2S$, which became shiny again after HF acid etching. We believe the surface was covered by thin oxide after soaking in $(NH_4)_2S$. The plated gold dot would also peel off very easily which happens normally whenever there is a thin oxide. So $(NH_4)_2S$ treatment had no effect on our work contrary to the reports of Polyakov et al. [47] who observed a significant improvement in the reverse leakage current.

The I-V data was acquired using a computer IEEE 488 bus (see Fig. 4.2) which communicated with two HP digital voltmeters and a lock-in amplifier. The circuit consisted of a KEPCO power supply driven by a programmable power supply from the lock in amplifier, in series with the Schottky diode and a resistor. The voltage drop across the resistor was used to determine the current through the diode. The computer program for the I-V data acquisition was written in C language. The curve fitting to the data was carried out using IDL software installed in the main frame.

C-V measurements were performed using HP 4284A Precision LCR Meter at an operating frequency of 1MHz. The HP 4284A was driven through IEEE 488 Bus by a computer program developed by Materials Development Corporation (MDC). The program allowed the direct computation of the built in voltage, V_{bi} and carrier concentration, N_d from C^{-2}-V where C-V relation is given as: $C^{-2} = [2(V_{bi}-V_R)/(q\varepsilon_s N_d)]^{1/2}$. The theory for this can be found in any of today's semiconductor text book.

RESULTS AND DISCUSSION

D.3 I-V CHARACTERISTICS OF SCHOTTKY DIODE

Except otherwise noted, all the I-V and C-V measurements were carried out at room temperature (300°K) under normal room light conditions. Figures 4.3(a) and 4.3(b) exhibit the typical I-V characteristics of the two Schottky diodes on LPEE GaSb layers grown at two different temperatures . Though the characteristics are similar for both the diodes, there are a few important differences. The layer grown at lower temperature (Fig. 4.3(a)) exhibit a higher onset voltage of 0.3 V for a dopant concentration of $5.0 \times 10^{16}/cm^3$ while the diodes on H- layers exhibit a lower onset voltage of 0.2V for the doping concentration of $2.0 \times 10^{17}/cm^{-3}$.

The reverse saturation current typically is about 5 μA at a reverse bias of 0.5V, which is substantially small as compared to the value of 140μA as reported by Milnes et al[57]. The breakdown voltage varies but generally is in the range of 1.5-2.0V for concentration range of $2\text{-}5x10^{17}/cm^3$ and 5-10V for concentration range of $5\text{-}9x10^{16}/cm^3$

D.4 I-V DATA ON Au/n-GaSb SCHOTTKY DIODE

I-V was analyzed using the thermionic emission theory: [58,59]

$$I=A_{eff}A^*T^2 \exp(-q\phi_{Bn}/kT)\exp[q(V-IR)/nkT] \qquad (4.1)$$

where A_{eff} = effective area of the diode, $A^*(=5.04cm^{-2}K^{-2}A)$is the effective Richardson constant for GaSb, which is related to corresponding effective mass by:

$$A^*/A = m^*/m_o, \qquad (4.2)$$

where A is equal to 120 $A/cm^2/K^2$ for free electrons and $m^* = 0.042m_o$ = effective electron mass of GaSb. ϕ_{Bn} is Schottky barrier height, k is the Boltzman constant, and R is the diode series resistance. There are a couple of ways one can determine these three unknown parameters: ϕ_{Bn}, R, and n. One method is the determination of these parameters manually from the slope of the I-V characteristics as reported by Wang et al.[46], and Basu et al. [60], which is somewhat tedious. Another method is by simulation of the experimental I-V characteristics. IDL software was used and the best fit I-V characteristics were obtained by trial and error where the above three parameters were treated as variables until the best fit between the experimental and computer data were achieved. This method is more convenient than the former one.

Figure 4.4 shows a typical fitting of Au/n-GaSb Schottky diode with LPEE layer grown at 530°C with a carrier concentration of $2.0x10^{17}cm^{-3}$. A good fitting was obtained for ϕ_{Bn}=0.48V, n=1.30, and R=8.5 ohm which are in good agreement with the values reported in literature [56,58-60]. The values of the barrier heights for the L-series samples was found to be consistently 0.04V higher than the H-series samples as listed in Table 4.1. It may be noted that the reported values in the literature were obtained from Schottky diodes made by

evaporation under either high vacuum or ultra high vacuum. None of these reports uses electroplating as the metal deposition method.

The reverse saturation current for the Schottky diodes was estimated from

$$I_{s(sch)} = A_{eff}A^*T^2\exp(-q\phi_{Bn}/kT) \qquad (4.3)$$

where $A_{eff} = 3.8 \times 10^{-4}$ cm^2 (for diameter of 220 μm), $A^* = 5.04$ Acm^{-2}K^{-2}, and $\phi_{Bn} = 0.48$ V (see Table 4.1), and we get

$$I_{s(sch)} = 1.5 \times 10^{-6} \text{ A} = 1.5 \ \mu\text{A}$$

This value compares fairly well with the experimental value of 5μA.

Reverse breakdown voltage in the Schottky diode can be estimated by considering the metal interfacial barrier to be a one sided abrupt junction, hence the breakdown voltage is a function of the carrier concentration in the semiconductor as given below[61].

$$V_B = 60\ (E_g/1.1)^{3/2}(N_d/10^{16})^{-3/4} \qquad (4.4)$$

where E_g is in eV , and N_d is doping concentration in cm^{-3}. For sample HE-5 with $N_d = 5.7 \times 10^{17}$cm^{-3} and LP-19 with $N_d = 5.0 \times 10^{16}$/cm^3, the computed values of V_B are 1.5 V and 9.5 V which are in excellent agreement with the experimental values of 1.0 and 8.0 V, respectively.

D.5 C-V DATA ON Au/n-GaSb SCHOTTKY DIODE

Due to the narrow band gap of GaSb and presence of large interfacial defects, Schottky diode made on n-GaSb tend to have larger leakage currents than on Si and GaAs. Once the leakage current exceeds a certain limit, C-V data acquired is not accurate. For samples with carrier concentration exceeding mid 10^{17} range, due to the large increase in the tunneling current component it was not possible to perform C-V measurements. For example, the leakage current of a diode with C = 60 pF at a reverse bias of 0.5 V should not exceed 60 μA. For the lower dopant concentrations (for a L-series layer exhibiting a carrier concentration of 6.4×10^{16}/cm^3) $1/C^2$ versus V plot is linear as shown in Fig 4.5. V_{bi} for this sample was determined from the intercept to be 0.316 V.

Considerable variations in the values of the built-in voltage is noticed as indicated in Table 4.1. This is probably due to the quality of the grown layers, as normally layers exhibit some sort of terracing and pin holes on the surfaces. These surface irregularities undoubtedly will affect the results of the C-V measurements. However, the values for ϕ_{Bn} obtained from I-V are quiet consistent. This is probably because I-V method is based upon forward bias condition with large current passing through the Schottky diode while C-V method is based upon reverse bias conditions and any surface defects will contribute to the increase in reverse leakage current and thereby affect the C-V results.

D.6 CONTROVERSIES OVER THE BARRIER HEIGHT FOR Au/n-GaSb

In literature, the values of barrier heights reported for Au/n-GaSb fall in two different ranges. Milnes et al.[57] , Sze [61] and Spitzer et al.[62], reported a value of 0.60 V and suggested that ϕ_{Bn} does not follow the well-known "two-third E_g Rule", while more recently Wang et al.[46], Murawala et al.[49], Basu et al.[60] reported ϕ_{Bn}=0.46-0.51V consistent with the "two-third E_g Rule". Our results on ϕ_{Bn} (0.48 - 0.52 V from I-V) is close to latter reports. Murawala et al.[49] suggested that values of the barrier heights can vary significantly in the presence of an interfacial layer between the Au and GaSb. They suggested that in the presence of an oxide layer (as GaSb has a high oxidation rate), the ideality factor n generally becomes large and the barrier height ϕ_{Bn} increases with the increase of ideality factor n. The lowest n reported by them is 1.12 and the barrier height computed from both C-V and I-V is 0.47 V. Our results are in good agreement with the above values with the value of n being 1.3 and ϕ_{Bn} in the range of 0.48-0.52V from I-V fitting.

We believe that the high values of n = 1.9-2.0 and ϕ_{Bn}= 0.6V reported by Milnes et al. [57] are due to the presence of oxide layer at the interface because they used $(NH_4)_2S$ as a surface treatment just before the deposition of Au. As mentioned earlier our observations indicated that $(NH_4)_2S$ oxides GaSb very quickly and the GaSb surface would turn dark within 3 minutes of soaking in $(NH_4)_2S$. This suggests the presence of thick oxide layer on the GaSb surface and hence the ideality factor n from these Schottky diodes are large leading to a considerable inaccuracy in the determination of the barrier height.

D.7 THE DIFFERENCES BETWEEN BARRIER HEIGHT OBTAINED FROM I-V AND C-V

The barrier heights are computed from both I-V and C-V measurements. I-V measurement provides direct determination of ϕ_{Bn} while C-V measurement provides information on V_{bi} which is then used for the computation of ϕ_{Bn}. The relation between ϕ_{Bn} and V_{bi} is given by,

$$\phi_{Bn}+\Delta\phi=V_{bi}+V_n=V_{bi}+(E_c-E_f)$$

so
$$\phi_{Bn}=V_{bi}+(E_c-E_f)-\Delta\phi \qquad (4.5)$$

where $\Delta\phi$ is due to the barrier lowering effect also called Schottky effect and

$$\Delta\phi=\sqrt{\frac{q\epsilon}{4\pi\rho_s}} \qquad (4.6)$$

If electric field ε is in the order of 10^5 V/cm then the barrier lowering $\Delta\phi$ is about 0.015V. The value of E_c-E_f will depend on the doping concentration of the semiconductor. The

values of E_c-E_f are estimated to be much larger than $\Delta\phi$ hence ϕ_{Bn} should be larger than V_{bi} as indicated in Eq.(4.5). Our results seem to support the above conclusions because as V_{bi} obtained by C-V method fell between 0.3V-0.4V compared to 0.48V-0.52V for ϕ_{Bn} obtained by I-V method. Further, V_{bi} increases with the increase in doping concentration which is in good agreement with the theoretical predictions

$$n = n_i \exp[(E_c-E_f)/kT] \qquad (4.7)$$

If the barrier heights of 0.3V (low temperature grown layers) and 0.4V (high temperature grown layers) are estimated from C-V measurements, then Eq. (4.5) yields

$$\phi_{Bn}(H) - \phi_{Bn}(L) = V_{bi}(H) - V_{bi}(L) + (E_c - E_{fH}) - (E_c - E_{fL})$$

$$= V_{bi}(H) - V_{bi}(L) + (E_{fL} - E_{fH}) \qquad (4.8)$$

where $\phi_{Bn}(H)$, $\phi_{Bn}(L)$ refer to the barrier height obtained on layers grown at high and low temperatures, respectively.
Using Eq. (4.7),

$$n_H/n_L = \exp[(E_{fL} - E_{fH})/kT] \qquad (4.9)$$

$$E_{fL} - E_{fH} = kT[\ln(n_H/n_L)] \qquad (4.10)$$

For example, n_H(HE5) = $5.0\times10^{17}/cm^3$ (grown at 530°C) , n_L(LP-15)=$5.7\times10^{16}/cm^3$ (grown at 474°C), then we get

$$E_{fL} - E_{fH} = 0.056 \text{ V}$$

Using Eq. (4.5), $V_{bi}(H) = 0.4$V and $V_{bi}(L) = 0.3$V, we get

$$\phi_{Bn}(H) - \phi_{Bn}(L) = 0.4 - 0.3 - 0.056 = 0.044 \text{ V}$$

This difference in the barrier heights for samples grown at different temperatures is consistent with the 0.04V difference obtained from I-V method.

D.8 THE DIFFERENCES IN VALUES OF ϕ_{Bn} FOR LAYERS GROWN AT DIFFERENT TEMPERATURES

The values of ϕ_{Bn} for lower temperature are higher than the corresponding value on layers grown at higher temperatures (see Table 4.1). This variation can be explained using the defect model employed in the literature by Wang et al[46]. They found that for Schottky barrier on MBE grown GaSb epilayers, the breakdown voltage and the barrier height was found to decrease with increasing Sb_4/Ga ratios which was attributed to the increase in surface state densities for samples grown at higher Sb_4/Ga ratios. The surface

state densities were estimated from the dependence of the barrier heights on metal work functions for various metal-GaSb interfaces. The surface state densities were estimated to be in the range of 2.3×10^{14} to 1.2×10^{15} states/cm^2/eV for Sb_4/Ga ratios varying from 2 to 9.

The variation of the barrier height with metal work function can be described by

$$\phi_o = E_g/q - (c_2\chi + c_3 + \Delta\phi)/(1-c_2) \qquad (4.11)$$

$$\phi_{Bn} = c_2\phi_m + c_3 \qquad (4.12)$$

$$D_s \cong 1.1 \times 10^{13}(1-c_2)/c_2 \qquad (4.13)$$

where ϕ_o and ϕ_m refer to the energy level of the surface and metal work function, respectively, c_2 and c_3 are constants that were determined experimentally. From the variation of the barrier height of the diode to the different metals for a given Sb_4/Ga ratio, and using the parametric values of d=5Å [46], χ=4.06eV[63] and E_g=0.7eV for the thickness of the interfacial layer, electron affinity and band gap of GaSb, the following results were obtained.

$$\phi_{Bn} = 0.04643\phi_m + 0.264 \quad (\text{for } Sb_4/Ga = 2)$$

$$\phi_{Bn} = 0.03690\phi_m + 0.293 \quad (\text{for } Sb_4/Ga = 3.6)$$

$$\phi_{Bn} = 0.01071\phi_m + 0.395 \quad (\text{for } Sb_4/Ga = 5.8)$$

$$\phi_{Bn} = 0.00952\phi_m + 0.398 \quad (\text{for } Sb_4/Ga = 9) \qquad (4.14)$$

The corresponding surface energies were then estimated to be 0.233, 0.246, 0.257, and 0.260 eV for Sb_4/Ga = 2, 3.6, 5.8, and 9, respectively. As mentioned, higher Sb_4/Ga ratio leads to higher values of surface energy ϕ_o. Note the largest value for c_1 is 0.04643, which is considerably small compared to the value of 0.27 for Si and 0.07 observed in GaAs. This suggests that the barrier height for Au/n-GaSb is relatively more independent of metal work function than Au/n-GaAs. The low value of c_2 is also an indication of Fermi level pinning at the interface by the surface states, and thus barrier height becomes independent of the work function, being entirely determined by the doping and surface properties of the semiconductor. Therefore, the following approximate equation could be used to calculate the Schottky barrier height on GaSb.

$$q\phi_{Bn} = (Eg - q\,\phi_o) - q\Delta\phi \qquad (4.15)$$

Using this equation, the calculated barrier height was found to be close to those measured by I-V method by Wang et al.[46]

It is well established[64] that high temperature LPE grown GaSb layers exhibit higher intrinsic defects than those grown at low temperature , it is expected that the surface energy will be higher in the former case. The differences in the surface energy values is expected to be reflected in the barrier height

$$\phi_{Bn}(L) - \phi_{Bn}(H) = \phi_o(H) - \phi_o(L) = 0.52 - 0.48 = 0.04 \text{ V}$$

which compares well with the values obtained in MBE grown diode

$$\phi_o(Sb_4/Ga = 9) - \phi_o(Sb_4/Ga = 2) = 0.260 - 0.233 = 0.027 \text{ V}$$

This allowed us to estimate the defect density in our LPEE grown epilayers to be in the range of 10^{14} - 10^{15} states/cm^2/eV.

V PN JUNCTION

E.1 INTRODUCTION

One of the main application of the GaSb semiconductor is in the optoelectronic devices. However, to realize this potential fully much needs to be done to understand the properties of the basic units of electronic devices, namely p-n junctions. Our efforts were concentrated towards the fabrication of p-n junctions using Zn diffusion.

E.2 Zn DIFFUSION IN III-V COMPOUNDS

Junctions of GaSb may be prepared by diffusion or by ion implantation. Zn diffusion is a common way to obtain p-type conductivity in GaSb and also in other III-V semiconductors. While extensive work has been done on the Zn diffusion in GaAs, InP etc.,[65-73] relatively little examination has been made of Zn diffusion in GaSb. Heinz et al[67]. successfully diffused Zn in GaSb from Zn/Silica emulsitone and p-n junctions were fabricated with breakdown voltages as high as 20-30V with the N_A concentration in the p-region to be 5 x $10^{15}cm^{-3}$. The occurrence of this p-region has not been fully explained, neither forward nor reverse biased characteristics have been extensively studied for diffused homojunction structure. In our laboratory we tried to duplicate the same effort but were unable to get good controllable diffusion.

The second method that has been widely used is the diffusion in sealed ampoules in III-V semiconductors. However, this method is cumbersome and time consuming. Further, the sealed ampoule method is generally used in device fabrication where control of junction depth is not critical[70].

Third technique, diffusion by open tube method has not been popular, as the most common problem with III-V semiconductors is the dissociation of V element at elevated temperatures. GaSb has a melting point of 712°C which is substantially lower than the 1240°C of GaAs. This can present more serious processing problem such as loss of Sb at moderate temperatures (the energy for dissociation is 10-14Kcal/mol). We discovered that even at 500°C , if GaSb is placed in either N_2 or H_2 for a few minutes, the surface of the GaSb turns dark, SIMS tests on the samples clearly showed the loss of Sb at the surface. Figure 5.1 shows the SIMS measurements on the Zn diffused n-GaSb at 500°C for 5 minutes. A modified version of this method, namely the open-tube diffusion under controlled ambient has been successfully used in III-V compound semiconductors. Open tube diffusion with phosphorus overpressure[26], use of encapsulants[27], ion implantation as a prediffusion source layers[28], and spin-on diffusion source layers[29], have been described in the literature for GaAs and InP. Other various specific experimental details include use of different sources, encapsulants, spin-on sources and combined measures.

Ghandhi et al[69]. reported, precisely controlled shallow p^+ diffusions in GaAs using ZnO/SiO_2 as a doped oxide source for zinc, phosphosilicate glass(PSG) layer as a cap. Phatak et al.[65] proposed a novel method for Zn in II-VI compounds. Using this technique, an appropriate vapor pressure of Zn and P could be localized and confined directly over the InP wafer. The technique requires specially designed graphite diffusion boats, which contain the

diffusion source charges and samples. We decided to adopt this open-tube method in a controlled ambient due to its simplicity. Further, in this method the diffusion front is controlled reproducibly by the two basic parameters: time and temperature. The volatile diffusing species are highly localized and contained within the apparatus in close proximity to the wafer. This technique has been applied to form diffused contacts to various devices, such as planar lasers and photodiodes, where the junction location can be accurately controlled.

E.3 EXPERIMENTAL

A graphite diffusion boat of approximately 2cm x 2cm x 1.5cm = 6 cm^3 volume was machined in our machine shop as shown in Fig 5.2(a). It consists of a substrate recess with a graphite basket on top. This basket had numerous holes in the bottom to create the Sb overpressure.

The charge consisted of metallic Zn and Sb with Ga as a solvent. Sb was added to suppress thermal etch pitting of the GaSb wafer to prevent Sb dissociation at elevated temperatures. The typical weight of the melt used was 3g Ga, 0.35g Zn, and 0.3g Sb. Similar ratios were used to diffuse Zn into both GaAs and InP successfully[65-73]. Also as mentioned in the literature, varying the ratio of these elements in a certain range did not affect the result of the diffusion[68,69]. Hence the weight of these three elements is not very critical. However cleanliness of these elements are crucial as the impurities in the diffusion charge will readily diffuse into the samples thereby affecting the behavior of the PN junctions.

The charge is initially baked at 700°C for 5 hours in H_2 ambient. Zn diffusion was carried out on Te-doped LPEE grown (100) GaSb layers with carrier concentration in the range of 6 x $10^{16}/cm^3$ - 2 x $10^{17}/cm^3$ as determined by C-V measurements. Prior to diffusion, the samples were cleaned in the standard organic solvent, then soaked in HCl acid for about 5 minute in order to eliminate residual metallic impurities like Hg, etc. and oxide layer[46]. The diffusion was carried out in H_2 ambient at 550°C for 5 minutes. The ramping of the furnace is as shown in the Fig. 5.2(b). One batch of charge could be used for about 10 runs of diffusions.

The top p-side of the junction was electroplated with Au as in the Schottky diode. The Au served both as a mesa etching mask and contact metal to the p-side of the p-n junction. Mesa etching was accomplished using CH_3COOH : HNO_3 : HF = 40 : 18 : 2[54] solution . Other etching solutions, namely Br_2-methanol (0.5% Br_2) was also attempted with not as good results in terms of surface finish leaving a cloudy surface. The typical etching rate for the former is about 8μm per second. Usually 5 seconds of etching is sufficient to isolate each individual p-n junction. Figure 5.3 gives the top view of the front-side of the sample after mesa etching. Electroplated Au-Sn was used for the back-side contact. Schematic summary of the p-n junction fabrication process is shown in the Fig. 5.4.

E.4 RESULTS AND DISCUSSIONS

Figure 5.5 shows a typical I-V characteristics of a mesa GaSb pn junction diode. The onset voltage is about 0.5V. The reverse leakage current is typically about 1-3 μA at a

reverse bias of 1V. The reverse leakage current for pn junctions is usually smaller than that of Schottky diode by a factor of 10 as expected. This leakage current is very close to the reported value by Heinz [67] (the diode diameter is 290μm by spin-on method) and Capasso [75] (the diode diameter is 350 μm by LPE method).

Figure 5.6 shows the analytical fitting of the forward I-V characteristics which is described by the equation:

$$I = I_{s(pn)}\exp[q(V-IR)/nkT] \qquad (5.1)$$

where

$$I_{s_{(pn)}} = A_{eff}\left(\frac{qD_p p_{no}}{L_p} + \frac{qD_n n_{po}}{L_n}\right) \qquad (5.2)$$

The parameters $I_{s(pn)}$, R, and n were used as fitting parameters. The values of R and n that resulted in a best fit for I-V curve of PN junctions are close to that determined for Schottky diodes, however n is not a constant for the entire I-V curve. This will be discussed in the subsequent section. The value for $I_{s(pn)}$ was computed to be 2.2 x 10^{-9} A.

Assuming the junction to be an ideal abrupt junction, the theoretical value of the reverse saturation current for pn junction was estimated from,

$$I_s(pn) = A_{eff}\left(\frac{qD_p p_{no}}{L_p} + \frac{qD_n n_{po}}{L_n}\right)$$

where we have A_{eff} = 3.8 x 10^{-4}cm^2, L_p = 1 μm, L_n = 1.5 μm, $\tau_p = \tau_n$ = 2 x 10^{-9} s [47], and n_i = 1.0 x 10^{13} cm^{-3}, $n_{no} = p_{po}$ = 1.0 x 10^{17}cm^{-3} , then

$$D_p = L_p^2/\tau_p = 5 \text{ cm}^2/\text{s}$$

$$D_n = L_n^2/\tau_n = 11.25 \text{ cm}^2/\text{s}$$

$$p_{no} = n_i^2/n_{no} = 1.0 \times 10^9 \text{cm}^{-3}$$

$$n_{po} = n_i^2/p_{po} = 1.0 \times 10^9 \text{cm}^{-3}$$

then, we have $I_{s\,(pn)} = 7.6 \times 10^{-9}$ A.

This value compares very well with the estimated value of 2.2x10^{-9}A determined earlier from the I-V fitting, if we take into consideration the complex nature of $I_{s(pn)}$.

One of the problem with devices based on GaSb and the related compounds is the presence of large dark current. This in conjunction with low break-down voltage have restricted the application of these diodes up to now.

The estimation of break-down voltage for p-n junctions is not as straight forward as

Schottky diode because the diffused p-n junction is not an abrupt junction. We observed that in general, the break-down voltage of pn junction is smaller than that of Schottky diodes for similar doping concentrations.

E.5 THE DIFFERENCE IN THE VALUE OF 'n' FOR PN JUNCTION AND SCHOTTKY DIODE

As stated in the above section E.4, I-V characteristics of P-N junctions cannot be described by one characteristic value of 'n'. This is also expected from the theoretical considerations. For pn junctions, the ideality factor (n) will be changing under different forward current densities. Under low current densities and low recombination current, the n will be close to 1. At higher current densities for which the injected minority carrier concentration is comparable to the majority concentration, both the drift and the diffusion current components have to be taken into consideration. Under high injection conditions, n is roughly proportional to exp(qV/2kT), where n = 2.

The mechanism of current transport for Schottky diode is also different from that of pn junction. The current transport in metal-semiconductor contacts is mainly due to majority carriers, in contrast to pn junctions, where minority carriers are responsible. So the ideality factor (n) does not change under different forward current densities. The ideality factor (n) is affected only by the interfacial layer between the metal and the semiconductor, and temperature[76], hence a unique value would suffice in describing the entire I-V characteristics.

VI. ION IMPLANTATION DAMAGE AND ANNEALING IN GaSb

F.1 INTRODUCTION

In the previous sections electrically active impurities were introduced into semiconductors (a) during growth of the epitaxial growth from the melt and (b) by diffusion from the surface. None of these processes is controllable enough to produce the required electrical conductivity in a precisely defined volume of semiconductor. It is very easy for the dopant source to become depleted at some stage ruining the complete growth run. Further, the process cannot readily be monitored so as to determine the actual number of atoms entering the semiconductor. Hence, we have investigated the third technique of doping the semiconductor, by ion implantation. This technique overcomes the above major drawbacks of the diffusion technique and in addition exhibits numerous advantages that include reproducibility , uniformity and a better control of the dopant profile. Hence, in recent years, ion-implantation technology has become very important in the preparation of doped semiconductors. Generally it is a two step process sequence, the implantation being followed by an annealing stage in order to remove the lattice disorder introduced by implantation and to achieve electrical activation of the dopants.

It is well documented, particularly in the case of Si [77-79] that if sufficient energy is deposited into elastic (nuclear) collisions during ion implantation, the material will undergo a phase transformation from the crystalline to amorphous state. Amorphization in the case of Si is known to reduce the random channeling tails of light ion implants and to increase dopant activation. Amorphization followed by solid phase epitaxial regrowth results in significant decrease in the concentration and stability of implantation related dislocation loops[80]. The studies on compound semiconductors have been limited [81,82]. In general compound semiconductor have lower solubilities for implanted species than elemental semiconductors, as well there are severe problems with defect related compensation of electrically active dopants. These studies seem to suggest that implantation induced amorphization should be avoided because on annealing, during the solid phase regrowth , the defect microstructure which may evolve from high densities of stacking faults and microtwins into dislocation networks. The presence of these defects are reported to lower dopant activation[83] .

A review of the published work in ion implanted GaSb is given in ref. 84 and is attached in the Appendix-D. It is evident from the literature survey [85-88] that the damage related processes involving GaSb implantation doping have not yet been sufficiently studied let alone understood. However, it is clear that the damage removal process in GaSb seems to be more complex in comparison to other III-V compounds because even at moderate dosages, the near surface regions are amorphized and the regrowth process has been unsuccessful [85]. In order to predict better the conditions of the solid state regrowth, there is a need to understand the threshold damage density for a variety of different species and implant conditions. This requires both a fundamental understanding of what solid state properties dominate the amorphization process and accurate experimental data.

To date, all the published reports have been on room temperature implanted GaSb. Hence, we have tried to study the solid phase regrowth mechanisms in shallow implants as a function of atomic weight of the implanted species for different dosages. The implant was

carried at 77K to ensure that the surface region is definitely amorphized. RBS/channeling was used to quantify the amount of damage produced in the form of atoms displaced from their normal sites in the as implanted samples and after rapid thermal annealing, thus estimating the percentage of damage recovery.

F.2 EXPERIMENTAL

Undoped (100) GaSb were implanted with Te, Er, Hg and Pb at liquid nitrogen temperature for three different fluences in the range of 10^{13}, 10^{14} and 10^{15} /cm^2 at 146 KeV, 180 KeV, 200 KeV and 206 KeV, respectively. The initial choice of the dopants were primarily dictated by the use of RBS for the direct determination of the concentration of the implanted materials. The dosages and the implantation energies were chosen so that the same amounts of energy were deposited by nuclear collisions on the substrate in roughly the same volume. The TRIM calculations indicated the projected range to be ~ 447Å . The details of the Rutherford backscattering/channeling , and rapid thermal annealing are given in Ref. 84 (see Appendix-D). Depth profile of the implanted species on as implanted and channeled samples were carried out using Secondary Ion Mass Spectroscopy (SIMS) instrument, Perkin Elmer 6300 system at Microelectronics Center of North Carolina. Mass seperated Cs^+ ion beam incident at an angle of 60° to the sample surface with an ion energy of 3 KeV was used. The Cs^+ beam current was typically 148 nA with a beam spot size of about 200x600 μm. The beam was raster \scanned to erode a 600x600 μm area. For depth profiling , negative ions were detected from a 80x80 μm area in the center of the eroded area using electron gating. The secondary extraction voltage was -200V. The pressure during Cs^+ bombardment was $5x10^{-9}$ torr.

F.3 RESULTS AND DISCUSSION

Figure 6.1 shows the RBS spectra of 2 MeV He^+ ions scattered at 170^0 from a GaSb sample, aligned along <100>, as implanted with 10^{14} Te ions/cm^2 and after annealing at 600°C for 60 and 120s. Also shown is a spectrum of the same sample in random orientation. The details of the measurement of the fractional residual damages and the χ_{min} are given in the Ref. 84. The shape of the random spectra is characteristic of a diatomic target with a first edge at the highest energy due to the alpha particles backscattered by the heaviest nucleus (Sb) and second edge superimposed at a lower energy and due to the particles backscattered by the lowest mass element (Ga). No significant peak is observed in the energy window above the edge. This is an indication of a low contamination of the surface with heavy elements (mass greater than Sb), taking into account that the detection threshold of the RBS technique for this element is as low as one monolayer (10^{15}/cm^2) . As shown in Fig. 6.1, the height of the damage peak of the as implanted sample reaches that of the random orientation, indicative of an amorphized surface layer. This was indeed observed for all the as implanted samples. Upon annealing at 600°C, the area under the damaged peak as well as χ_{min}, decrease, showing partial recovery of the damage. These values for different annealing durations are listed in Table 6.1.

As Te implanted GaSb has a potential application for devices, the study was mostly

focussed on these samples. The results of RBS/channeling spectra of the GaSb samples implanted with 10^{13} Te ions/cm^2, before and after annealing at 600°C for 30,60,90 and 120 s are tabulated in Table 6.1. Durations of 30- 60 s appear to be the optimum annealing time for achieving low χ_{min} and low residual damage. For longer annealing, χ_{min} either degrades or remains the same. Examination of surface morphology by SEM revealed significant degradation of the surface for annealing durations beyond 90 s as shown in Fig. 6.2. The lowest residual disorder and χ_{min} is obtained at lower implantation doses as expected. The samples with 10^{13} Te ions/cm^2 annealed for 30 s had a backscattering yield as low as 11%. For comparison we also carried out RBS/channeling in undoped and Te doped GaSb substrates obtained from different vendors and on liquid phase electro-epitaxially grown epilayers. The bulk substrates and the epilayers are indicated by the letter V and L at the beginning of the sample name as indicated in Table 6.2. There is a considerable variation in the χ_{min} of the substrates and the layers, but on annealing the scatter in the values of χ_{min} decrease and saturated between 5-10. The epilayers seem to exhibit somewhat lower χ_{min} than the substrates indicating a better crystalline quality with a minor improvement in χ_{min} on annealing. There does not seem to be any variation in % damage which was measured as the ratio of area under the channeled spectra to the corresponding total counts in the random spectra.

The samples implanted with 10^{14} ions/cm^2 as shown in Fig. 6.1 indicates a similar behavior as ion implanted samples of 10^{13} dosages with annealing duration of 30-60 seconds to be the optimum annealing time. However, in the ion implanted samples with 10^{15} ions/cm^2, a considerable deficit in the backscattering yield from Sb atoms near the surface was noticed when annealed at 600°C beyond 60 s. This may be either due to the preferential evaporation of Sb or due to oxygen adsorption at the surface by highly damaged surface as reported earlier by Pearton et al. [85]. As a result the Sb surface peak almost disappears. No oxygen was detected by RBS when measured at grazing angle. We also compared the random spectra of the ion implanted material with that of the virgin substrate . This was done in order to see if there were any differences in the slope of the characteristics resulting from oxygen adsorption in the implanted materials. No differences were noticed. However, there are evidences of preferential evaporation of Sb at the surface and of enhanced oxygen incorporation in these samples from SIMS data. The latter data is more reliable as in RBS the oxygen peak could be easily masked by the high background scattering yield of the matrix elements.

SIMS depth profile of the Te implanted samples of 10^{13} and 10^{14} dosages/cm^2 as shown in Figs. 6.3 and 6.4 do not indicate any significant redistribution of the dopant on annealing . The depth profile of the 10^{13} dosage/cm^2 as implanted sample is in excellent agreement with those predicted by TRIM, as shown in the Figs. 6.3, but the discrepancy increases with the Te concentration. For samples implanted with 10^{15} ions /cm^2, the surface was extremely rough and the depth of the crater formed from the ion beam was not well defined.

Surface morphology of these layers exhibited systematic change from smooth to sponge like appearance with increasing dosages as shown in Fig. 6.5. In addition anomalous expansion from 30-40 Å to 600Å of the implanted surface region was also observed with increasing dopant dosages. This is consistent with the observations reported in room

temperature implanted GaSb where swellings up to 6μm were observed for Ar^+ implantations of similar energies and dosages [88]. The swelling phenomenon was attributed to the formation of a porous layer and was found to be a function of the atomic mass of the dopant, energy of implantation and dosage of the implanted ions [88].

RBS/channeling analysis of the samples implanted with Er, Pb and Hg showed that the scattering yield from the damaged layer reached the random level, indicating the amorphization of the near surface region. In these samples the extent of damage production/removal appears to be dependent on the mass of the implanted ions. The details of this work is again provided in the Ref. 84 and hence is not repeated. The SIMS data on Er doped samples did not indicate the presence of Er in the sample. At this point it is not clear if it is due to the bad implantation or problem due to SIMS. Low temperature PL measurements were also carried out on all of these samples . The PL spectra were identical to that of undoped GaSb which is explicable as the depth of the excitation volume about 1 μm is much deeper than the implant depth, hence one does not expect to see any changes in the PL spectra.

It should be noted that we have used rapid thermal annealing treatments throughout this work. It is quite likely that furnace annealing under group V element overpressure would lead to different redistribution properties of implanted dopants in the materials we have investigated. This is because during proximity capless annealing there will be a loss to the surface of the more volatile lattice constituent (usually the group V elements) making significant concentrations of the vacancies of this type which assist the motion of substitutional and interstitial diffuses. We have concentrated on the use of RTA because this will be the unique choice for the most important applications in multilayered epitaxially grown structures in which redistribution of implanted dopant must be kept to a minimum. TEM micrographs of a Te implanted annealed sample showed the presence of trapezoidal shaped stacking faults as shown in Fig. 6.6.

VII CONCLUSIONS

Good optical-device-quality layers of GaSb and GaInAaSb have been grown by LPEE technique as evidenced by the narrow spectral width of x-ray diffraction and PL spectra. A systematic trend in the low temperature PL spectra is observed with the change in the composition of GaInAsSb. The optical activation energy of the acceptor is about 35meV and its phonon replica is shifted by about 30 meV towards the lower energy, consistent with the reported values in GaSb. The dissociation energies of the bound excitons in quaternary layers were also in good agreement with those in the binary layers.

Au/n-GaSb Schottky barrier was accomplished by electroplating. I-V and C-V measurements can now be routinely performed on the Schottky diode to determine the carrier concentration and barrier height, and also to examine the quality of these grown layers. The reverse saturation currents observed from these diodes are typically smaller than reported values and the break-down voltages are in good agreement with the predicted values. The barrier heights measured from I-V were either of 0.48V or 0.52V, the exact value appears to depend on the defect density of the grown epilayer. The barrier heights measured from C-V are generally smaller and more diverse than those obtained from I-V due to the presence of the surface defects.

Well behaved p-n homojunctions were obtained by Zn diffusion in Te-doped LPEE grown GaSb in an open tube configuration with Sb overpressure. The reverse saturation currents are close to the reported values. Computer simulations of I-V characteristics reveal a reasonably good agreement between experimental data and theoretical predictions.

In Te-doped GaSb layers low temperature PL spectra exhibit numerous additional transitions at lower energy levels. A doubly ionizable native residual acceptor (A/A^-) is observableat 97meV above the valence band. In addition another native acceptor level (B) at 54meV, three Te-related acceptor levels at 68, 80 and 86meV above the valence band are observed. The relative dominance of each of these transitions depends on the degree of Te compensation and incident excitation intensity. At lower intensity the deeper impurity levels are active and with increasing intensity, due to an increase in the probability of "infilteration" under the barrier, the shallow acceptors predominate. The limited data on the output integrated intensity dependence on excitation intensity further confirms the nature of the transitions. Finally, the bound excitonic transitions are seen even under the heaviest doping conditions which indicates good crystal quality.

Study on the dependence of damages on atomic weight and dosages of the implanted species on (100) GaSb indicate that the degree of disorder of the implanted region increases significantly with both of the above parameters. RTA at 600°C for 30-60 secs was found to be optimum annealing conditions that yield the lowest χ_{min} value without any surface degradation. Excellent recovery was obtained for Te-implanted samples with no significant distribution of Te on annealing.

VIII. TABLES AND FIGURES

TABLE 3.1 Low temperature characteristics of Te doped GaSb layers as a function of growth temperature & incident excitation level.

			Growth Temp 474°C					Growth Temp530°C		
	Ref4.	Ref12.	0.7W/cm^2		19W/cm^2		1W/cm^2		16W/cm^2	
Iden	Energy (meV)	Energy (meV)	Energy (meV)	Rel. Int.	Energy (meV)	Rel. Int.	Energy (meV)	Rel. Int.	Energy (meV)	Rel. Int.
FE	810	808.5								
UI	808.7									
UI	807.95									
BE_1	805.4	805.4							804	.07
BE_2	803.4	802.2								
BE_3	800.1	799.1			799	.02			800	.03
BE_4	796.1	795.8							796	.3-.14
UI	795				793	.02			790	.9-.1
UI		784.5								
A	777.5	777.5	777-81	.1-.4	780-4	1	777	.07	779-80	.1-.6
A'			771-3	.2-.03	771-4	.07-.12			770-4	.1-.3
BE_4-LO	765	765.5	761-2	.03	765-9	.02-.1	766-.045		766	.03
B	758	756.36	756-60	.03	761-2	.04-.11			756-9	.65-1
UI	752		750-51	.09	751-2	.08				
A-LO	748.5	748.2								
C			745-47	.10			741-5	1	744	.5-1
D			730-1	1	734-740	.2-.4				
B-LO	728									
E	722		724-25	.2-.4	724-5	.05-.08			722-725	.05-.5
C-LO			714-17	.09	717-9	.07	714-8	.15-.4	717	.17
A"	710		703-07	.16	705-8	.06	704-9	.15-.18	708-10.	.16-0.004
UI	694		690-7	.01-.09	696	.03	697	.1	694-8	0.07

TABLE 3.2 Low temperature PL characteristics of Te doped GaSb layers grown at 530°C by LPEE technique for incident intensity levels of 1.0W/cm^2

	HAK9 ($1x10^{17}/cm^3$)			HF6 ($2x10^{17}/cm^3$)			HE6 ($6.2x10^{17}/cm^3$)		
Iden	Energy (meV)	Rel. Int.	II	Energy (meV)	Rel. Int.	II	Energy (meV)	Rel. Int.	II
A							777	0.07	0.03
BE_4-LO							766	0.05	0.01
C	744	1.0	1.0	745	1.0	1.0	741	1.0	1.0
D	731	0.50	0.66	730	0.55	0.44	731	0.06	0.25
C-LO	714	0.15	0.12	717	0.40	0.32	718	0.37	0.10
A`				709	0.18	0.13	704	0.22	0.02
UI	697	0.07	0.07				697	0.1	

II-Integrated Intensity

TABLE 3.3. Low temperature PL characteristics of Te doped GaSb layers grown at 530°C by LPEE technique for incident intensity levels of 16W/cm^2

	HAK9 ($1x10^{17}/cm^3$)			HF6 ($2x10^{17}/cm^3$)			HE6 ($6.2x10^{17}/cm^3$)		
Iden	Energy (meV)	Rel. Int.	II	Energy (meV)	Rel. Int.	II	Energy (meV)	Rel. Int.	II.
BE_1	804	0.14	0.06	804	0.07	0.04			
BE_2									
BE_3	800	0.03	0.01						
BE_4	796	0.3	0.67	796	0.14	0.08			
UI	790	0.9	0.5	790	0.11	0.04	791	0.45	0.28
A	779	0.65	0.27	780	0.19	0.04	780	0.1	0.03
A'	770	0.28	0.12	770	0.12	0.10	774	0.08	0.01
BE_4-LO							767	0.04	0.01
B	756	0.65	0.58	759	1	1.0	753	1	1.0
C	744	1	1.0	744	0.54	0.49			
UI							736	0.07	0.31
B-LO							728	0.03	0.01
E	725	0.2	0.16	725	0.51	0.42	722	0.27	0.24
C-LO	717	0.17	0.15						
A'				710	0.16	0.1	708	0.03	0.01
UI	698	0.08	0.09				694	0.06	0.03

TABLE 3.4. Low temperature PL characteristics of Te doped GaSb layers grown at 474°C by LPEE technique for incident intensity levels of 0.7W/cm^2

	LP11 (6×10^{16}/cm^3)			LP30 (9.3×10^{16}/cm^3)			LS7 (3×10^{17}/cm^3)		
Iden.	Energy (meV)	Rel. Int.	II (meV)	Energy Int.	Rel. (meV)	II Int.	Energy (meV)	Rel. Int.	II
A	777	0.43	.25	780	0.43	.30	779	0.21	.16
A'	772	0.23	.22	771	0.09	.08	771	0.06	.33
BE_4-LO	761	0.03	.01	761	0.04	.03	766	0.01	.01
B	756	0.04	.23				760	0.04	.04
UI				750	0.08	.07	753	0.03	.02
C	745	0.11	.11				748	0.09	.05
UI							731	0.05	.01
UI							727	0.02	.01
D	731	1	1	735	1	1	735	1	1
E	721	0.19	.11	724	0.25	.06	724	0.37	.33
C-LO	714	0.08	.04	717	0.09	.06	714	0.03	.02
A"	703	0.16	.21	705	0.16	.18	705	0.17	.27
UI	690	0.09	.01	697	0.02	.07	691	0.03	.01
UI	685	0.02	.01						

II-Integrated Intensity

TABLE 3.5 Low temperature PL characteristics of Te doped GaSb layers grown at 474°C by LPEE technique for incident intensity levels of 19W/cm^2

	LP-11 ($6x10^{16}$/cm^3)		LP-30 ($9.3x10^{16}$/cm^3)		LS-7 ($3X10^{17}$/cm^3)	
Iden	Energy (meV)	Rel Int.	Energy (meV)	Rel. Int.	Energy (meV)	Rel. Int.
FE						
UI						
UI						
BE_1						
BE_2						
BE_3			799	0.022		
BE_4					796	0.033
UI	793	0.020				
UI						
A	780	1	782	1	782	1
UI	771	0.110	772	0.074	772	0.180
BE_4LO	765	0.020			766	0.060
B	761	0.040	762	0.1	762	0.054
UI	751	0.080	751	0.089	754	0.108
A-LO						
D	734	0.210	738	0.258	738	0.263
B-LO			731	0.008	731	0.030
E			725	0.048	725	0.084
UI			719	0.074		
UI	713	0.01	713	0.033	715	0.033
A	708	0.070	705	0.055	707	0.069
UI			696	0.026		

II-Integrated Intensity

TABLE 3.6 Low temperature (4K) PL characteristics of quaternary composition under two different incident intensity levels.

	Ref5.	1W/cm^2		20W/cm^2	
Iden	Energy (meV)	Energy (meV)	Rel. Int.	Energy (meV)	Rel. Int.
FE					
BE_1	703.8				
BE_2	697.9				
BE_3	691.1	683	1.00	679	0.30
A	670.9	661	0.02		
		653	0.14	652	0.01
		634	0.28	626	1.00
A-LO	640.2				
		614	0.20		
		595	0.08	595	0.64
		577	0.06		
				552	0.06
				527	0.07

TABLE 4.1. Summary of electrical characteristics of Au/n-GaSb Schottky diode.

SAMPLE	$N_d(cm^{-3})$	V_{bi}(C-V) (V)	ϕ_{Bn}(I-V) (V)	V_B (V)	R(ohm)	n
HB-15	3.2×10^{17}	0.37-0.47	0.48	0.5	8.5	1.30
HE-5	5.6×10^{17}	0.41	0.48	1.5	8.5	1.30
HD-5	2.0×10^{17}	0.40	0.48	2.0	8.6	1.30
HD-6	5.0×10^{17}	0.44	0.48	0.8	8.9	1.30
(Above samples were grown at 530°C)						
LS-6	1.02×10^{17} – 2.85×10^{17}	0.37-0.47	0.52	1.5	9.5	1.32
LP-29	9.3×10^{16}	0.32-0.35	0.52	8.5	9.8	1.32
LP-15	$5.7\text{-}6.4 \times 10^{16}$	0.23-0.31	0.52	10	10.6	1.35
LP-19	Too leaky	Too leaky	0.52	Too leaky	10.5	1.34
(Above samples were grown at 476°C)						

TABLE 6.1 Implantation dosages and RBS data on the annealing behavior of different elements in undoped (100) GaSb.

ELEMENT	DOSAGE (/cm^2)	FRACTION OF DAMAGE (%) AFTER ANNEALING DURATION (SEC)				χ_{min} (%) ANNEALING DURATION (SEC)			
		30	60	90	120	AI	30	60	90
Te	$1.2x10^{13}$		5	6	4	50	11	12	13
	$1.2x10^{14}$	13	12	16	13	54	17	12	
	$1.2x10^{15}$	25	18	--	--	54	33	26	27
Er	$1.1x10^{13}$	58	18			54	17		
	$1.1x10^{14}$	22				49	18		
	$1.1x10^{15}$	28	13			48	25		
Hg	$1.1x10^{13}$					34			
	$1.1x10^{14}$					46			
	$1.1x10^{15}$					84			
Pb	$1.1x10^{13}$	30				52	26		
	$1.1x10^{14}$	39				60	52		
	$1.1x10^{15}$								

TABLE 6.2. RBS data on the annealing behaviour of undoped and Te-doped (100) GaSb substrates and LPEE grown epilayers.

SAMPLE	FRACTION OF DAMAGE (%) AFTER ANNEALING DURATION (SEC)			χ_{min} (%) ANNEALING DURATION(SEC)			
	30	60	90	U	30	60	90
VSM-U/D	74	86	87	6	7	7	10
VMS651848-U/D	95	80		9	8	7	
VSM-Te	54	90		12	10	9	
VMS-Te	76	67		11	6	5	
VMS55W-Te				16	8		
LGS52-U/D	67	67		14	17	10	
LS9-Te	84	87		9	9	6	

SM - Sumitomo
MS - Metal Specialties
U/D - Undoped

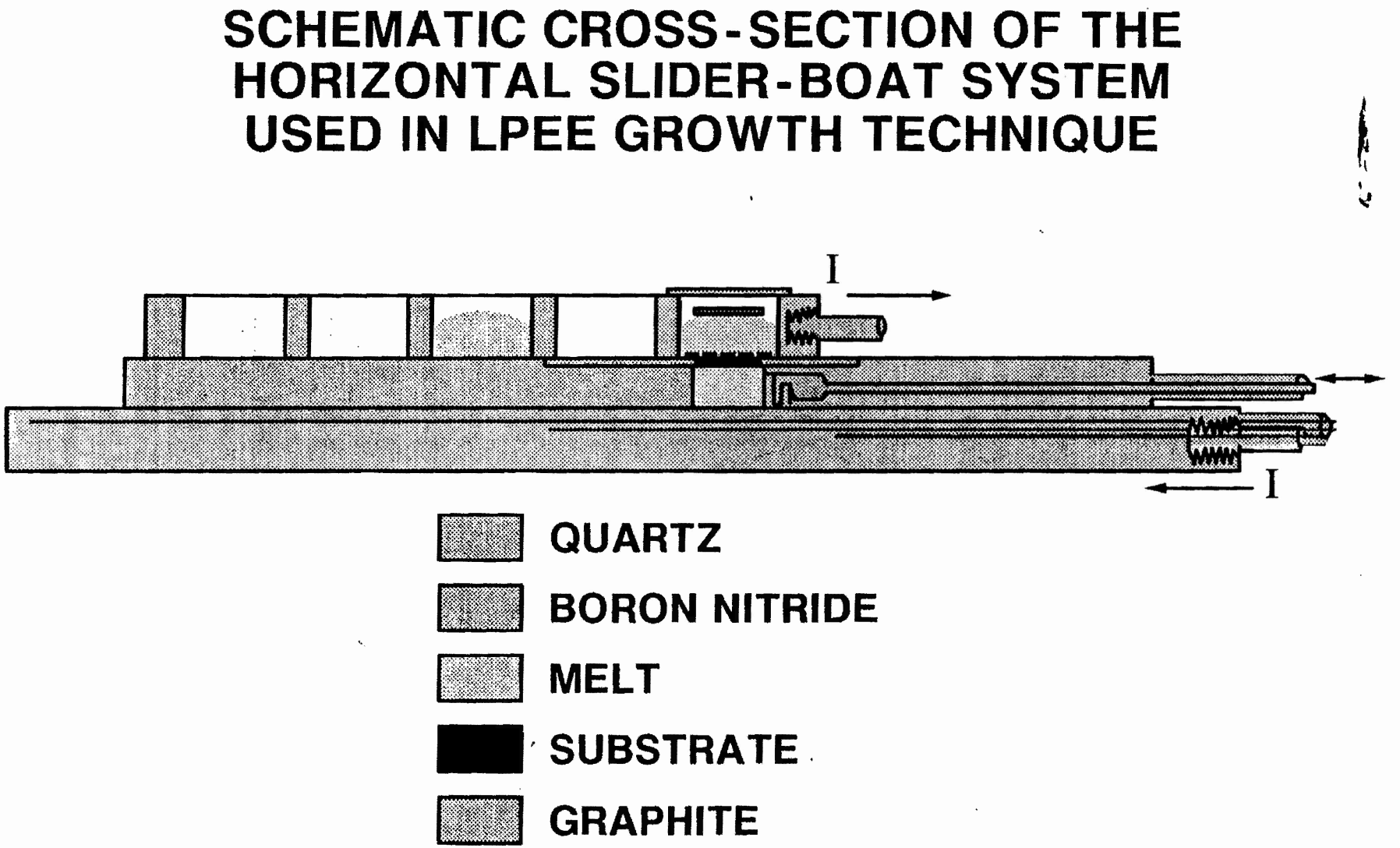

Fig. 2.1. Schematic diagram of the LPEE growth set-up.

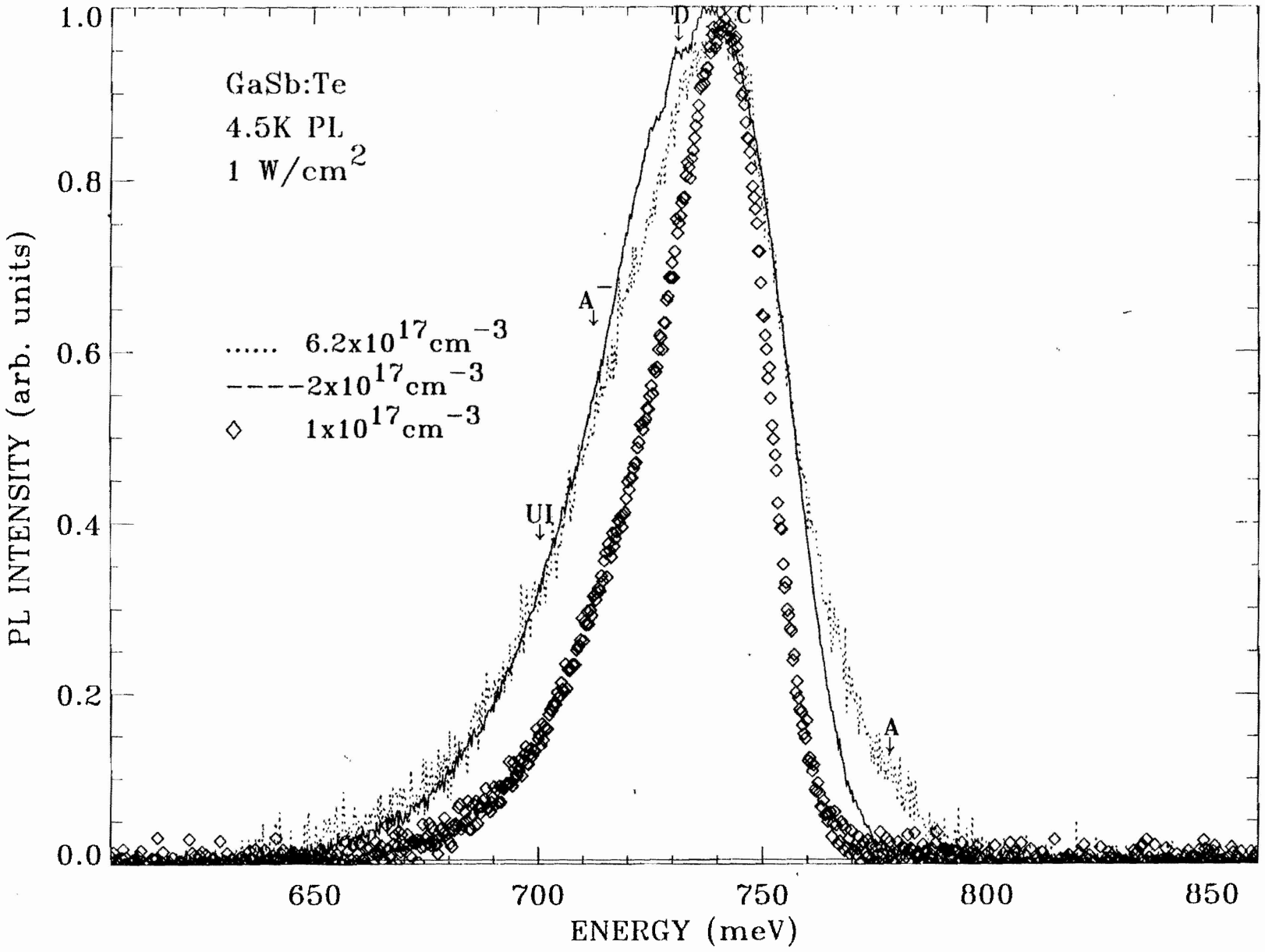

Fig. 3.1. Low temperature PL spectra of LPEE GaSb layers grown at 530°C at different Te concentrations.

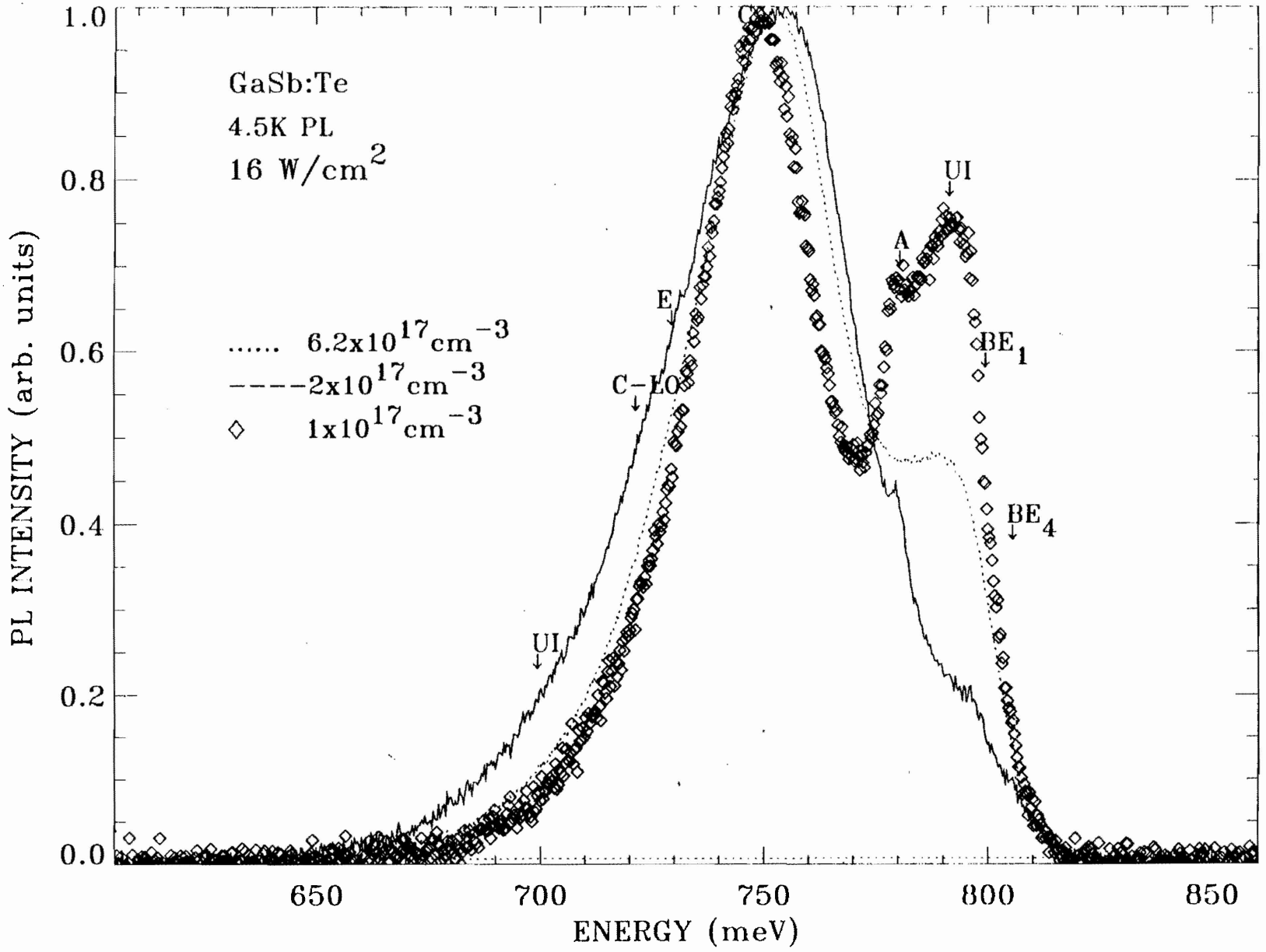

Fig. 3.2. Variation of 4K PL spectra with Te concentration for LPEE GaSb layers grown at 530°C.

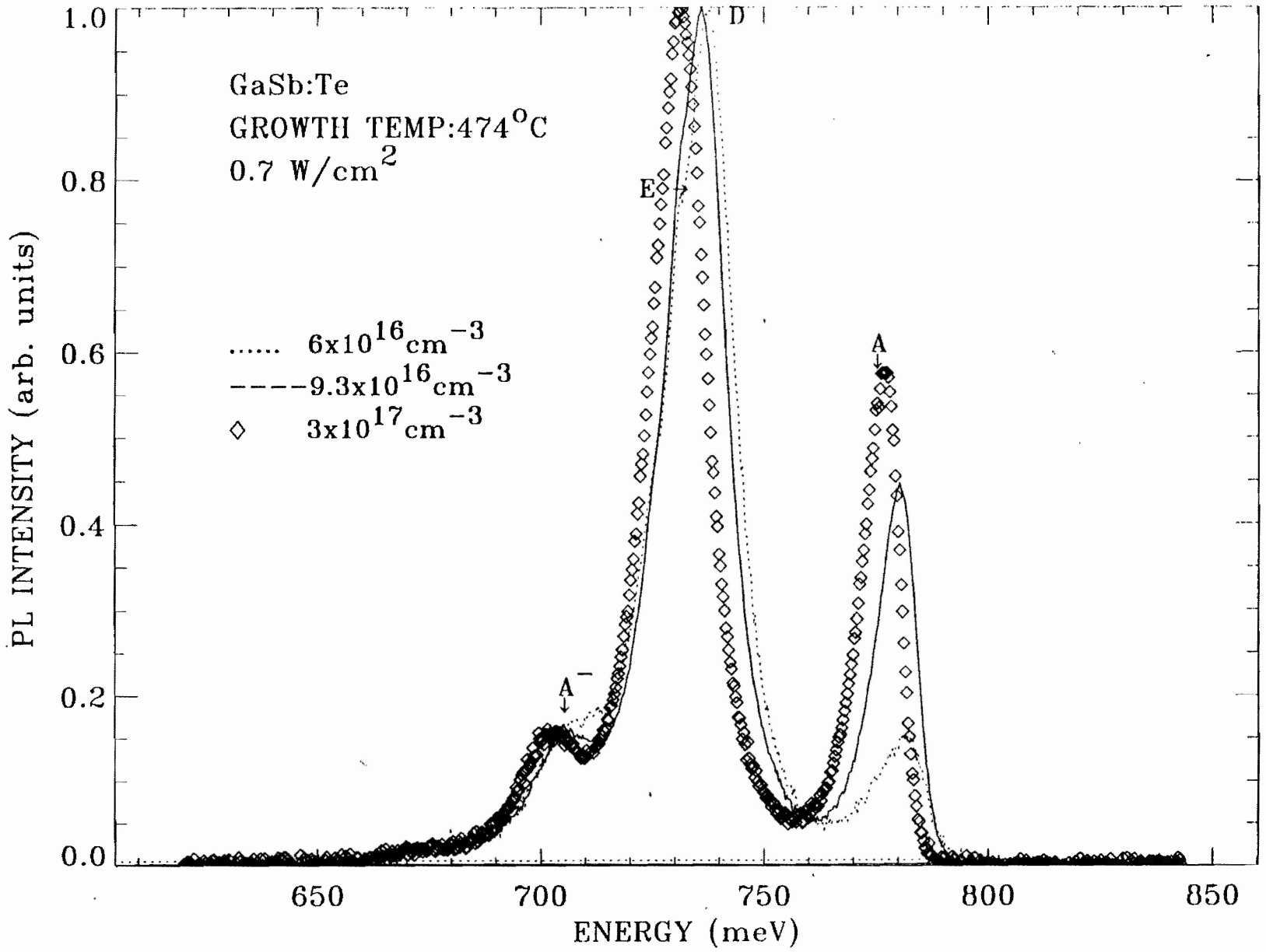

Fig. 3.3. Variation of 4K PL spectra with Te concentration of LPEE GaSb layers grown at 474°C.

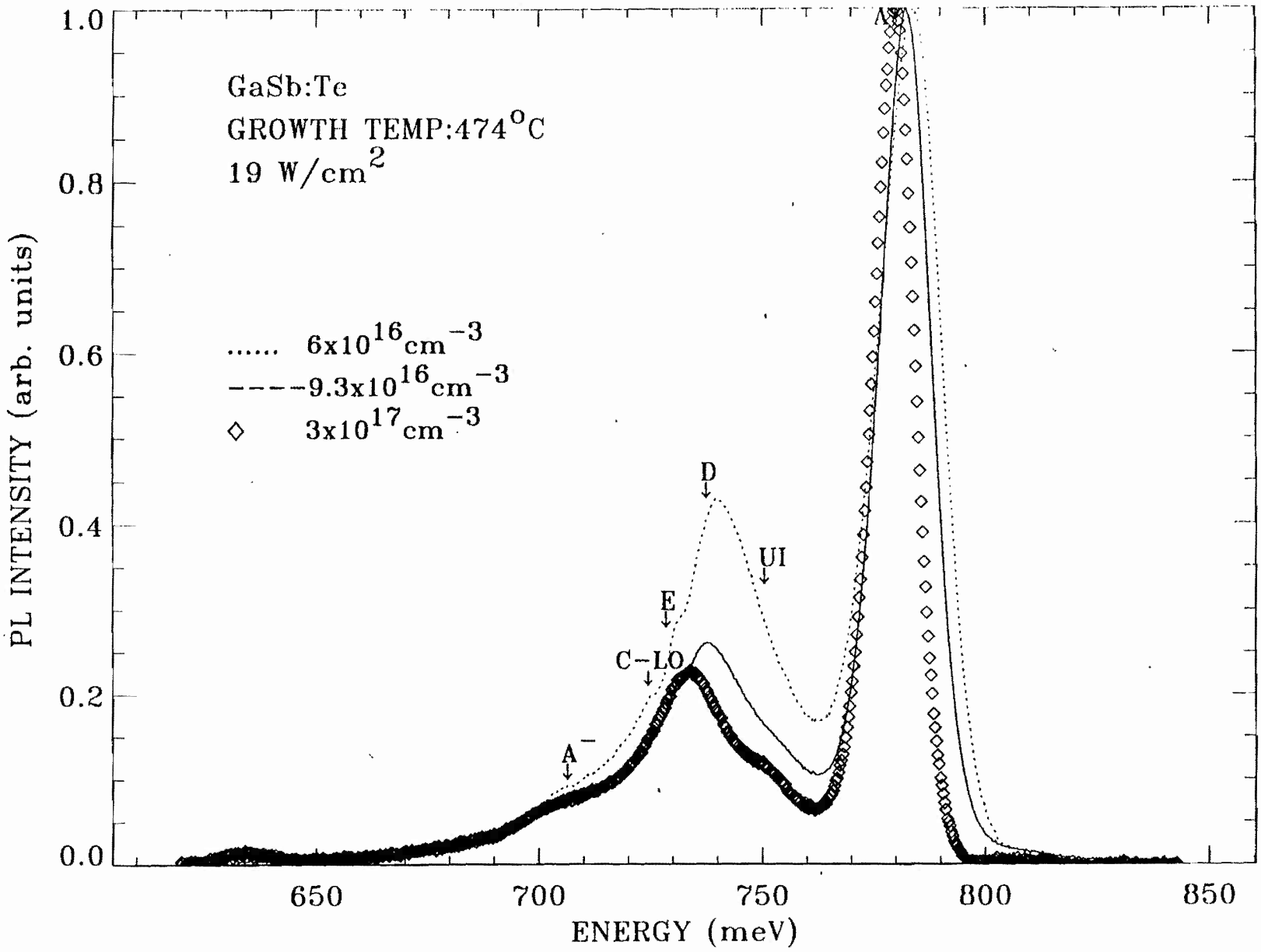

Fig. 3.4. Low temperature PL spectra of LPEE GaSb layers at 474°C for different Te concentrations.

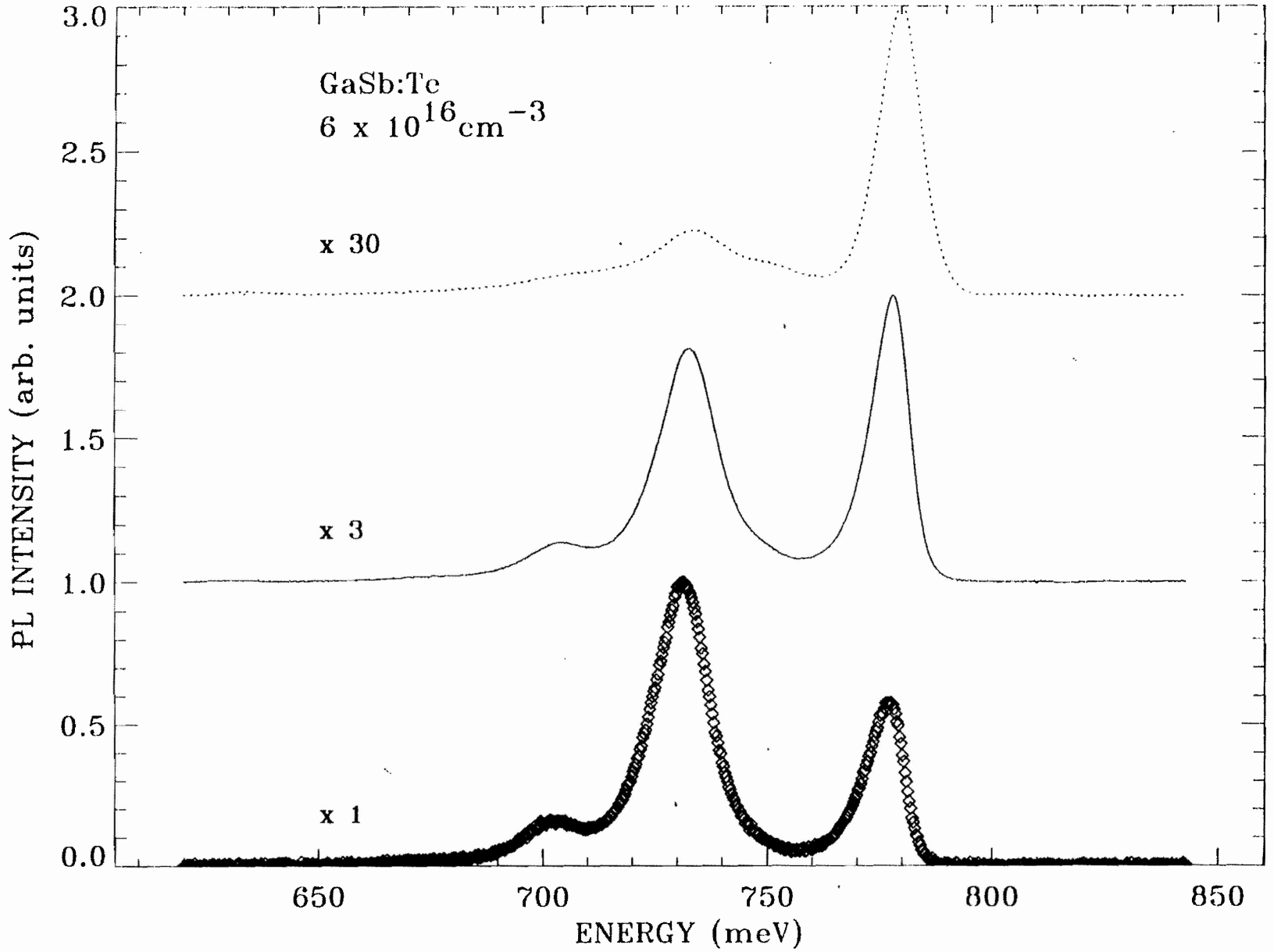

Fig. 3.5. Intensity dependence of the PL spectra of the Te-doped LPEE grown binary layers.

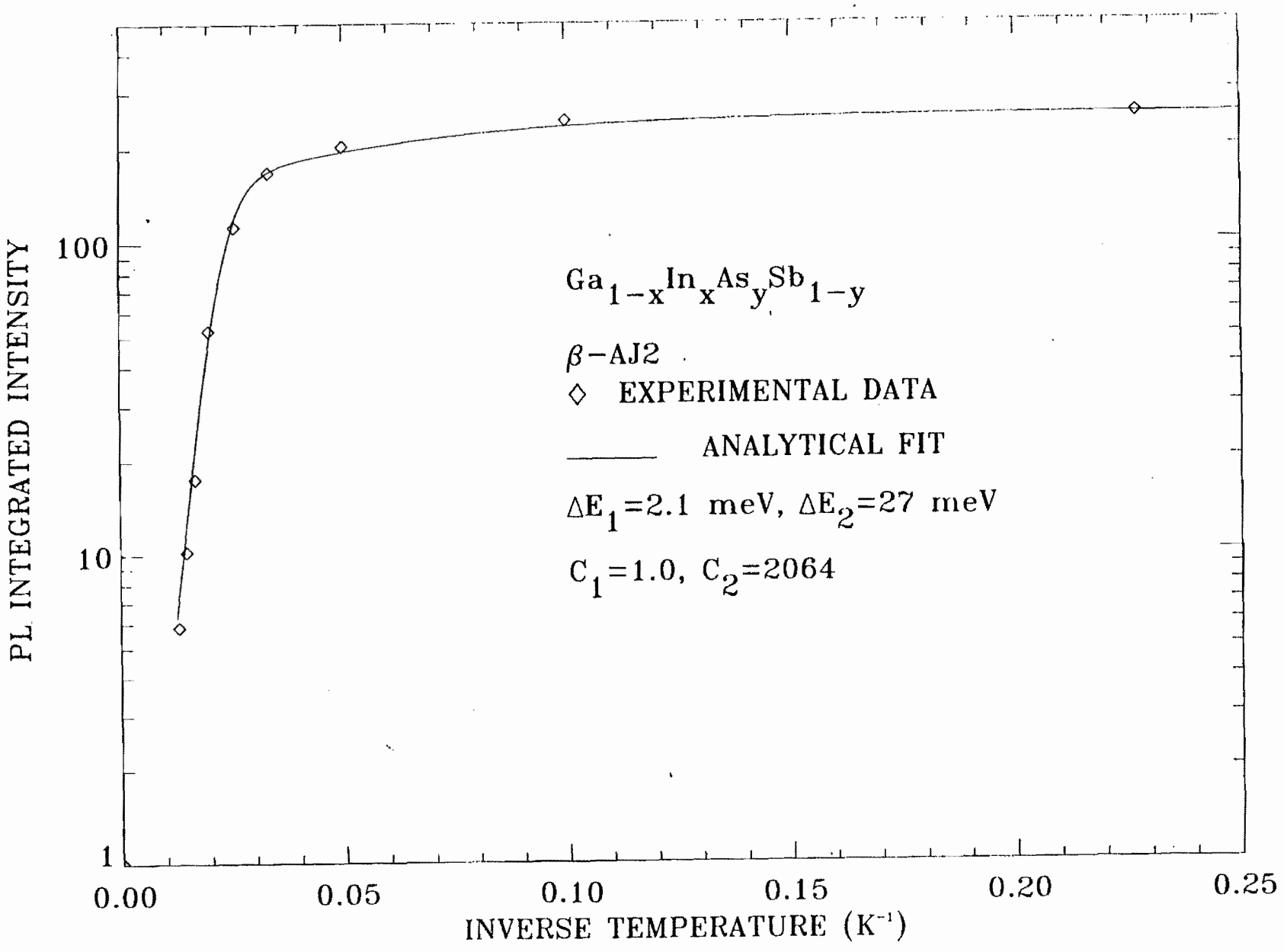

Fig. 3.6. Theoretical fit to the temperature dependence of integrated intensity of bound exciton transition (681 meV) at low temperatures. The values of C_1 and C_2 were in excellent agreement with that of undoped GaSb layers though the binding energies were higher.

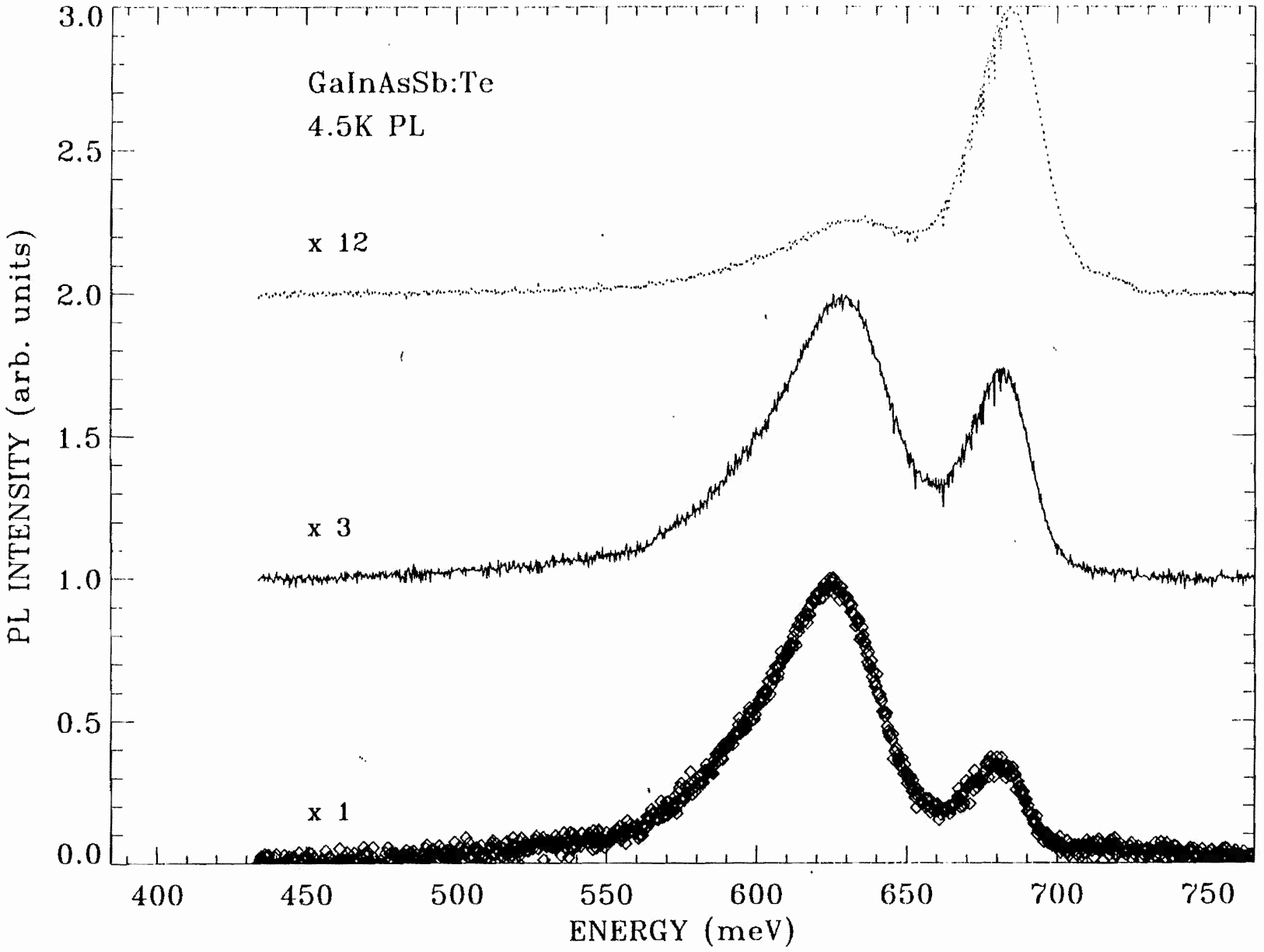

Fig. 3.7. Intensity dependence of the PL spectra of the doped quaternary LPEE layers.

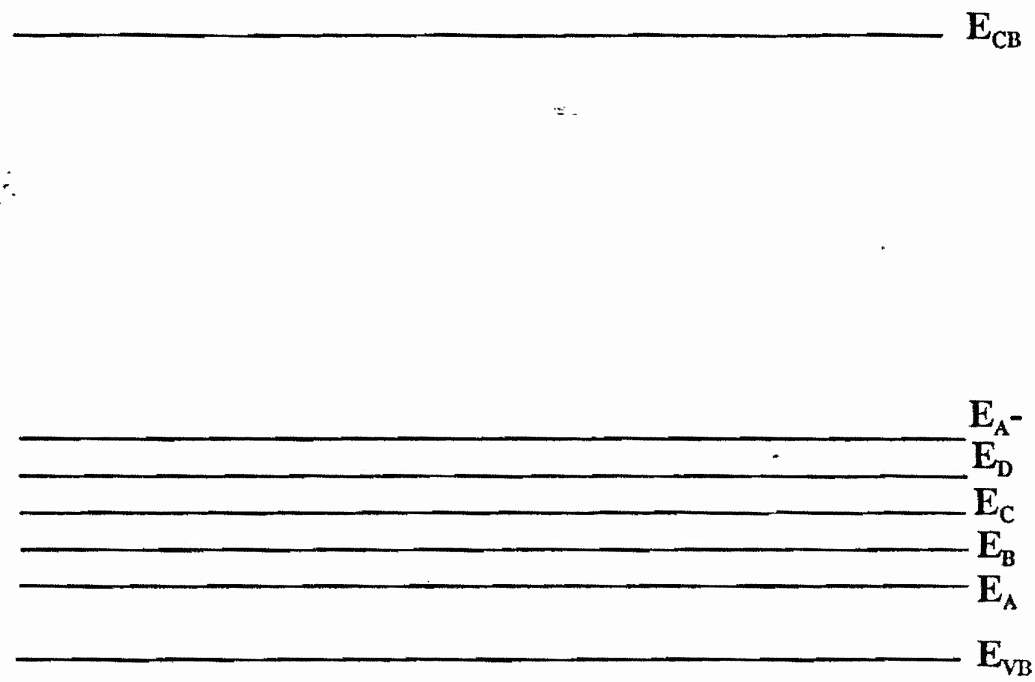

Fig. 3.8. Energy band diagram of Te-doped GaSb at 4.5 K, where E_{cB}=conduction band, E_{vB}=valence band, E_A=neutral residual acceptor, E_B=another neutral residual acceptor, E_C=Te related deep acceptor, E_D=another Te related deep acceptor, E_A^-=singly ionized level of residual acceptor A.

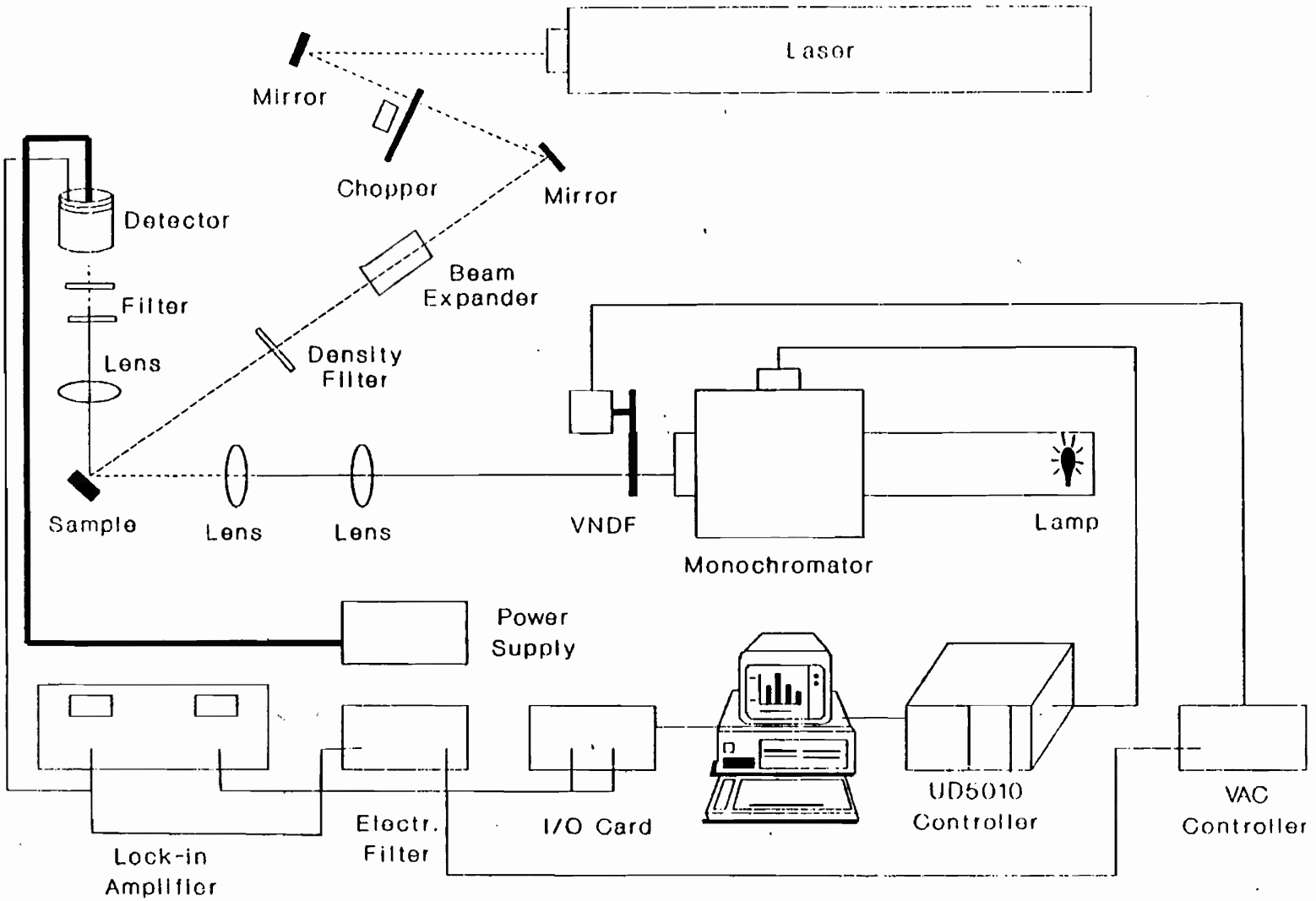

Fig. 3.9. Schematic representation of a photoreflectance experimental set-up.

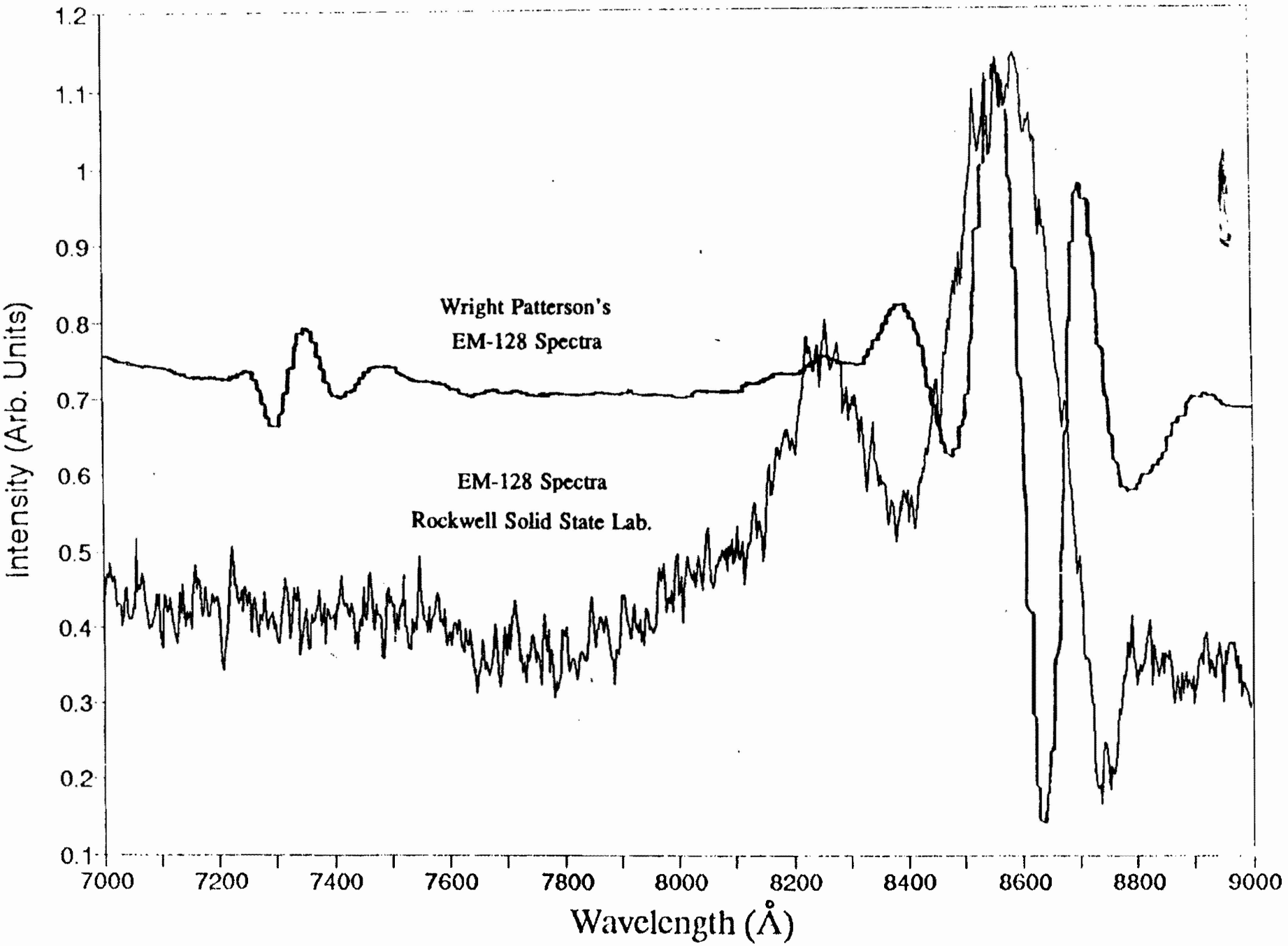

Fig. 3.10. Comparison of PR spectra of a GaAs/AlGaAs HEMT structure acquired at Wright Patterson and RSSEL (our laboratory).

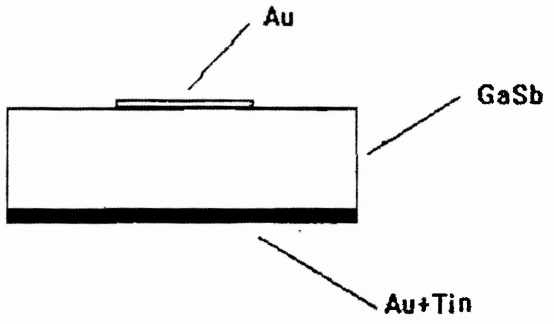

Fig. 4.1(a). The structure of the Au-GaSb Schottky diode.

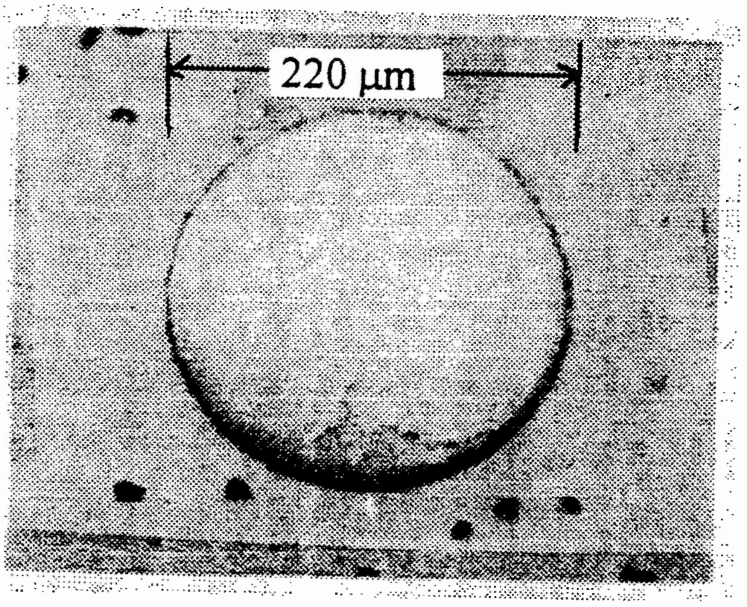

Fig. 4.1(b). The top view of the Au-GaSb Schottky diode.

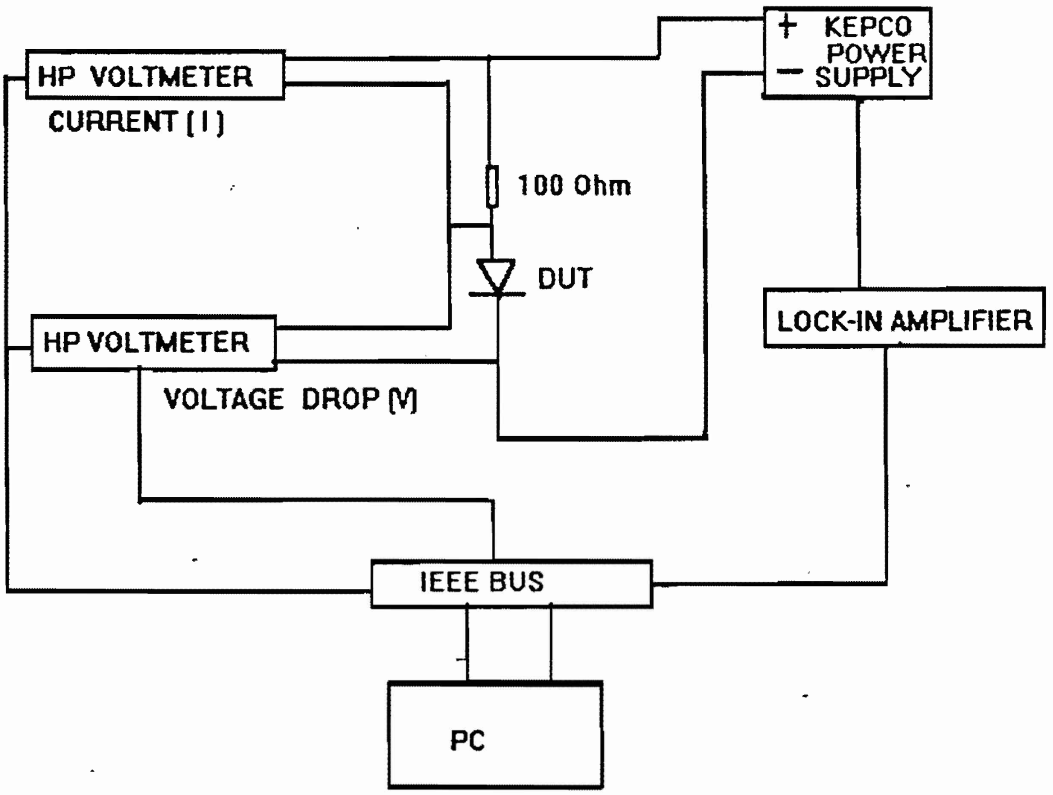

Fig. 4.2 Diagram of I-V data acquisition system.

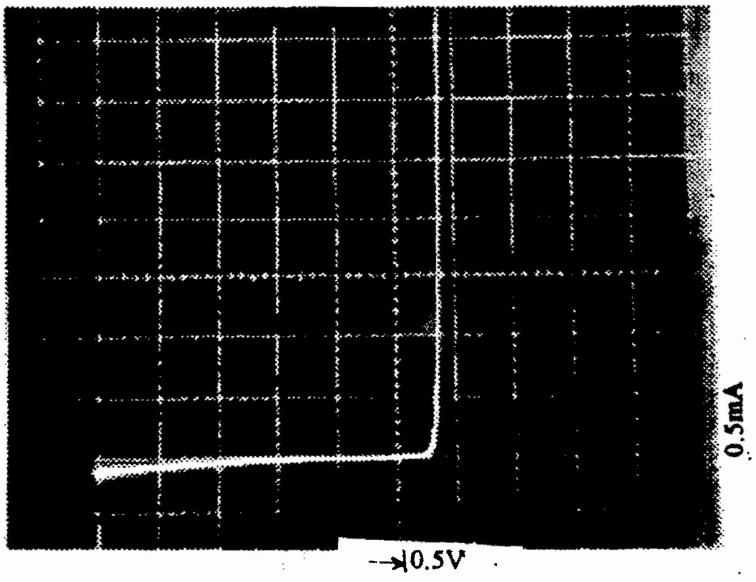

Fig. 4.3(a) Schottky diode on layers grown at 474°C.

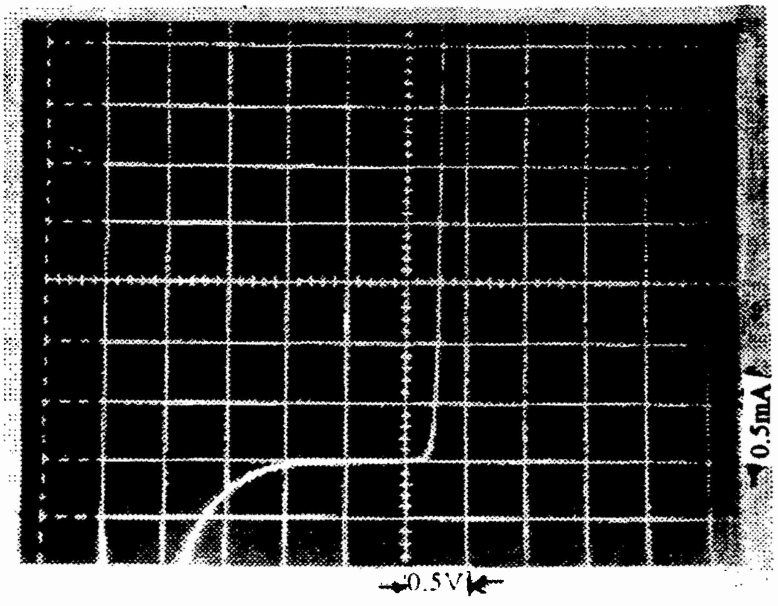

Fig. 4.3(b) Schottky diode on layers grown at 530°C.

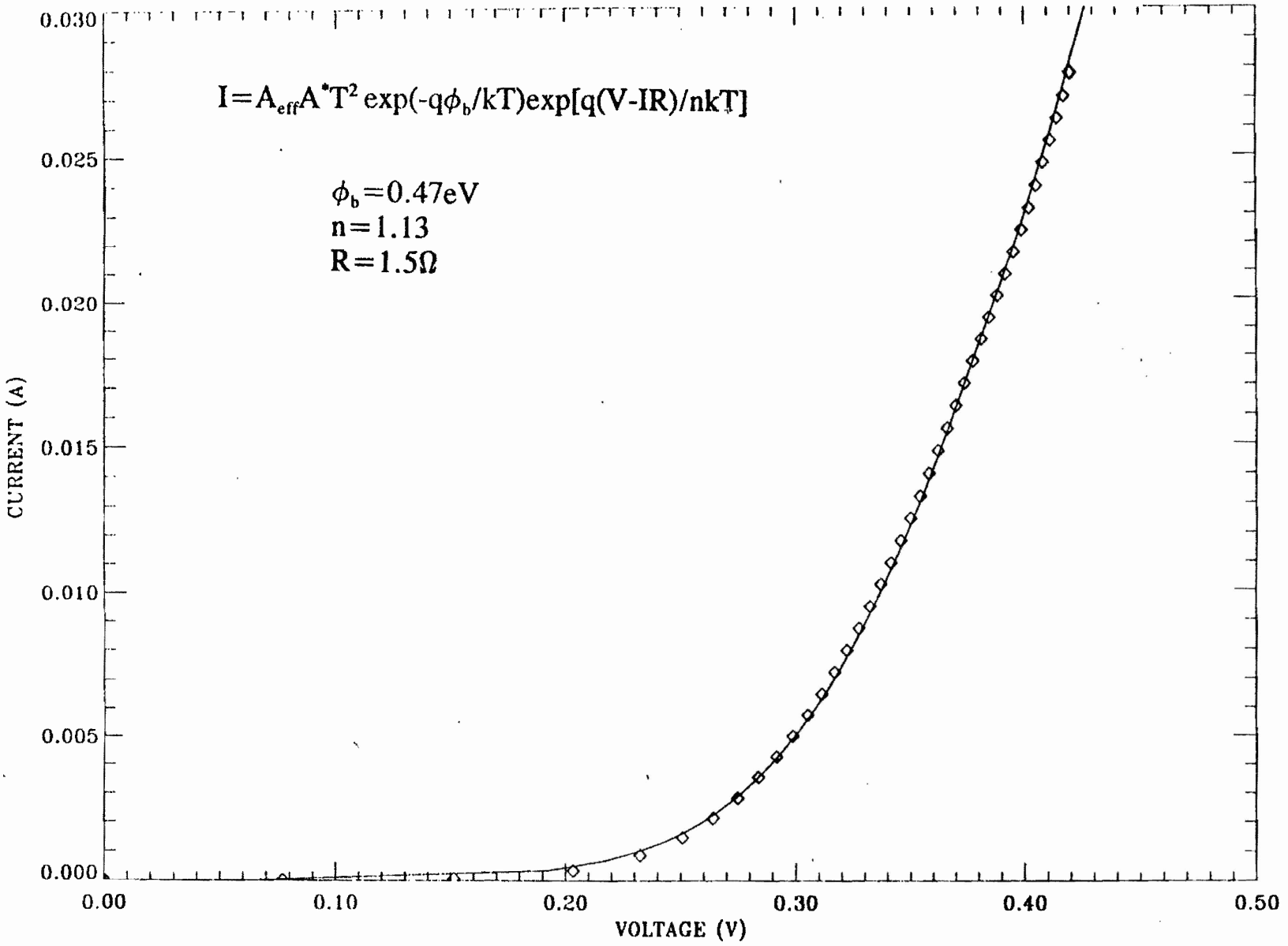

Fig. 4.4 Computer fitting of I-V characteristics of Au/n-GaSb Schottky diode.

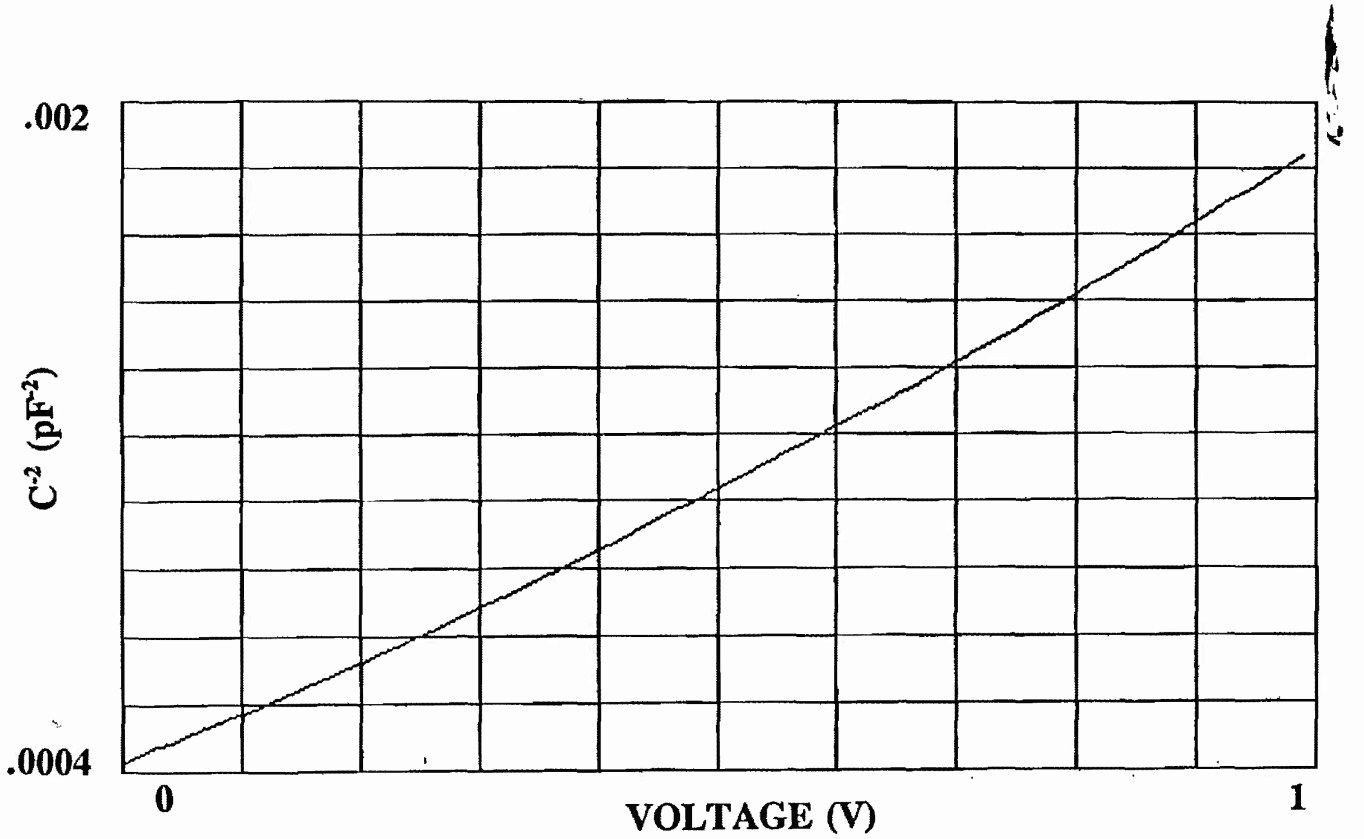

Fig. 4.5 C^{-2}-V plot for Au/n-GaSb Schottky diode.

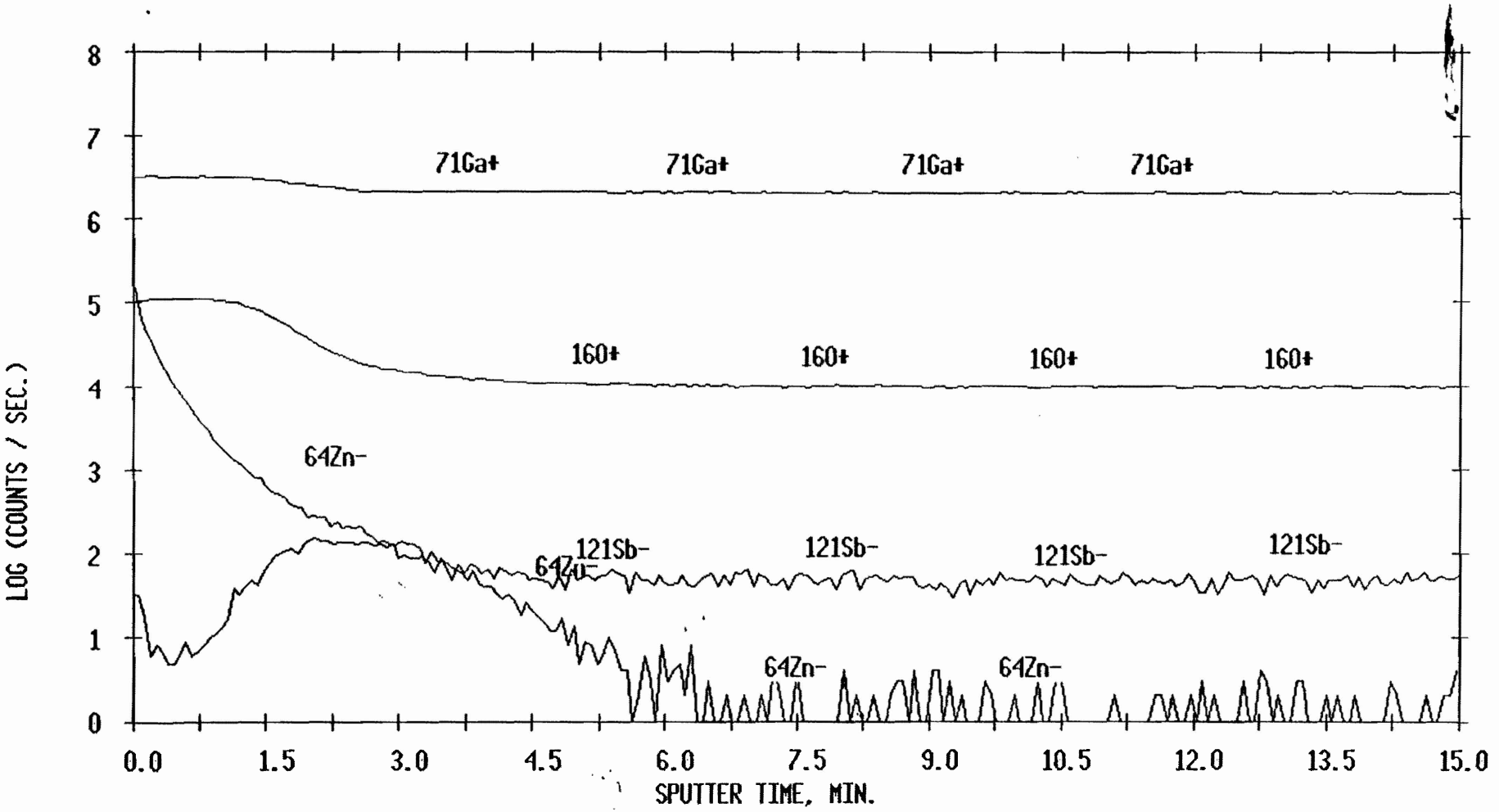

Fig. 5.1 SIMS measurements on the Zn diffused n-GaSb.

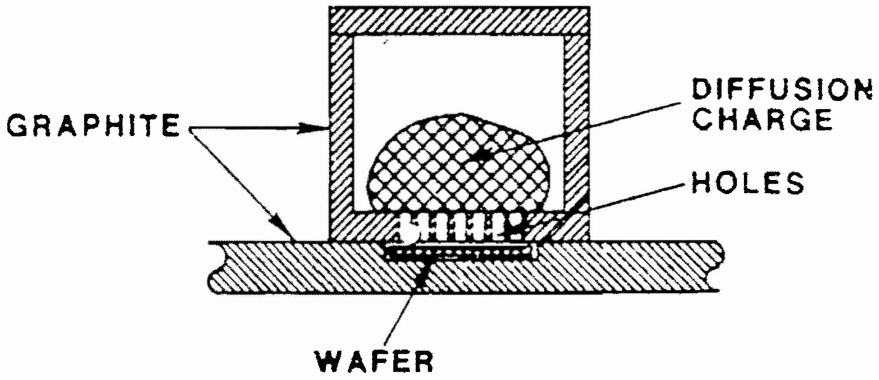

Fig. 5.2(a) Schematic cross-sectional illustration of the graphite boat used for diffusion.

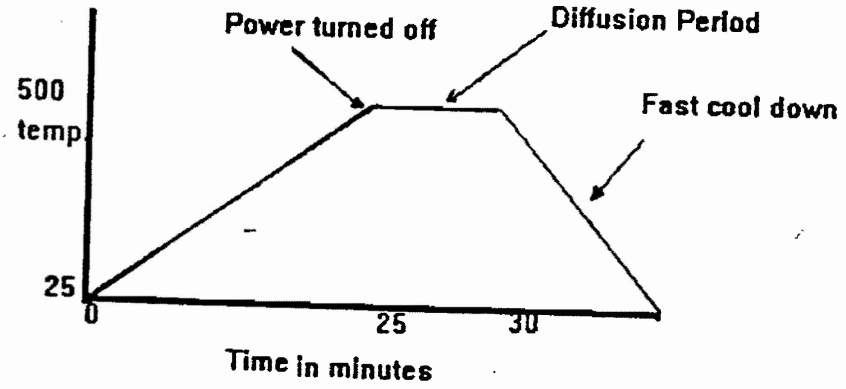

Fig. 5.2(b) Furnace temperature profile used for diffusion.

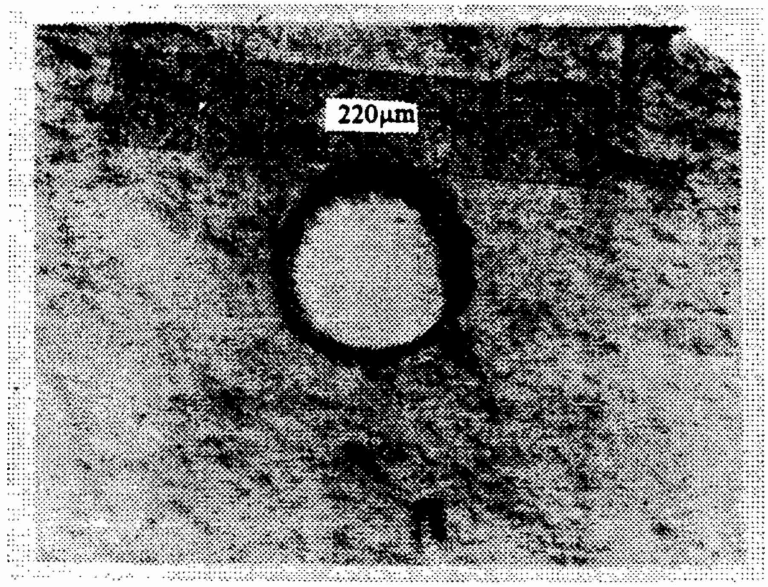

Fig. 5.3 Top view of the sample after mesa etching.

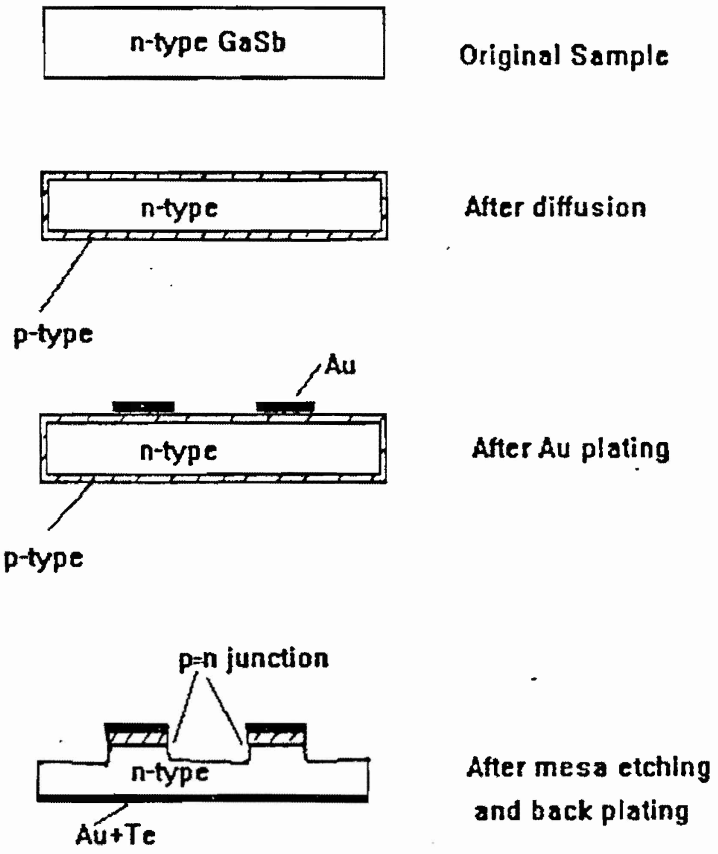

Fig. 5.4 Mesa p-n junction fabrication process.

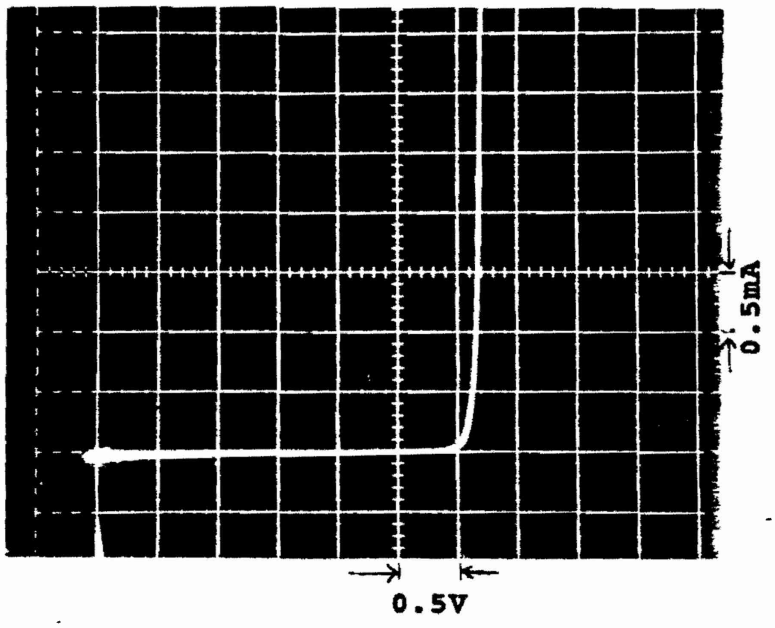

Fig. 5.5 I-V characteristics of a GaSb pn junction diode.

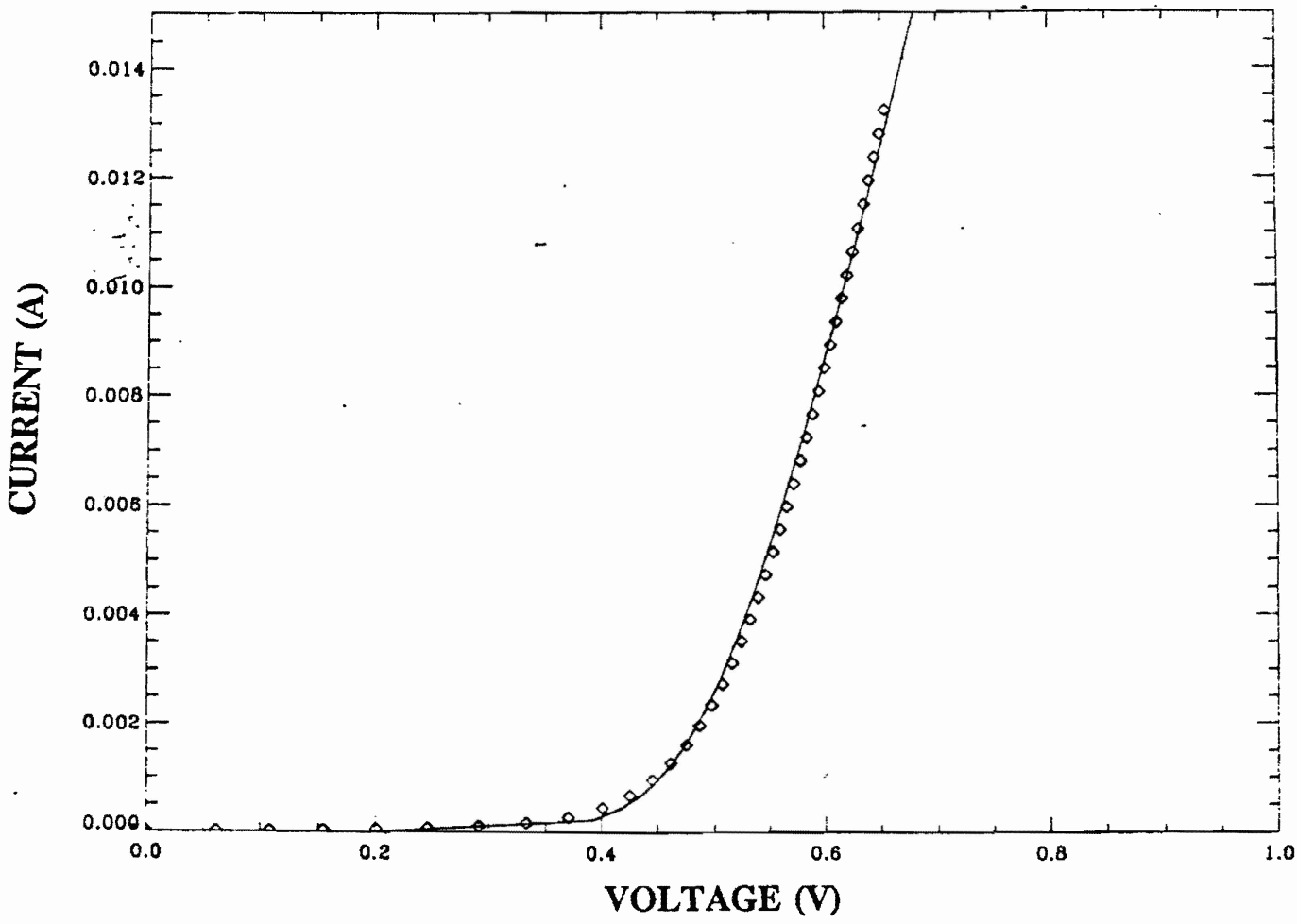

Fig. 5.6 IDL fitting of a typical I-V characteristics of a pn junction on LPEE grown Te-doped GaSb

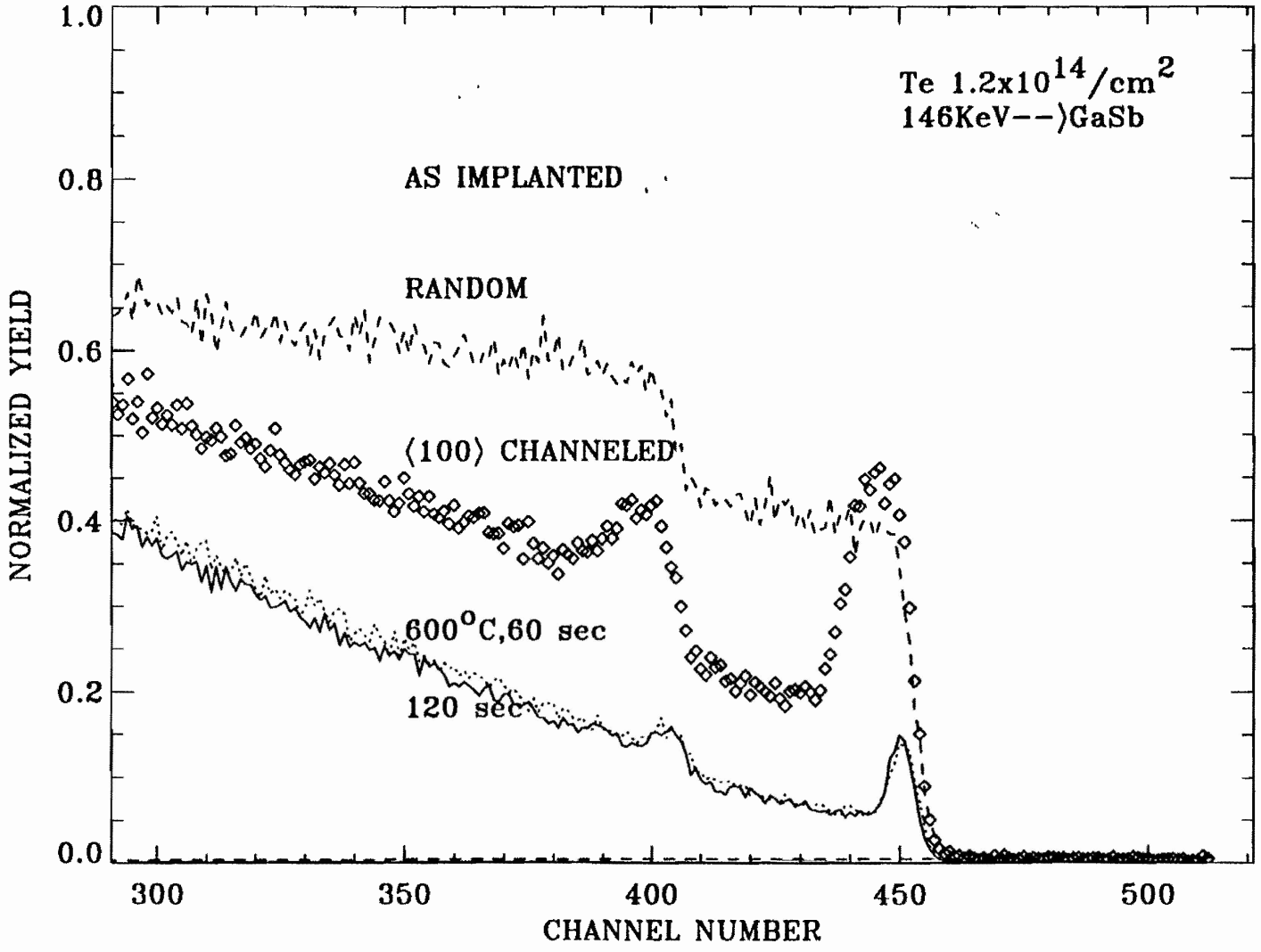

Fig. 6.1. RBS spectra of GaSb sample implanted with 1.2x10^{14}/cm^2 Te at 146 KeV. The yields for the As-implanted GaSb and of the sample rapid themal annealed at 600°C for 60 and 120 sec.

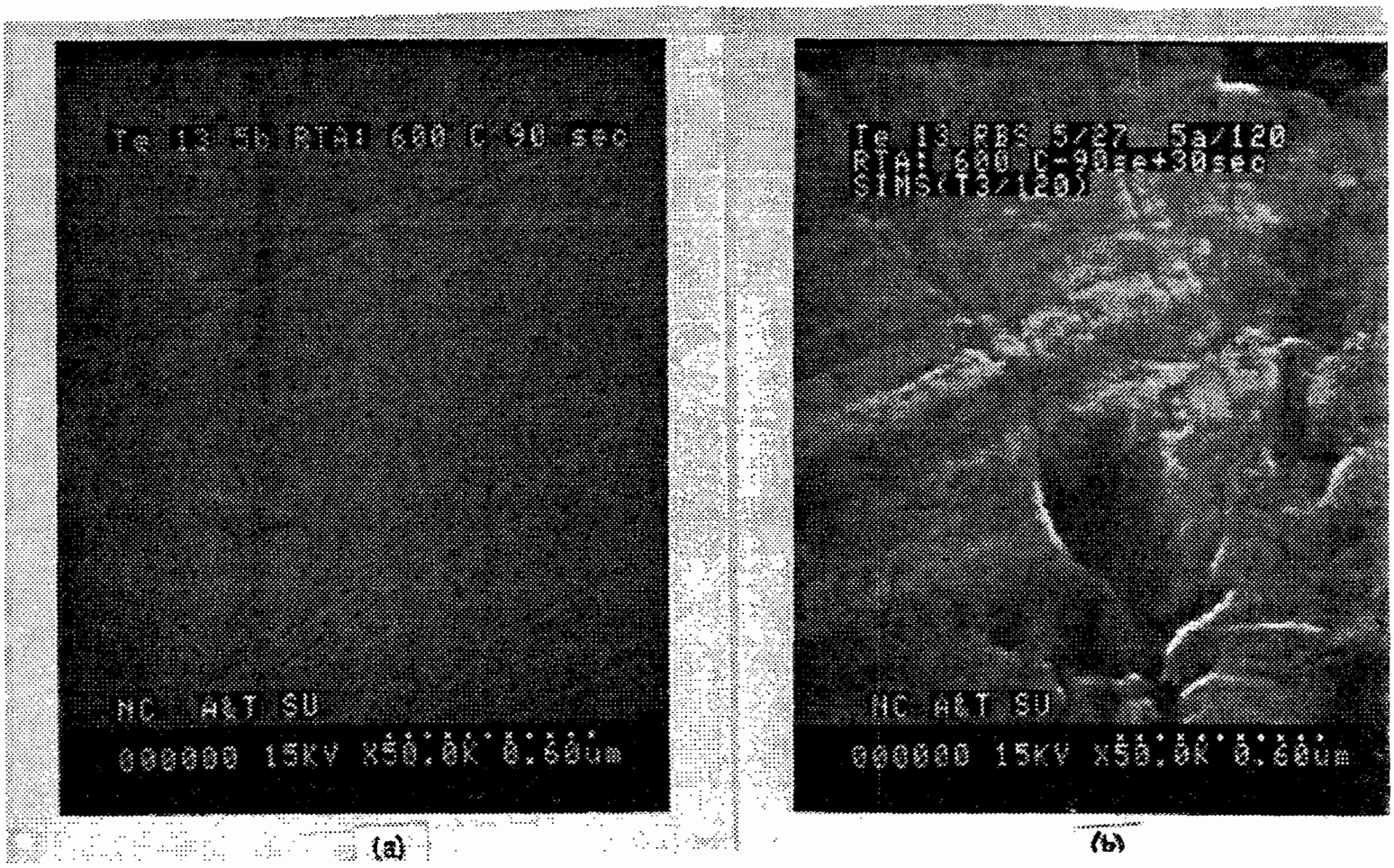

Fig. 6.2. SEM micrographs of Te implanted sample (1.2×10^{13} ions/cm^2) annealed for (a) 90 and (b) 120 secs.

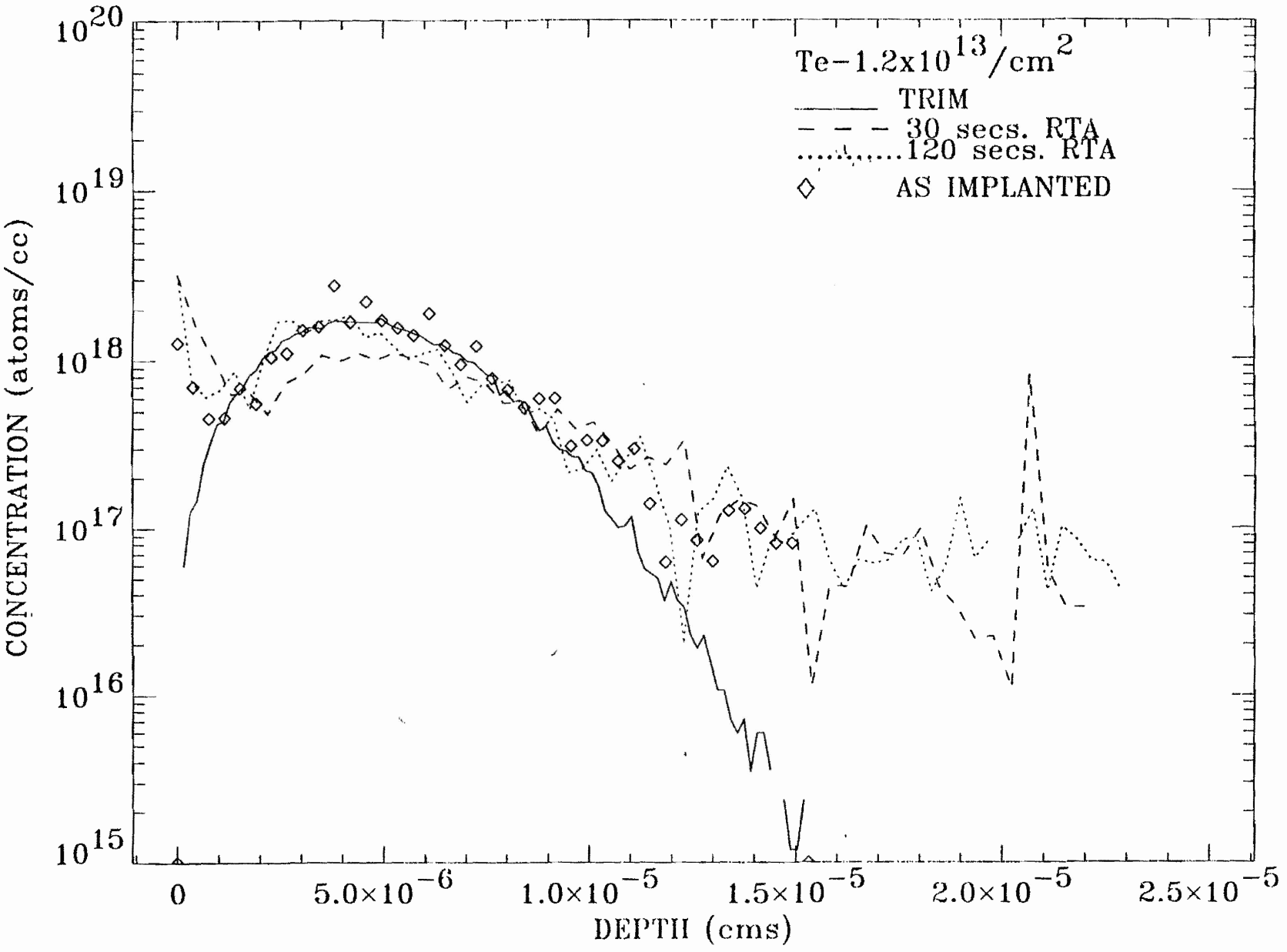

Fig. 6.3. Comparison of experimental SIMS depth profiles with the TRIM data of as implanted and annealed GaSb samples with dosages of $10^{13}/cm^2$.

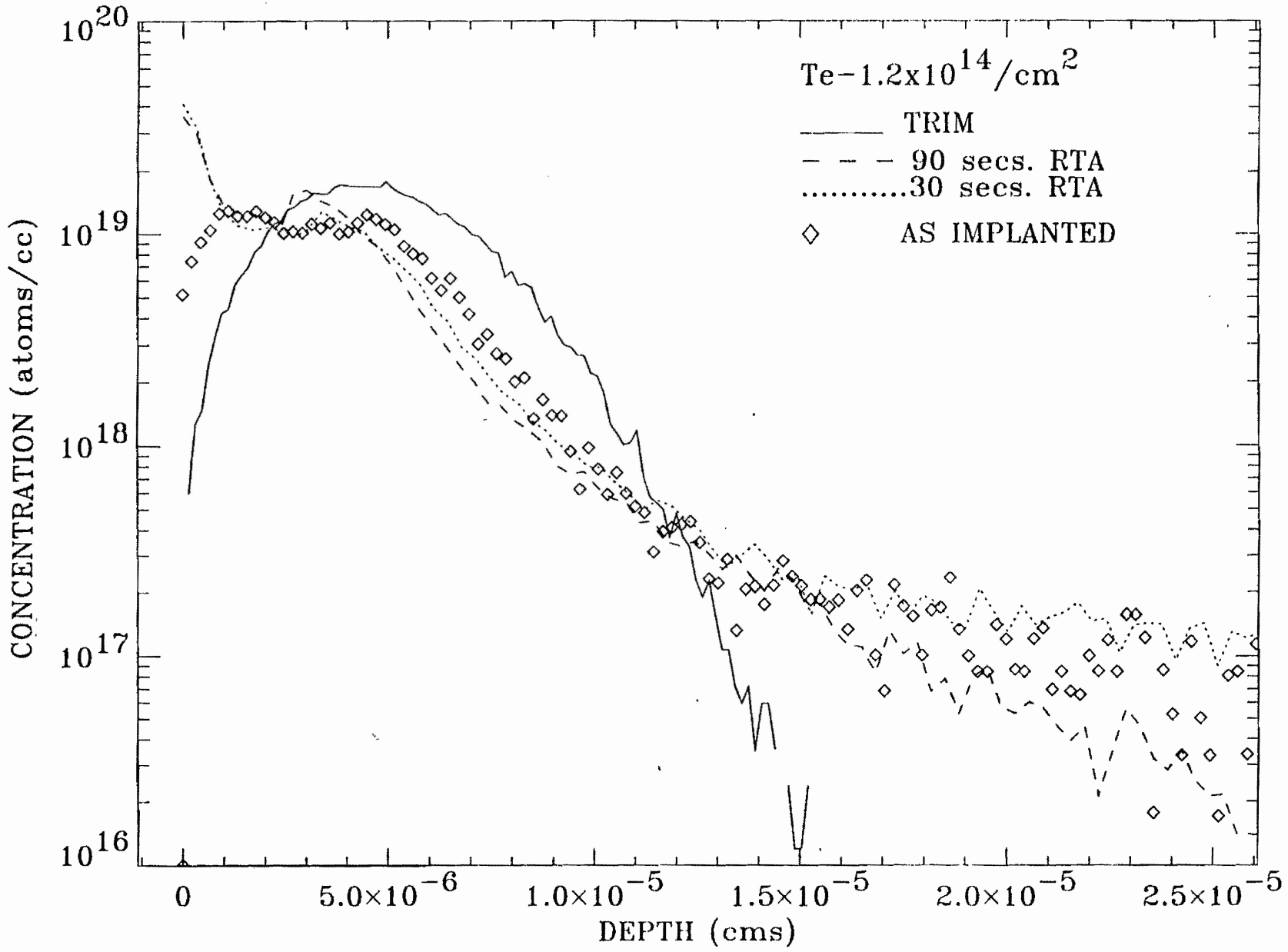

Fig. 6.4. Te distribution in a (100) GaSb for as implanted and annealed samples of ion dosage $10^{14}/cm^2$. The experimental data is compared with the TRIM data.

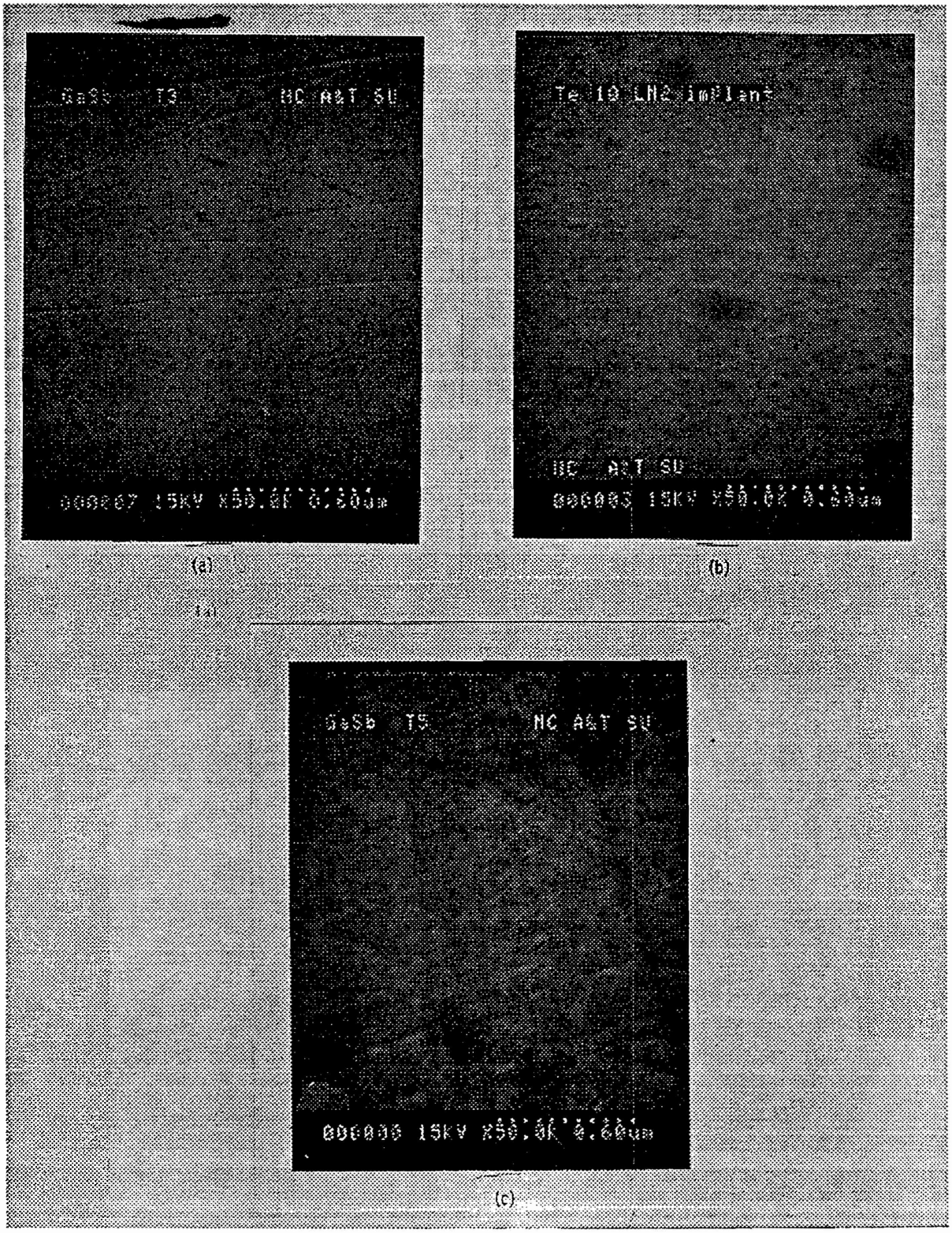

Fig. 6.5. The surface morphology of Te implanted samples for ion dosages of a) $1.2x10^{13}/cm^2$, b)$1.2x10^{14}/cm^2$ and c)$1.2x10^{15}/cm^2$.

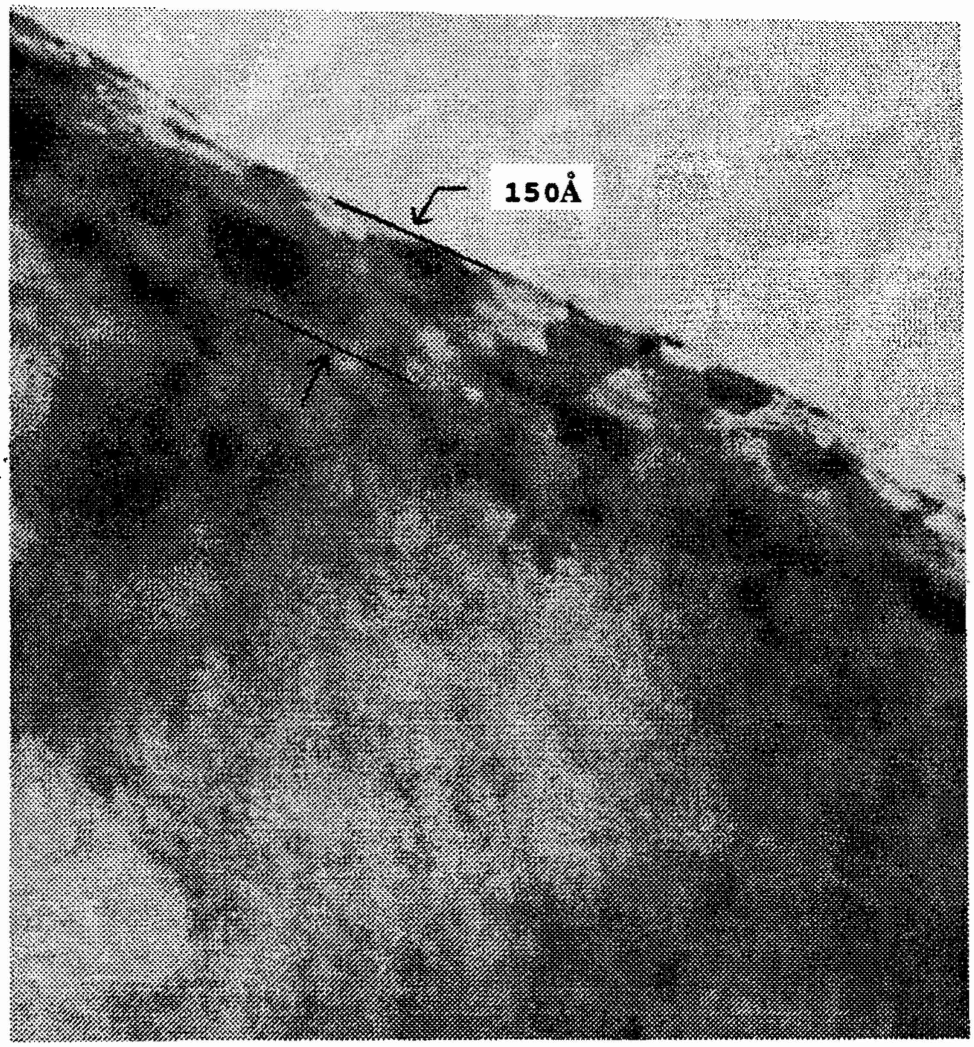

Fig. 6.6 Cross-sectional micrograph of Te implanted sample ($1.2x10^{13}$ions/cms^2) annealed for 30secs.

IX BIBLIOGRAPHY

1. T.H. Chiu, J.L. Zyskind and W.T. Tsang, *J. Electron. Mat.* **16**, 57(1987).
2. W.T. Tsang, T.H. Chiu, D.W. Kisker and J.A. Ditzenberger, *Appl. Phys. Lett.* **46**, 283 (1985).
3. M.J. Cherng, H.R. Jen, C.A. Larsen, G.B. Stringfellow, H. Lundt and P.C. Taylor, *J. Cryst. Growth* **77**, 408 (1986).
4. M.J. Cherng, G.B. Stringfellow, D.W. Kisker, A.K. Srivastava and J. L. Zyskind, *Appl. Phys. Lett.* **48**,419 (1986).
5. J.C. DeWinter, M.A. Pollack, A.K. Srivastava and J.L. Zyskind, *J. Electron.Mat.***14**, 729 (1985).
6. A. Joullie, F. Jia Hua, F. Karouta and H. Mani, *J. Cryst. Growth* **75**, 309 (1986).
7. M. Astles, H.Hill, A.J. Williams, P.J. Wright and M.L. Young, *J. Electron. Mat.* **15**, 41 (1986).
8. R.Sankaran and G.A.Antypas, *J. Cryst. Growth* **36**,198 (1976).
9. E. R.Gertner, A.M. Andrews, L.O. Bubulac, D.T. Cheung, M. J. Ludowise and R. A. Riedel, *J. Electron. Mat.* **8,** 545 (1979).
10. N. Kobayashi and Y. Horikoshi, *Jpn. J. Appl. Phys.* **20,** 2253 (1981).
11. Shanthi N. Iyer, Ali Abul-Fadl, Albert T. Macrander, Jonathan H. Lewis, Ward J. Collis and James W. Sulhoff, *Mat. Res. Symp. Proc.* **160**, 445 (1990).
12. Shanthi N. Iyer, S. Hegde, A. Abul-Fadl, K.K. Bajaj and W. Mitchel, *Phys. Rev. B* **47**, 1329 (1993)
13. S. Iyer, S. Hegde, K. K. Bajaj, A. Abul-Fadl, and W. Mitchel, *J.Appl.Phys.* **73**, 3948 (1993)
14. G.B. Stringfellow, *J. Cryst. Growth* **58,** 194 (1982).
15. A. Okamoto, J. Lagowski and H.C. Gatos, *J. Appl. Phys.* **53**, 1706 (1982).
16. Y. Imamura, L. Jastrzebski and H.C. Gatos, *J. Electrochem. Soc.* **125**, 1560 (1978).
17. J.J. Daniele and A. Lewis, *J. Electron. Mater.* **12**, 1015 (1983).
18. J. J. Daniele and A. J. Hebling, *J. Appl. Phys.* **52**, 4325 (1981).
19. W. Ruhle and D. Bimberg, *Phys. Rev. B* **12**, 2382 (1975).
20. W. Ruhle, W. Jakowetz,C. Wolk, R. Linnebach and M. Pilkuhn, *Phys. Stat. Sol.(B)* **73**, 255 (1976).
21. C. Benoit a la Guillaume and P. Lavallard, *Phys. Rev. B* **5**, 4900 (1972).
22. M.H. van Maaren, *J. Phys. Chem. Solids* **27**, 472 (1966).
23. Y.J. Van Der Meulen, *J. Phys. Chem. Solids* **28,** 25 (1967).
24. C.Anayama, T.Tanahashi, H. Kuwatsuka, S. Nishiyama, S. Isozumi and K.Nakajima, *Appl.Phys.Lett.* **56**, 239 (1990).
25. S.J.Eglash and H.K. Choi, Gallium Arsenide and Related Compounds,1991; *Inst. Phys. Conf. Ser. No.* **120** ed. G.B Stringfellow (America Inst. of Physics, 1992) p.4
26. Y.P.Varshi, *Physica* **34**,149(1967)
27. J.Camassel and D.Auvergene, *Phys. Rev.* B **12,** 3258 (1975).
28. A. I. Lebedev and I. A. Stel'nikova, *Sov. Phys. Semicond.* **13**, 229 (1979).
29. A. S. Kyuregyan, I. K. Lazareva, V. M. Stuhebnikov, and A. E.Yunovich, *Sov. Phys. Semicond. 6, 208 (1972).*

30. A. A. Kastal'skii, S. B. Mal'tsev, and Y. G. Shreter, *Sov. Phys. Semicond.* **5**, 1391 (1972).
31. Y. E. Pokrovskii, K. I. Svistunova, and A.S. Kaminskii, *Sov. Phys. Semicond.* **1**, 26 (1967).
32. I. K. Lazareva and V. M. Stuchebnikov, *Sov. Phys. Semicond.* **4**, 550 (1970).
33. A.I.Lebedev and I.A. Strel'nilova, and A.E.Yunovich, *Sov. Phys. Semicond.*, **10**,773 (1976).
34. A.I.Lebedev, I.A. Strel'nikova and A.E.Yunovich, *Sov. Phys. Semicond.* **11**,1246, (1977).
35. A.N. Imenkov, T.P. Lideikis,B.V.Tsarenkov, Yu.M. Shernyakov,. and Yu. P. Yakovlev, *Sov.Phys-Semicond.***10**, 748(1976)
36. M. C. Wu, and C. C. Chen, *J. Appl. Phys.* **72**, 4275 (1992).
37. N. Kitamura, H. Uekita, M. Ichimura, A. Usami and T. Wada, Mat.
38. S. C. Chen and Y. K. Su, *J. Appl. Phys.* **66**, 350 (1989).
39. M. C. Wu, and C. C. Chen, *J. Appl. Phys.* **73**,8495 (1993).
40. M. C. Wu, and C. C. Chen, *J. Appl. Phys.* **71**, 6116 (1992).
41. M. Lee, D.J. Nicholas, K.E. Singer and B. Hamilton, *J. Appl. Phys.* **59**, 2895 (1986).
42. D.J. Nicholas, M. Lee, B. Hamilton, and K.E. Singer, *J. of Cryst. Growth, B*, 298 (1987).
43. W. Jakowetz, W. Ruhle, K. Breuninger, and M. Pilkuhn, *Phys. Stat. Sol.* **12**, 169, (1972).
44. R.D. Baxter, R.T. Bate, and F.J. Reid, *J. phys. Chem. Solids* **26**, 41 (1965).
45. D. Bimberg, M. Sondergeld and E. Grobe, *Phys. Rev.B* **4**, 3451 (1971).
46. Y.H.Wang, M. P. Houng, and P. W. Sze, *J. Appl. Phys.* **71(6)**, 2760 (1992)
47. A.Y. Polyakov, M. Stam, A.G. Milnes, and T. E. Schlesinger, *Mater. Sci. Engg,* **B12**, 337 (1992)
48. S.A. Waters and R.H. Williams, *Mater. Sci. Engg.* **B9**, 51 (1991)
49. Prakash A. Murawala, *J. Appl. Phys.* **12**, L2434 (1990)
50. A.B. McLean, and R.H. Williams, *J. Phys. C.* **21**, 783 (1988)
51. Newman, T. Kendelewicz, L. Bowman, and W.E. Spicer, *Appl. Phys. Lett.* **46**, 1176 (1985).
52. I. Poole, M.E. Lee, M. Missous, And K.E. Singer, *J. Appl. Phys.* **62**, 3988 (1987).
53. J. Tersoff, Heterojunction Band Discontinuities, 3-59 (1987).
54. A. Y. Polyakov, A.G. Milnes, N.B. Smirnov, L.V. Druzhinina, and I.V. Tunitskaya, *Solid State Electron.*, **36**, 1371 (1993)
55. W.E. Spicer, P.W. Chye, P.R. Skeath, C.Y. Su and I. Lindau, *J. Vac. Sci. Technol.*, **16**, 1422 (1979)
56. W.E. Spicer, Z. Liliental-Webee, E. Weber, N. Newman, T. Kendeliewicz, R. Cao, C. McCants, and I. Lindau, *J. Vac. Sci. Technol.*, **B6**, 1257 (1988)
57. A.G.Milnes and A.Y.Polyakov, *Solid-State Electron.*, **36**, 803 (1993)
58. K.Sato, *J. Appl. Phys.*, **58**, 3655 (1985)
59. S.K. Cheung and N.W. Cheung, *Appl. Phys. Lett.*, **49**, 85 (1986)
60. S.Basu and U.N. Roy, *Mater. Sci. Engg,* **B8**, 1 (1991)

61. S.M.Sze, Physics of Semiconductor Devices (John Wiley & Son, New York, 1981)
62. W.G. Spitzer and C.A. Mead, *Phys. Rev.* **134**, 713 (1964)
63. B.L. Sharma, Metal Semiconductor Schottky Barrier Junctions and Their Applications (Plenum, New York, 1984), P199
64. Hamiya Keyoto, *Materials Letters,* **10**, 417 (1991)
65. S.B. Phatak, *IEEE Electron. Device Lett.*, **EDL-3**, No.5 (1982)
66. J.C. Marinace, *J. Electrochem. Soc*, Nov. 1153 (1963)
67. C. Heinz, *Electron Lett.*, **22**, 276 (1986)
68. Harry Chou and Wayne V. Sorin, *Hewlett-Packard Journal*, **50**, (1993)
69. S.K. Ghandhi and R.J. Field, *Appl. Phys. Lett.*, **38**(4), 267 (1981)
70. A. Borghesi, G. Guizzetti, M. Patrini, A. Caligiore, R.C. Chen, and S. Pellegrino, *J. Appl. Phys.*, **74**, 2445 (1993)
71. P.N. Favenne, *Electron. Lett.*, **10,** 832(1980)
72. J.R. Shealy, *Electron. Device Lett.*, **EDL-1**, 119 (1980)
73. M.C. Boissy and D.Dignet, *J. Electronchem. Soci.*, **125**, No.9, 1505 (1978)
74. S.Aytac and A. Schlachetzki, *Solid-State Electron.*, **24,** 57 (1981)
75. F.Capasso, M.B.Panish, S. Sumski, and P.W. Foy , *Appl. Phys. Lett.* **36**, 165 (1980)
76. E.H. Rhoderick, Metal-semiconductor Contact (Clarendon, Oxford, 1978) p. 136.
77. Kou-Wei Wwang, William G. Spitzer, Graham K. Hubler, and Devendra K. Sadana, *J. Appl. Phys.* **58**, 4553 (1985).
78. Roger Kelly, *Nucl. Instrum. Methods* **182/183**, 351 (1981).
79. J.S. Poate and J.M. Williams, Ion Implantation and Beam Processing (Academic Press, New York, 1984).
80. K.S. Jones, S. Prussin, and E.R. Weber, *Appl. Phys. A* **45**, 1 (1988).
81. D.K. Sadana, *Nucl. Instrum. Methods in Phys. Res.* **B7/8**, 375 (1985).
82. D.K. Sadana, H. Choski, J. Washburn, P.F. Byrne, and N.W. Cheung, *Appl. Phys. Lett.* **44**, 301 (1984).
83. K.S. Jones, S. Prussin and E.R. Weber, *Appl. Phys. A*, **45**, 1 (1988)
84. S. Iyer, R. Prakkat, B. Patnaik, N. Parikh and S. Hegde, *Mat. Res. Soc. Symp. Proc.*, **316**, 185 (1994)
85. S. J. Pearton,A. R. Von Neida, J. M. Brown, K. T. Short, L. J. Oster and U. K. Chakrabarti, J. *Appl. Phys.* **64**, 629 (1988).
86. A. R. Von Neida, K. T. Short, J. M. Brown and S. J. Pearton, *Mat. Res. Soc. Symp. Proc.* **100,** 689 (1988).
87. Y. K. Su, K. J. Gan, J. S. Hwang and S. L. Tyan, *J. Appl. Phys.* **68**, 5584 (1990).
88. R. Callec, P. N. Favennec, M. Salvi, H.L'Haridon and M. Gauneau, *Appl. Phys. Lett.* **59**, 1872 (1991).

X. LIST OF PUBLICATIONS, TECHNICAL REPORTS AND THESIS

REFEREED PUBLICATIONS

1. Shanthi N. Iyer, S. Hegde, A. Abul-Fadl, K.K. Bajaj and W. Mitchel, "Growth and Photoluminescence Study of GaSb & $Ga_{1-x}In_xAs_ySb_{1-y}$ Grown on Gasb Substrates by Liquid-Phase Electroepitaxy",Phys. Rev.B, 47, 1329-39 (1993)

2. Shanthi N.Iyer,S.Hegde,K.K.Bajaj, A.Abul-Fadl, and W.Mitchel, "Photoluminescence Study of Liquid Phase Electroepitaxially Grown GaInAsSb On (100) GaSb" J. App. Phys., 73, 3948-3951 (1993)

3. Shanthi N.Iyer,S.Hegde,K.K.Bajaj, A.Abul-Fadl, and W.Mitchel, " Low Temperature PL Characterization of LPEE Grown GaSb and GaInAsSb Layers on GaSb" Mat. Res. Symp. Proc. 299,41-46 (1993)

4. S. Iyer, R. Parakkat, B. Patnaik, N. Parikh and S. Hegde, "Ion Implantation Damage and Annealing in GaSb", Mat. Res. Soc. Symp. Proc., 316, 185-190 (1994)

NON-REFEREED PUBLICATIONS AND PRESENTATIONS (by S.Iyer)

1. "Low Temperature PL Characterisitics of Te-Doped LPEE Grown GaSb and Devices", presented at APS Meeting, Pittsburgh, March 24, 1994.

2. "Ion Implantation and Damage and Annealing in GaSb", presented at MRS Fall Meeting, Boston, Dec. 1993.

3. "Growth and Characterization of GaSb and GaInAsSb by LPEE", presented at Science and Technology Alliance Materials Conference, NCA&T State University, October 27, 1993.

4. "Growth and Photoluminescence Study of GaSb and $Ga_xIn_xAs_ySb_{1-y}$ Grown on GaSb substrates by LPEE", presented at Mat. Res. Soc. Symp. Proc. Spring Meeting, San Francisco, April (1993).

5. "Photoluminescence Study of LPEE Grown GaInAsSb epilayers on GaSb", presented at American Physical Society Spring Meeting, Seattle, Washington, March (1993).

6. L. Small, S. Iyer, "Photoluminescence Spectral Analysis of GaInAsSb Semiconductor Layers", Proc. of 3rd Annual Symposium on CSA, Greensboro, NC, p. 527-30 (1992)

7. D.L. Simpson, S. Iyer, and A. Abul-Fadl, "Liquid Phase Electroepitaxial (LPEE) Growth and Photoluminescence Characterization of Undoped GaInAsSb (2.25μm) at 530°C," ibid, p. 525-6 (1992).

8. "LPEE Growth & Characteristics of GaInAsSb alloys", presented at Emory University, Feb. 27 (1992).

9. S. Iyer, A. Abul-Fadl, S. Vaddi, and W.J. Collis, "Photoluminescence Study of LPEE Grown GaInAsSb Epilayers on GaSb", Proc. of 2nd Annual Symposium on CSA, Greensboro, NC, p.53-6 (1991).

10. R. Cardona, S. Iyer, and A. Abul-Fadl, "Photoreflectance as an Optical Characterization Tool", ibid., p.58 (1991).

11. S. Vaddi, S Iyer and A. Abul-Fadl, "LPEE Growth of GaInAsSb System", ibid., p.108-109 (1991).

12. C. Durham, A. Abul-Fadl, and S. Iyer, "Photoluminescence / Photoreflectance Data Acquisition", ibid., p.106-107 (1991).

13. "LPEE Growth & Photoluminescence Characteristics of GaSb & GaInAsSb alloys", presented at Wright Patterson Laboratory, June (1991)

14. S. Iyer, A. Abul-Fadl, S. Vaddi, and W.J. Collis, "Photoluminescence Study of LPEE Epilayers on GaSb", Proc. of 2nd Annual Symposium on CSA, Greensboro, NC, p. 53-6 (1991).

15. "LPEE Growth & Characterization of GaInAsSb", presented at 1st HBCU Meeting on PMMS' 90, Howard University, Washington, May 16, (1990)

16. J. Lewis, S. Iyer, A. Abul-Fadl and W. Collis, "Liquid Phase Electroepitaxial Growth and Characterization of InGaAsSb lattice Matched to (100) GaSb in the 1.7 to 2.3 μm", Proc. of 1st Annual Symposium on CSA, Greensboro, NC, p.57 (1990)

PRESENTATIONS BY STUDENTS

1. "Damage and Annealing of Te-Implanted GaSb", **R.Parakkat**, Materials Conference, NC A&T State University, October 29, 1993.

2. "Schottky Barrier on LPEE Grown n-GaSb Layers", **Gaojun Qiu**, Materials Conference, NCA&T State University, October 29, 1993.

3. "Low Temperature PL Spectral Analysis of LPEE Grown Te-doped GaSb and GaInAsSb Layers", **Lori Small**, Materials Conference, NCA&T University, October 29, 1993.

4. "Liquid Phase Electroepitaxial (LPEE) Growth and Photoluminescence Characterization of Undoped GaInAsSb (2.25μm) at 530°C", **D.L. Simpson**, 3rd Annual Symposium on CSA, Greensboro, NC, p. 525-6 (1992)

5. "Photoreflectance as an Optical Characterization Tool", **R. Cardona**, 2nd Annual Symposium on CSA, Greensboro, NC, p.58 (1991).

6. "LPEE Growth of GaInAsSb System", **S .Vaddi**, 2nd Annual Symposium on CSA, Greensboro, NC, p.108- 109 (1991).

7. "Photoluminescence / Photoreflectance Data Acquisition", **C. Durham**, 2nd Annual Symposium on CSA, Greensboro, NC, p.106-107 (1991).

8. "Liquid Phase Electroepitaxial Growth and Characterization of InGaAsSb lattice Matched to (100) GaSb in the 1.7 to 2.3 μm", **J. Lewis**, 1st Annual Symposium on CSA, Greensboro, NC, p.57 (1990)

PUBLICATIONS IN PREPARATION

1. "Low Temperature Photoluminescence Study of LPEE Grown Te-doped GaSb and Schottky Barriers on (100) GaSb" by S.Iyer et al.

2. "Ion Implantation Damage and Annealing in GaSb", S.Iyer et al.

UNDERGRADUATE PROJECTS

1. Lori Small, "Photoluminescence Spectral Analysis of GaInAsSb Semiconductor layers" , Dec. 1991.

2. Christopher Durham, "Photoreflectance/Photoluminescence Data Acquisition", April 1991.

3. Karen Slater, "Computer Simulation of Photoluminescence Spectra", Sept. 1992

REPORTS SUBMITTED

1. S.Iyer and A.Abul-Fadl, "LPEE growth and Characterization of $In_xGa_{1-x}As_ySb_{1-y}$ Lattice Matched to GaSb and InAs for Photodetectors",
USARO Semi-Annual Reports,

Jan 1, 1990 - Jun 30, 1990	Jul 1, 1990 - Dec 31,1990
Jan 1, 1991 - Jun 30, 1991	Jul 1, 1991 - Dec 31, 1991
Jan 1, 1992 - Jun 30, 1992	Jul 1, 1992 - Dec 31, 1992
Jan 1, 1993 - Jun 30, 1993	

GRADUATE DEGREES AWARDED

1. S. Vaddi,M.S.E.E. "Photoluminescence Study of LPEE Grown GaSb and GaInAsSb Layers on (100) GaSb",Dec. 1991.

2. D. Moxey, M.S.E.E. "LPEE Growth and Characterization of Te-Doped GaSb and GaInAsSb on (100) GaSb at 574°C", May 1992.

3. Rufino Cardona, M.S.E.E., "Photoreflectance characterization of semiconductors", August,1992.

4. Darrell Simpson, M.S.E.E "LPEE Growth of Te-doped GaSb & GaInAsSb for Photodetector Applications", March 1993

5. Lori Small, M.S.E.E "Photoluminescence characterization of LPEE grown Te doped GaSb and GaInAsSb", July 1993

6. Jen-Sheng Huang, M.S.E.E "LPEE Growth Of Te-Doped GaSb Layers at 474°C And Electrical Properties Of Au/n-GaSb Schottky Diodes", February, 1994.

7. Gaojun Qiu, "Schottky Diodes and p-n Junctions on LPEE Grown n-GaSb" February, 1994.

MASTERS THESIS IN PREPARATION

Rajiv Parakkat, "Ion Implantation Damage and Annealing in GaSb"

XI. PARTICIPATING SCIENTIFIC PERSONNEL

Faculty

1. Shanthi Iyer, Associate Professor
2. Ali Abul-Fadl, Associate Professor
3. Ward Collis, Associate Professor
4. Clinton Lee, Assistant Professor

Graduate Students

1. S. Vaddi, MSEE
2. Darrell Simpson, MSEE
3. Lori Small, MSEE
4. G. Qiu, MSEE
5. Rajiv Parakkat, MSEE Candidate
6. Jenseng Huang,MSEE
7. P. Walha
8. Donovan Moxey, MSEE
9. Rufino Cardona, MSEE

Undergraduate Students

1. Nidhi Sangal
2. Norman Sanchez
3. Andrea Thornton
4. Richard Bowling
5. Christopher Durham
6. Karen Slater

COLLABORATORS

Dr. Krishna Bajaj (Chairperson, Emory Unuversity)
Dr. William Mitchel (Wright Patterson Laboratory, Materials Directorate)
Dr. S. Hegde (University of Dayton Research Institute)
Dr. Nalin Parikh (University of North Carolina, Chapel Hill)
Dr. Bijoy Patnaik (University of North CArolina, Chapel Hill)
Dr. Mark Ray (Microelectronics Center of North Carolina, Research Triangle Park)
Dr. Mark Denker (Microelectronics Center of North Carolina, Research Triangle Park)

XII. APPENDICES

APPENDIX A

Phys. Rev. B 47,1329-39 (1993)

Growth and photoluminescence of GaSb and $Ga_{1-x}In_xAs_ySb_{1-y}$ grown on GaSb substrates by liquid-phase electroepitaxy

S. Iyer
Department of Electrical Engineering, North Carolina A&T State University, Greensboro, North Carolina 27411

S. Hegde
University of Dayton Research Institute, Dayton, Ohio 45469-0178

Ali Abul-Fadl
Department of Electrical Engineering, North Carolina A&T State University, Greensboro, North Carolina 27411

K. K. Bajaj
Department of Physics, Emory University, Atlanta, Georgia 30322

W. Mitchel
Materials Directorate, Wright Laboratory, Wright–Patterson Air Force Base, Dayton, Ohio 45433-6533
(Received 5 February 1992; revised manuscript received 13 August 1992)

We report on the liquid-phase electroepitaxial (LPEE) growth of GaSb and $Ga_{1-x}In_xAs_ySb_{1-y}$ alloys on undoped (100) GaSb substrates. Alloys with room-temperature photoluminescence peak wavelengths as long as 2.32 μm have been grown. These layers were assessed by x-ray diffraction, energy-dispersive x-ray analysis, and low-temperature Fourier-transform photoluminescence (PL), with emphasis on the latter. The variation in the low-temperature photoluminescence bands as a function of the alloy composition has been investigated. The low-temperature (4.5 K) PL spectra of the alloys exhibited narrow peaks with full width half maxima in the range 3–7 meV, indicating an excellent quality of the LPEE-grown epilayers. The temperature and intensity dependences of the PL spectra were investigated to identify the nature of the recombination processes.

I. INTRODUCTION

The quaternary alloys $Ga_{1-x}In_xAs_ySb_{1-y}$ are currently of great interest for use in infrared devices (1.7–4.1 μm). The unique feature of this alloy system is the presence of the miscibility gap which covers almost the entire composition range at typical growth temperatures (Fig. 1). Nonequilibrium techniques, namely, organometallic vapor-phase epitaxy[1,2] (OMVPE) and molecular-beam epitaxy,[3,4] (MBE), have been used successfully for the growth of these layers in the miscibility gap region. The layers grown by liquid phase epitaxy[5–10] (LPE) are limited by the presence of the miscibility gap, and the composition with the longest wavelength reported inside the gap is 2.33 μm,[5] corresponding to x of 0.22 and 0.18 on GaSb substrates. For compositions away from the substrate corresponding to $x \geq 0.8$ (Refs. 8 and 9) difficulties have been encountered due to the growth solutions tending to dissolve the substrate. Hence, most of the LPE work has been concentrated over a very narrow composition range, for $x < 0.25$ (Refs. 5–7) on GaSb substrates and for $x \leq 0.2$ (Refs. 7 and 8) and $x \geq 0.83$ (Refs. 8 and 10) on InAs substrates.

Iyer *et al.*[11] have reported the growth of these layers lattice matched to GaSb by the liquid phase electroepitaxial (LPEE) technique. In the LPEE technique, unlike LPE, growth is carried out at a constant furnace temperature and is induced and sustained by an external parameter, in this case the current density. The advantages of LPEE over LPE-grown layers in terms of the interface stability,[12] surface morphology[13] and the compositional homogeneity[14,15] are well established. Epitaxial layers of InSb (Ref. 16) were the first binary III-V semiconductor compound layers grown by this technique. However, since then GaAs,[13] InSb,[16] InP,[17] GaP,[18] InAs,[19] $Ga_{1-x}Al_xAs$,[15] $In_{1-x}Ga_xAs$,[20,21] InGaP,[14] and $Ga_{1-x}In_xAs_yP_{1-y}$ (Ref. 22) have been grown by this technique.

GaSb, unlike other commonly known III-V semiconductors such as GaAs and InP, has a somewhat large concentration of residual acceptors. The dominant residual acceptor has been attributed to the native defect caused by Sb deficiency, predominantly due to either the Ga antisite,[23] or a Ga antisite in the vicinity of a Ga vacancy.[24–26] The nature of this acceptor has been a subject of extensive studies to determine whether the residual acceptor is a single acceptor[24,27] or a double acceptor.[28,30] The strong evidence of the latter has been shown in compensated materials,[28,29] namely, in donor-doped layers. The first and second ionization energy levels of this acceptor have been determined to be in the range 30–35 meV (Refs. 23, 28, and 29) and 70–120 meV (Refs. 28–30), respectively. In addition, another dominant acceptor level is present at 54 meV above the valence band

 ©1993 The American Physical Society

in GaSb.[27,31] However, the nature of this acceptor level is not well understood. Very little is known about the acceptors due to chemical impurities in this material.

The low-temperature photoluminescence has so far been an important characterization tool for assessing the quality of GaSb layers. Due to the presence of different acceptor levels in this material, the low-temperature PL spectra exhibit numerous transitions which include free excitons, recombinations at the different acceptor levels, and excitons bound to these neutral acceptor levels. Hence, if the layers grown are not of high purity, there is considerable misinterpretation of the origin of the PL peaks. The sharp structures near the band edge in GaSb have been attributed to excitons bound to different neutral acceptors.[27,32,33] In high-quality GaSb material, four bound excitons have been resolved[32,33] at low temperatures occurring at 805.4, 803.4, 800.1, and 796.1 meV, respectively. They will be referred to as BE_1, BE_2, BE_3, and BE_4, respectively, following the nomenclature of Ruhle and Bimberg,[32] which is now commonly used. The binding energies of excitons to the acceptors are significantly different and much larger than commonly observed in other III-V semiconductors such as GaAs, InP, and InSb. Both Johnson and Fan[30] and Benoit a la Guillaume and Lavallard[27] have identified BE_2 to correspond to an exciton bound to a native acceptor level at 34 meV, from Zeeman splitting and piezoemission experiments, respectively. The BE_4 transition has also been ascribed to an exciton bound to a neutral acceptor level[27,32] above the valence band from the piezoemission data.[27] However, Johnson and Fan[30] have suggested the possibility of this transition being due to an exciton bound to an ionized acceptor, while Pollak and Aggarwal[34] claimed to observe no splitting of the levels under uniaxial stress questioning the identity of the above transitions. The origin of the other two bound exciton transitions BE_1 and BE_3 is not yet clearly understood.

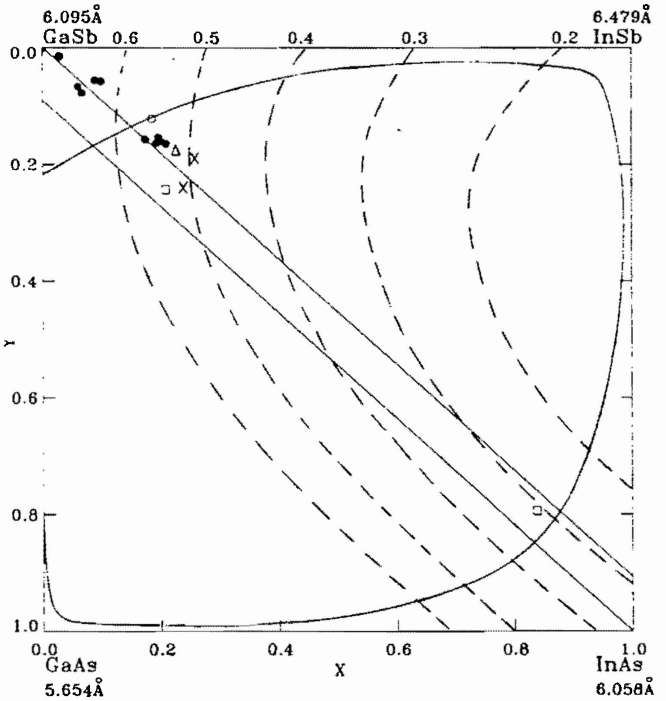

FIG. 1. Schematic diagram of the solid phase field for the quaternary alloy system $Ga_{1-x}In_xAs_ySb_{1-y}$. Isolattice constant lines for alloys lattice matched to GaSb and InAs are shown by the solid straight lines. Binodal isotherm at 600 °C and room-temperature band-gap plots are taken from Ref. 1. Indicated are our data points (●), previous LPE data corresponding to the highest value of x inside the gap lattice matched to GaSb, DeWinter *et al.* (Ref. 5) (Δ), Jouille *et al.* (Ref. 6) (×), and lattice matched to InAs, Sankaran and Antypas (Ref. 8) (□) and Astles *et al.* (Ref. 7) (○).

While there have been several reports on GaSb, there has been no detailed study of the radiative transitions in $Ga_{1-x}In_xAs_ySb_{1-y}$. As is well known for III-V semiconductor compounds and alloys in general, the properties of the material are growth specific. Hence, it becomes important to compare specific fundamental characteristics and the quality of the materials grown by LPEE technique with those grown using other techniques, in particular the LPE technique. In this work, we present a systematic study of the LPEE-grown $Ga_{1-x}In_xAs_ySb_{1-y}$ layers of compositions corresponding to the room-temperature wavelength in the range 1.7–2.28 μm. The results of the dependence of PL characteristics on the excitation laser power, temperature, and the alloy composition are reported.

II. EXPERIMENTAL DETAILS

A conventional horizontal slider boat system which was designed to allow the passage of current through the melt-substrate interface, was used for the LPEE growth of $Ga_{1-x}In_xAs_ySb_{1-y}$. The details of the growth system and the growth procedure have been described elsewhere.[11,20] Undoped (100) GaSb wafers of thickness 0.4 mm (16 mil) and an area of 6 mm × 6 mm were used as substrates. GaSb and three different compositions of the quaternary alloys were grown. The liquidus composition of the melt was determined by the source dissolution technique. Excess GaSb was added prior to epilayer growth to provide a continuous source of Sb. The lattice mismatch of the layers were determined either by double-crystal x-ray diffraction or by high-resolution x-ray diffraction. The rocking curves were recorded for the (400) reflection of Cu $K\alpha$ line from an InP and Si monochromator crystals, respectively.

The low-temperature PL spectra were obtained using a BOMEM Fourier-transform spectrometer at a resolution of 0.2 meV. An Ar-ion laser operating at 514.5 nm provided the excitation source. The maximum output power was limited to 140 mW. The spectra were taken using a focused laser spot on the sample and a liquid-nitrogen-cooled InAs as the detector. The beam diameter on the sample was 100–500 μm and typical excitation power density on the sample was ~ 1 W/cm^2. The low-temperature measurements were carried out in a variable temperature continuous-flow liquid-helium cryostat. A different setup was used for recording the room-temperature PL spectra. It consisted of a 0.5-m grating monochromator and a PbS detector with lock-in techniques, for dispersion and detection purposes, respectively.

The compositions of the layers were determined using an energy dispersive spectrophotometer attached to an ISI SS-40 scanning electron microscope. GaSb, GaP, and InAs were used as the binary standards for Sb, Ga, In, and As, respectively. The quantitative analysis was carried out using Tracor Northern Computer. The MICROQ program with ZAF correction was used to analyze the x-ray spectra.

III. RESULTS AND DISCUSSION

A. Growth Results

GaSb and $Ga_{1-x}In_xAs_ySb_{1-y}$ layers of different compositions corresponding to the room-temperature PL peak wavelength range of 1.7–2.32 μm were grown by the LPEE technique. $Ga_{1-x}In_xAs_ySb_{1-y}$ layers of compositions corresponding to room-temperature PL peak wavelengths around 1.8, 1.99, and 2.2 μm have been labeled as α, β, and γ samples, respectively. The quaternary α and β layers were grown at 580 °C, as better compositional homogeneity is expected due to the reduction in the As distribution coefficient[7] at higher temperatures. However, for the growth of γ composition, catastrophic dissolution of the substrate occurred at this temperature due to the unstable melt. Hence the growth temperature was lowered to 530 °C. The liquidus compositions of the different melts used were reported earlier.[11] The growth parameters together with the results of lattice mismatch and the layer composition, where available, are given in Table I. The growth rate exhibited a linear dependence with the current density,[11] which is indicative of the dominance of the electrotransport mechanism in the growth process. The typical values of the growth rates as reported earlier[11] are 0.8 μm/min at a current density of 10 A/cm^2. Layers in the thickness range of 1–10 μm have been grown by this technique. The layers used for the PL measurements were 2–4 μm thick.

X-ray-diffraction studies of the grown layers indicated that epitaxial layer–GaSb substrate mismatch, $\Delta a/a$, never exceeded 0.17%. The full width half maxima (FWHM) of the epilayers were in the range of 20–67 arc sec. The good quality of the crystalline epilayers becomes evident when this is compared to the half-width of the 25–30 arc sec normally seen on the substrate itself. For α and β layers smooth and shiny surfaces were obtained with ease under both lattice-matched and lattice-mismatched conditions. This indicates that lattice matching is not critical for obtaining specular surfaces for compositions close to the GaSb corner of the phase diagram. For γ layers, the surface morphology was comparatively inferior, in general exhibiting a cloudy appearance. However, the exact dependence of the surface morphology on the lattice mismatch was not examined in detail.

B. Near band-edge PL spectra at 4.5 K

Figure 2 illustrates the 4.5-K PL spectra of LPEE-grown GaSb and $Ga_{1-x}In_xAs_ySb_{1-y}$ epilayers. The PL

TABLE I. Summary of growth conditions and characterization results. An asterisk indicates that the lattice mismatch was determined by high-resolution x-ray diffraction.

Sample No.	Growth temp. (°C)	Current density (A/cm^2)	Thickness (μm)	λ_{pl} (μm)	Eg (eV)	ΔEg (meV)	$\Delta a/a$ (%)	FWHM (arc sec)	x	y
GS-5	580	1.4	6.5	1.70	0.729	32				
GS-8				1.70	0.729	43			0.00	0.00
GS-29				1.71	0.729	37	0.00	24	0.00	0.00
*G*3α3				1.77	0.700	41		30		
αT-05	580	6.2		1.79	0.693	42	0.00	67		
αT-11	581	6.0		1.79	0.693	35	0.01	32	0.027	0.014
αT-02	580	8.2		1.81	0.685	37	−0.07	27		
α-23	581	10.4		1.81	0.685	39	0.00	31	0.028	0.016
αT-14	581	6.5		1.82	0.681	44	0.04	30		
α-21	581	9.9	5.5	1.84	0.674	35	0.04	20		
β-8				1.95	0.636	28				
β-9				1.96	0.633	32	0.048 *		0.088	0.056
β-120	574			1.96	0.633	35	0.001	30	0.098	0.058
βT-22	585	9.8	7.3	1.97	0.629	37	<0.050 *	42		
βT-27	572	7.5	3.7	1.99	0.623	35	−0.042	27	0.066	0.078
β-121	574			1.99	0.623	23	−0.083	40		
β-18	573	6.8	5.4	2.00	0.620	33	0.06	46		
γ-11	534	11.4	2.9	2.25	0.551		0.00 *	55		
γT-31	535	11.3	0.7	2.25	0.551	48	0.00	22	0.170	0.140
γT-47	532	18.7	3.7	2.26	0.549	37	−0.164 *	61	0.173	0.157
γT-46	535	14.4	4.0	2.27	0.546	37	−0.099 *	28	0.199	0.160
γT-44	535	8.9	3.7	2.27	0.546	45	0.083 *	66	0.191	0.164
γ-12	534	11.8	6.6	2.28	0.544	37	0.079 *	65	0.208	0.165
γ-14	533	11.7	3.7	2.30	0.539	41				
δAF-7	529	10.0	5.6	2.32	0.534	46			0.195	0.154

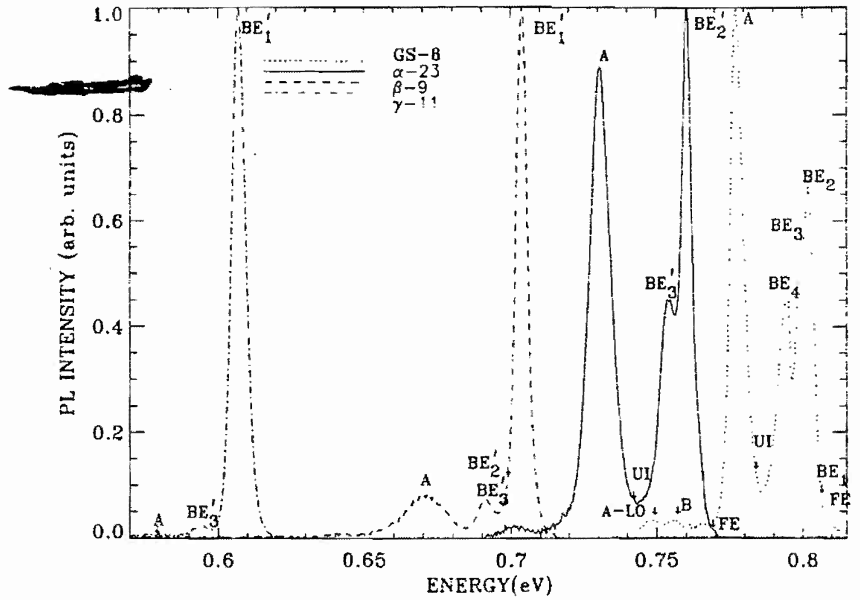

FIG. 2. Low-temperature (4.5 K) PL spectra of GaSb and $Ga_{1-x}In_xAs_ySb_{1-y}$ of three different compositions.

emission intensity of the spectra has been normalized with respect to the dominant peak present in each of the samples. A quantitative fit to the PL spectra, using the sum of Gaussian line shapes, has been utilized to accurately determine the peak positions and the spectral widths.

As shown in Fig. 2, in GaSb (sample GS-8) we observe four emission peaks labeled as BE_1, BE_2, BE_3, and BE_4 at 805.4, 802.2, 799.1, and 795.8 meV, respectively near the band edge. These peaks have been associated with the radiative decay of excitons bound to neutral acceptors. The origin of these acceptors is not definitely known though some have been conjectured as due to native defects. In addition, a weak transition associated with free excitons (FE) is also observed at 808.5 meV which attests to the high quality of the LPEE-grown layers. Amongst the bound exciton transitions, BE_2 is found to be the strongest and BE_1 appears to be hidden by the more pronounced emission peak BE_2, BE_3, and BE_4 also appear to be fairly strong.

The band-acceptor or donor-acceptor transition (A) at 777.5 meV is the dominant peak. In GaSb the donor levels are shallow ($\sim$2–3 meV) due to the small effective mass of the electron, which makes it difficult to distinguish between free-to-bound and donor-to-acceptor recombination processes. A broad band at the lower energy can be resolved to consist of impurity-related transitions (B) and a phonon replica of A (A-LO). In addition to most of the peaks reported in the literature in LPE-grown GaSb, an additional unidentified peak (UI) at 784.6 meV observed in MBE (Ref. 35) and OMVPE (Ref. 36) grown layers, is also seen.

The PL spectra of the quaternary layers exhibit features similar to those described for GaSb. PL spectral characteristics of the quaternary layers are summarized in Table II. Free-exciton transition is seen only in the α-23 sample, as a weak band centered at 765.0 meV on the high-energy side of the spectrum. This is seen in both GaSb and α-23 layers only under the highest excitation level used. The highest-energy transition line identified as BE_2' at 760.5 meV becomes strong. In addition, we observe transitions at 754.3, 742.2, 730.6, and 702.2 meV which are labeled as BE_3', UI, A, and A-LO, respectively. The transitions BE_2' and BE_3' are relatively sharp and are

TABLE II. Low-temperature PL characteristics of LPEE-grown $Ga_{1-x}In_xAs_ySb_{1-y}$ layers. Relative intensity is denoted by Relat. Int.

	α-23			β-9			γ-11		
Identity	Energy (meV)	FWHM (meV)	Relat. Int.	Energy (meV)	FWHM (meV)	Relat. Int.	Energy (meV)	FWHM (meV)	Relat. Int.
FE	765.0	4.7							
BE_1'				703.8	5.0	1.0	607.1	5.5	1.0
BE_2'	760.5	4.1	1.00	697.9	5.2	0.04			
BE_3'	754.3	7.6	0.48	691.1	6.7	0.07	594.1	7.6	0.02
UI	742.2	14.0	0.07						
A	730.6	8.5	0.97	670.9	15.7	0.08	578.1		0.002
A-LO	702.2	8.8	0.03	640.2					

only 4.5 and 10.7 meV lower in energy than the free-exciton line. We suggest that these two transitions are associated with the decay of excitons bound to two different neutral acceptors whose identities are not known at this time. As in GaSb the transitions A and A-LO are associated with the band-acceptor recombination and its optical phonon replica, respectively, and transition A is the most intense. The energy band gap of this sample is obtained by adding the free-exciton binding energy ($\sim$1.1 meV) to the free-exciton transition energy (765.0 meV).

In sample β-9, which has an alloy composition corresponding to a lower band gap, we observe at least five transitions at 703.8, 697.9, 691.1, 670.9, and 640.2 meV labeled as BE_1', BE_2', BE_3' A, and A-LO, respectively. We do not see any evidence of the free-exciton transition for the range of pumping power studied in this work, and therefore cannot accurately determine the value of the energy band gap in this sample. We find that the linewidths of BE_1', BE_2' and BE_3' transitions observed in this sample are comparable to those of acceptor-bound excitons in GaSb and α-23 sample. We therefore suggest, as before, that these transitions are associated with the radiative decay of excitons bound to neutral acceptors. Additional support for this assignment is also provided by the excitation and temperature-dependent behavior of these transitions as described in an upcoming part of this paper. Thus if we assume that BE_1' is an acceptor-bound exciton transition, we can estimate the band gap of this sample by adding approximately 4 meV (namely, the sum of the exciton dissociation energy and FE binding energy) to the transition energy of BE_1', namely, 703.8 meV. This gives us a band gap of about 708 meV. The A transition, associated with the radiative recombination of a free electron with a bound hole of an acceptor is rather weak in this sample, whereas in GaSb and in α-23 it is the most intense transition. It is not clear why this transition is so weak whereas an acceptor-bound exciton transition BE_1' is so strong. From the value of the band gap and the transition energy of A we determine the binding energy of the acceptor to be 38 meV. This value compares quite well with those determined in GaSb (34 meV) and the α-23 sample (35 meV).

A broad line shifted by $\sim$30 meV from the A peak towards lower energy appears, as in the other two samples. We label this structure the LO phonon replica of A (A-LO), as this energy corresponds to the optical phonon energy reported in GaSb.[37] In GaSb, α-23, and β-9 samples, the ratios of the intensity of the A peak and A-LO peak are in the range 32–40 and remain invariant within experimental error with excitation laser power intensity and decrease with increase in temperature. This trend conforms to the expected behavior of the phonon sideband further strengthening the assignment of this peak. However, $Ga_{1-x}In_xAs_ySb_{1-y}$ alloy have an unusual band structure and the peak designated as A-LO could be related to it. Even though this transition is proposed to be a phonon replica of A, this identification is by no means definite.

In sample γ-11, which has an alloy composition corresponding to even a lower band gap, we observe three transitions at 607.1, 594.1, and 578.1 meV labeled as BE_1', BE_3', and A, respectively. Again, we do not see a free excitonic transition. As in the case of sample β-9, we associate BE_1' and BE_3' with radiative recombination of excitons bound to two different neutral acceptors and estimate the band gap of this sample by adding about 4 meV to the transition energy of BE_1', namely, 607.1 meV. This leads to a band gap of about 611 meV. The transition A is very weak and could be detected only under high sensitivity. As before, we suggest that this transition is associated with radiative recombination of a free electron with a bound hole. The binding energy of an acceptor obtained in this case is about 33 meV which compares rather well with values obtained in GaSb and other two alloy samples. It should be pointed out that our observation of a single strong peak in γ samples is consistent with the experimental observation[2,38] on the layers grown by nonequilibrium techniques (OMVPE and MBE) where only one strong peak is seen for layers with compositions closer to or inside the miscibility gap region.

C. Intensity dependence of the PL spectra

To further confirm the identity of the various peaks, the PL spectra were studied as a function of incident laser power intensity. The integrated intensity of the BE_2' transition as a function of incident intensity for α samples is depicted in Fig. 3. It exhibits a power dependence of $P^{1.40}$. The transitions identified as BE_3' in all the quaternary layers exhibit an identical power dependence of $P^{1.22}$, though only the intensity dependence of BE_3' in α samples is shown, suggesting that the BE_3' transitions in the different quaternary layers have similar origin. These values are somewhat higher than the power dependence of $P^{0.96}$ and $P^{1.14}$, respectively, reported in GaSb layers for similar transitions by Chidley *et al.*[36]

In Fig. 4 we display the variation of the integrated intensity of BE_1' transition in β-9 sample as a function of the incident power. This transition exhibits a power dependence of 2.1. Similar power dependence for this transition is also found in the other quaternary alloy γ-11. We have calculated the power dependence of the integrated intensity of transitions associated with the radiative recombination of excitons bound to neutral acceptors using the well-known rate equations. We find that this dependence varies from $P^{1.0}$ to $P^{2.0}$ depending upon the values of the various recombination parameters which are highly sample dependent. Thus our assignment of BE_1', BE_2', and BE_3' transitions in $Ga_{1-x}In_xAs_ySb_{1-y}$ alloys to acceptor-bound excitons is consistent with their behavior as a function of incident power.

With the decrease of incident laser intensity, the higher-energy transitions gradually collapse and only the free electron to acceptor transitions persist at low intensities. The variation of the luminescence intensity of the free electron to acceptor peak in the β-9 layer at 670.9 meV as a function of incident intensity is also shown in Fig. 4. The intensity variation is perfectly linear with a slope of 1.0 confirming the assignment of this peak. No saturation effects in any of the peaks were observed in the limited range of incident laser power used.

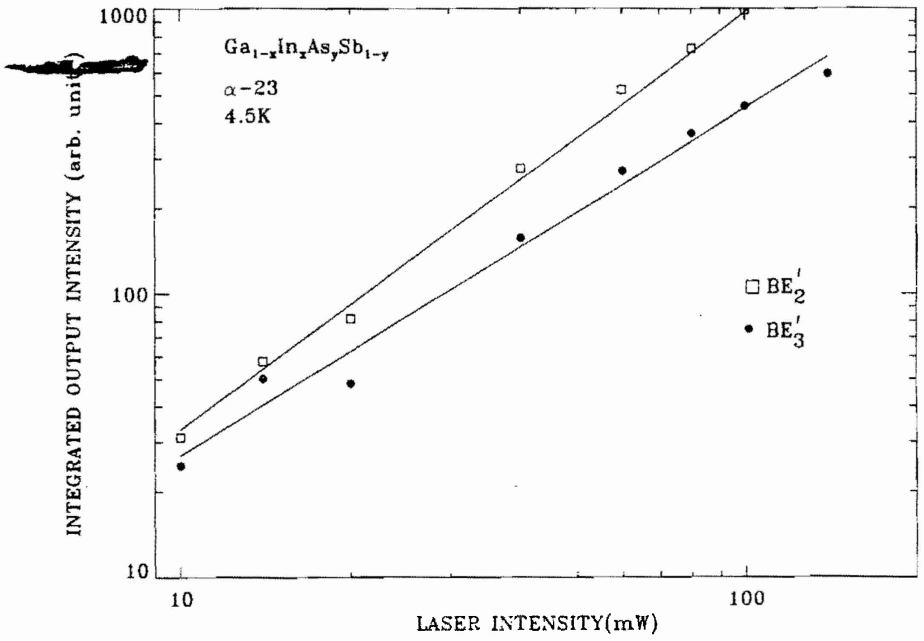

FIG. 3. Variation of PL-integrated intensity of the bound excitons as a function of the incident laser intensity in α layers.

D. Temperature dependence of the PL intensity

With increase in temperature, the overall integrated emission intensity of the quaternary PL spectra gradually decreases, indicating the presence of nonradiative mechanisms of decay with low activation energies. BE_2' in α layers shifts to higher energy by 0.57 meV with increasing temperature up to 30 K, and thereafter merges with the band-to-band transitions. The deeper bound exciton peak identified as BE_3' is rapidly quenched by 35–40 K with no significant shift in the position.

To determine the activation energies of the bound excitons, the low-temperature integrated intensity-dependent data for BE_3' were fitted as shown in Fig. 5, using the three-level Boltzmann distribution developed by Bimberg, Sondergeld, and Grobe,[39]

$$I_T/I_0 = 1/\{1 + C_1 \exp(-\Delta E_1/kT) + C_2 \exp(-\Delta E_2/kT)\}\ , \quad (1)$$

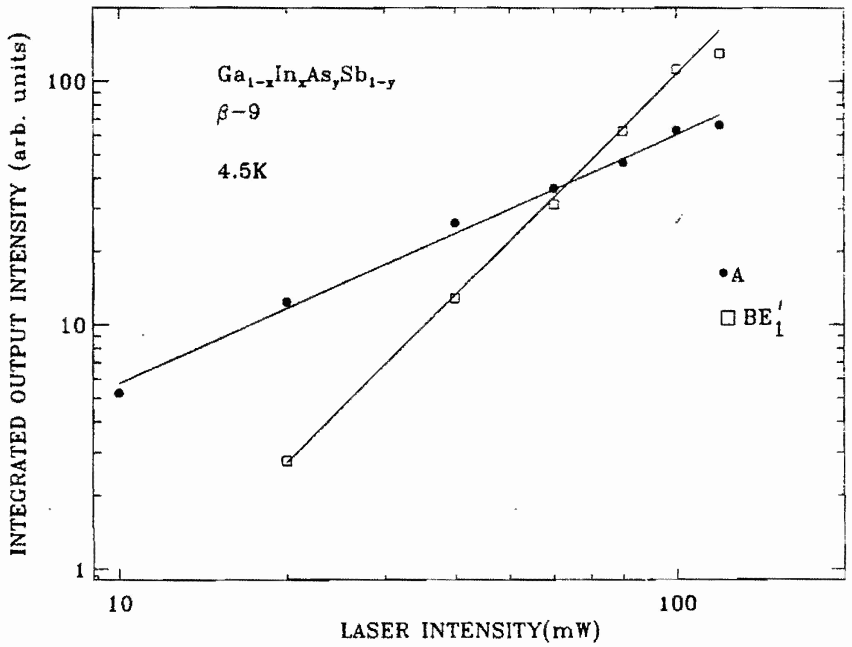

FIG. 4. PL-integrated intensity dependence of band-to-band transitions and band-to-acceptor transitions in β layers on the incident laser intensity.

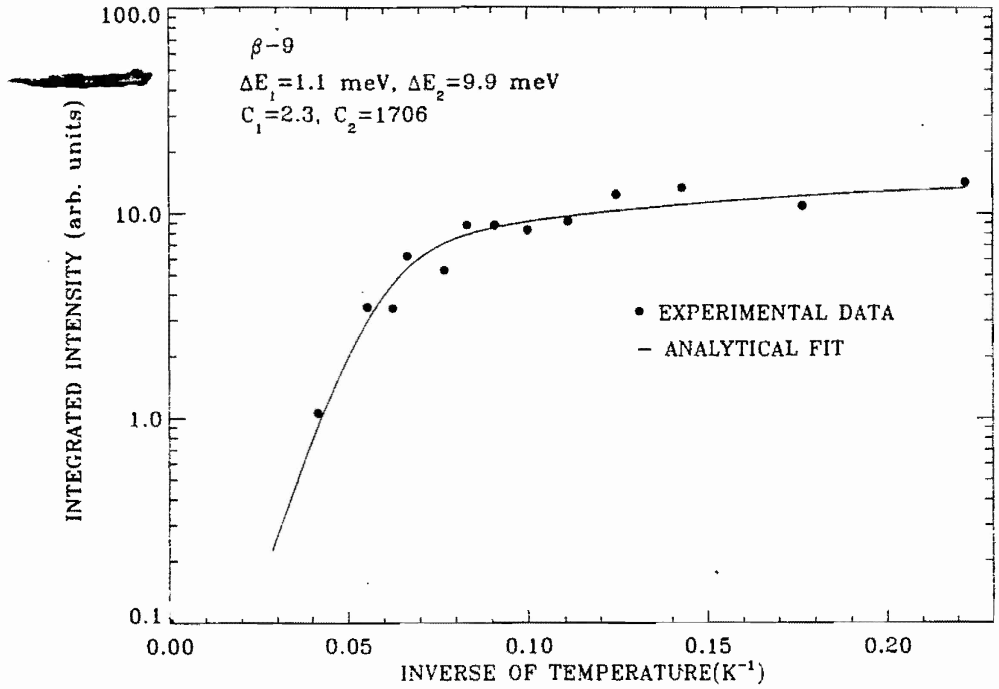

FIG. 5. Theoretical fit to the temperature dependence of integrated intensity of the deeper bound exciton transition (BE_3') at low temperatures. The values of C_1, C_2, and the binding energies are in excellent agreement with the results of GaSb (Ref. 33).

where I_T/I_0 represents the normalized integrated intensity at 4.5 K, ΔE_1 and ΔE_2 represent the effective-mass donor binding energy and dissociation energy of the bound exciton, respectively, and C_1 and C_2 are constants and are functions of the density of states. The values of ΔE_1 and ΔE_2 were found to be in the range 1.1–1.3 meV and 8.9–11 meV, respectively, in excellent agreement with the corresponding values reported in GaSb layers.[33] The binding energy of the second level ($\frac{4}{3}$ of the thermal activation energy) is in the range of 11.8–14.6 meV, which is also close to the values estimated from the PL peak positions. The intensity of BE_1' transitions as a function of temperature could not be fitted with a reasonable set of values for ΔE_1 and ΔE_2. The reason for this behavior is not clear at this time.

Integrated intensity of the band-to-acceptor transition also decreases with increase in temperature. However, it persists up to a temperature of 100–140 K. In α layers

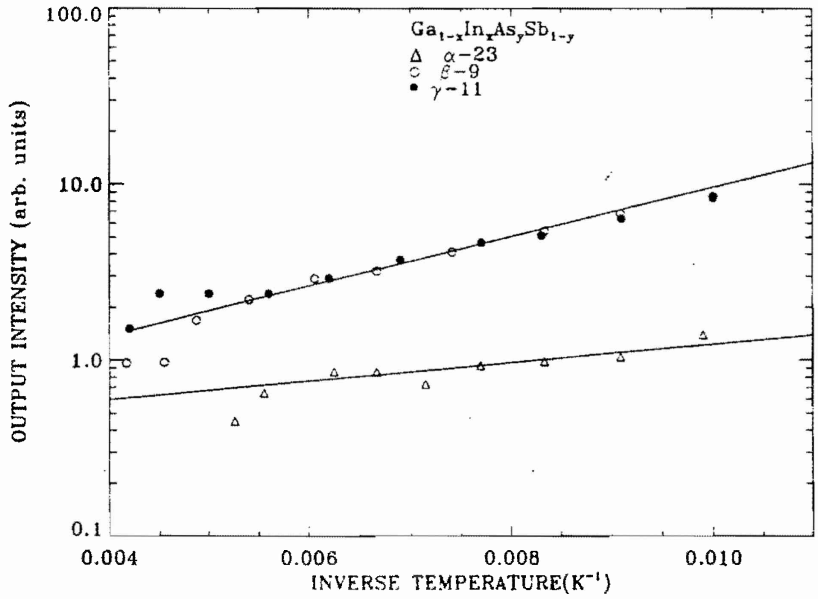

FIG. 6. Thermal quenching behavior of band-to-band PL emission for temperatures beyond 80 K. The intensity of the γ layers were scaled up so that they can be plotted on the same graph.

the A peak shifts to higher energy by 0.43 meV with a rise in temperature up to 35 K before it follows the band-gap variation. This may be caused by the shift in the quasi Fermi level to higher values in the conduction band, and consequent recombination of the free electrons above the Fermi level with the holes localized in the acceptor states.

The band-to-band transitions are the only recombination processes above 80 K in all the quaternary layers. With the rise in temperature the integrated intensity of the band-to-band transition decreases. The activation energy for this thermal quenching process has been determined using the configuration coordinate model, where the competing nonradiative recombination process can be described by the expression

$$I = I_0 \exp(E_a/kT) \tag{2}$$

where I and E_a represent the PL emission intensity and quenching activation energy, respectively. The semilogarithmic plot of intensity versus reciprocal temperature is linear as illustrated in Fig. 6 exhibiting an activation energy of 14 meV in α layer and 28 meV in β and γ layers. The fact that these energies do not correspond to the band-gap energy is indicative of the presence of various nonradiative centers in the quaternary layers. Such nonradiative recombination processes would degrade the performance of devices which have these alloys as active layers. They lead to a low value of T_0 for instance, which represents a characteristic temperature that relates to the laser threshold current density, J_{th} in the laser diode. The temperature dependence of J_{th} is described by

$$J_{th} = J_0 \exp(T/T_0) \tag{3}$$

where J_0 is the threshold current density at $T=0$ K. Phenomenologically, temperature dependence of the PL process could be expressed in terms of T_0 as

$$I \propto \exp(-T/T_0) . \tag{4}$$

The straight-line fit of the integrated intensity with temperature as shown in Fig. 7 yields the value of T_0 to be 225 K for the α sample and ~90 K for β and γ samples, respectively. The latter result is in good agreement with the reported value of 80 K in $Ga_{1-x}In_xAs_ySb_{1-y}/Al_{1-x}Ga_xAs_ySb_{1-y}$ cw lasers;[40] the emission wavelength at 190 K being 2.1 μm, close to that of γ sample.

E. Line-shape analysis

For GaSb and quaternary samples all the PL peaks could be well fitted by the sum of the Gaussian line distributions at low temperatures. With a rise in temperature the PL spectra become increasingly asymmetrical, and the asymmetry sets in around the 25–35 K range indicating the dominance of the band-to-band transitions. The PL spectral shape of the band-to-band transition is analyzed[41] using

$$I(\omega) \propto (\hbar\omega - E_g)^{1/2} \exp[-(\hbar\omega - E_g)/kT] , \quad \text{for } \hbar\omega > E_m \tag{5}$$

$$\propto \exp[(\hbar\omega - E_g)/\epsilon] , \quad \text{for } \hbar\omega < E_m , \tag{6}$$

where ϵ is the tail-state parameter and E_m is the PL peak energy. The slope of the high-energy side of the spectrum is dependent on the sample temperature, while the lower-energy side of the spectrum is determined by the shape of the band edges. Figure 8 shows the experimental spectra and analytical fit for the γ layer at 80 K. A

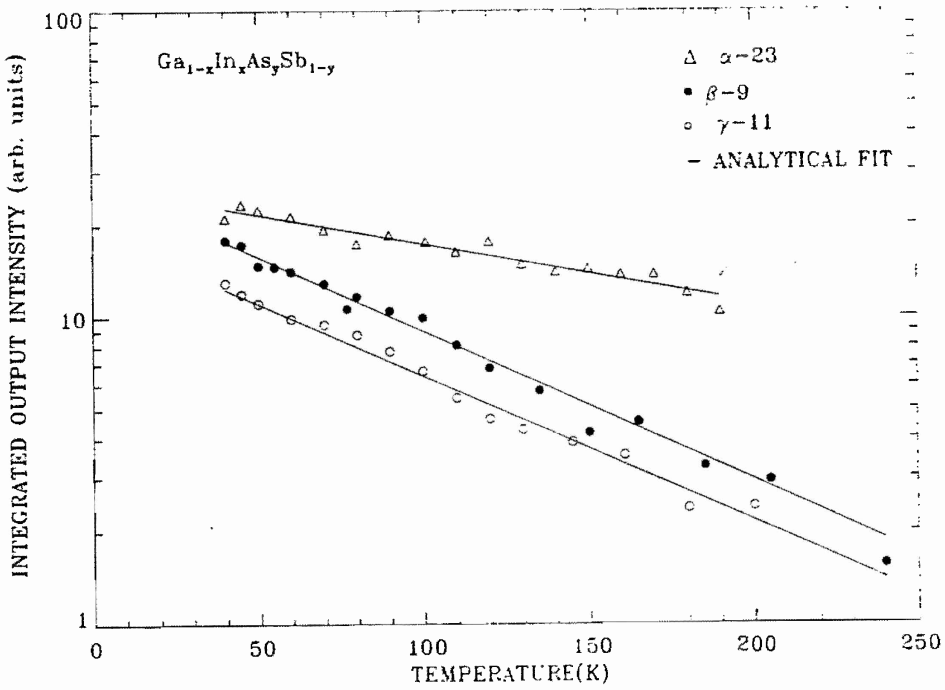

FIG. 7. Semilogarithmic plot of integrated intensity of band-to-band transitions as a function of temperature for all three different compositions of $Ga_{1-x}In_xAs_ySb_{1-y}$.

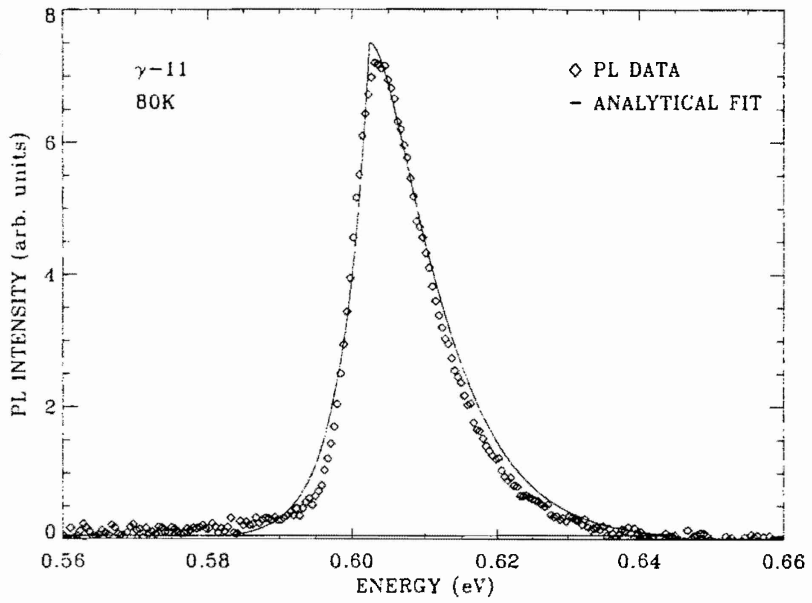

FIG. 8. Analytical fit to the PL spectra of γ layers at 80 K. The band-tail state parameter $\epsilon = 3$ meV was used to get the best fit to the lower-energy side of the spectrum.

similar fit has been obtained for all the quaternary layers in the temperature range 30–300 K with ϵ ranging from 3 to 10 meV. A similar behavior has also been observed in another quaternary $Ga_{1-x}In_xAs_yP_{1-y}/InP$ system.[42] This suggests that localized states formed either due to impurities or compositional grading contributes to the recombination processes. At higher temperatures, the emission spectra are narrower than the analytical spectra on the high-energy side, as self-absorption due to higher photon energy within the epilayer has not been taken into account. The value of E_g determined from this analysis was found to be $kT/2$ less than the PL peak energy indicative of k-conservation nature of the recombination processes.

The value of FWHM of the bound excitons for the quaternary alloys were in the range of 4–7 meV at 4 K. These are the smallest linewidths reported for $Ga_{1-x}In_xAs_ySb_{1-y}$ on GaSb so far. Variation of the FWHM of the band-to-band transitions the layers with temperature was also examined. Though there is a considerable scatter in the data, the experimental values for FWHM appear to increase linearly with temperature for all the layers, as shown in Fig. 9. The slopes of the lines are 1.0 k, 0.8 k, and 1.2 k for the three layers α, β, and γ,

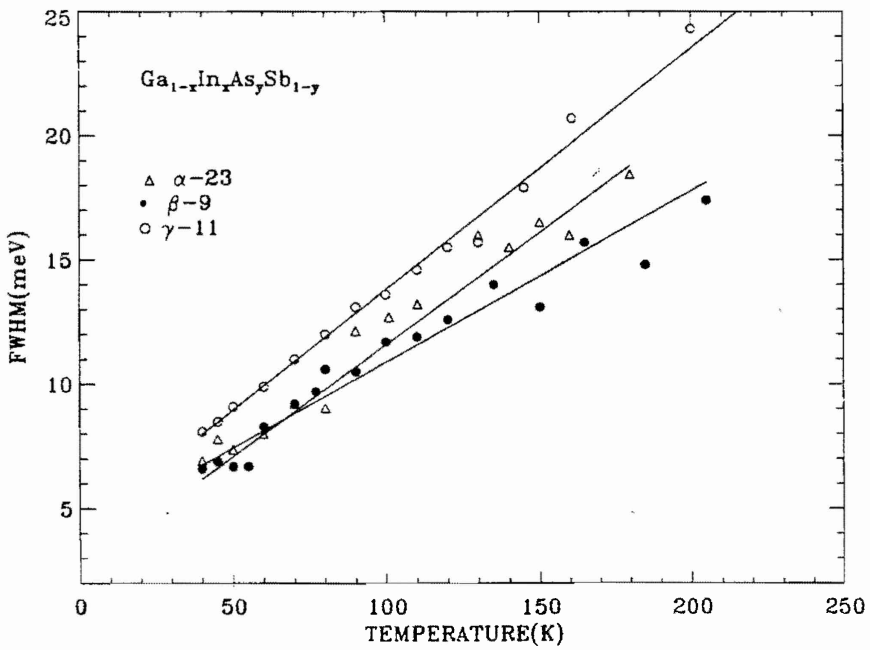

FIG. 9. Temperature dependence of the FWHM of band-to-band transitions in $Ga_{1-x}In_xAs_ySb_{1-y}$ layers.

respectively, and are much smaller than the analytical value of (1.8–2) k for an intrinsic band-to-band transition computed from Eq. (5). A similar discrepancy between the experimental and the computed half-width dependence on temperature has also been noticed in the $Ga_{1-x}In_xAs_yP_{1-y}$ system[43,44] and, as mentioned earlier, is commonly attributed to the overestimation of the spectral width by the van Roosbroeck–Shockley relation [Eq. (5)]. However, the narrow linewidths observed in our quaternary samples indicate the high quality of the crystalline layers.

And, finally, we would like to point out that our proposed assignment of the near band-edge emission peaks, BE_1', BE_2', and BE_3' to radiative recombination of excitons bound to different neutral acceptors in $Ga_{1-x}In_xAs_ySb_{1-y}$ layers is based on their relatively narrow widths and their behavior as a function of incident laser power and temperature. However, there are a few aspects of our data which are rather intriguing. For instance, in sample α-23, both the bound exciton peak BE_2' and electron-to-acceptor transition A are quite strong. However, in samples β-9 and γ-11, the intensities of peaks A are much smaller than those of BE_1'. If the BE_1' transition is due to exciton bound to neutral acceptors, as we have suggested, then the electron to the same acceptor transition should have been quite strong. Also in GaSb and sample α-23, we see several bound exciton peaks, but only one strong electron-to-acceptor transition. It is clear that more work needs to be done, especially in higher purity samples, to understand these features and to gain a better understanding of the nature of the acceptors.

IV. CONCLUSIONS

Good optical-device-quality layers of GaSb and $Ga_{1-x}In_xAs_ySb_{1-y}$ have been grown by LPEE technique as evidenced by the narrow spectral width of x-ray-diffraction and PL spectra. A systematic trend in the low-temperature PL spectra is observed with the change in the composition of $Ga_{1-x}In_xAs_ySb_{1-y}$. The optical activation energy of the acceptor is about 35 meV and its phonon replica is shifted by about 30 meV towards the lower energy, consistent with the reported values in GaSb. The dissociation energies of the bound excitons in quaternary layers were also in good agreement with those in the binary layers. A good fit to the PL spectral line shape due to band-to-band transition was obtained using the simple model of van Roosbroeck–Shockley at higher energies and exponential band edge at lower energies. The PL transitions appear to be k conserved from the data presented.

ACKNOWLEDGMENTS

We wish to thank Lori Small for assisting in the computer simulation of a few of the graphs, Soon Lau from AT&T Bell Labs and Mike Caparo for x-ray-diffraction measurements and Gernot Pomrenke for helpful suggestions. This work was supported by AFOSR (Contract No. F49620-89-C-004) and U.S ARO (Grant No. DAAL03-89-G-0115). The work of S.H. was supported by the U.S. Air Force (Contract No. F33615-88-C-5423).

[1]M. J. Cherng, H. R. Jen, C. A. Larsen, G. B. Stringfellow, H. Lundt, and P. C. Taylor, J. Cryst. Growth **77**, 408 (1986).
[2]M. J. Cherng, G. B. Stringfellow, D. W. Kisker, A. K. Srivastava, and J. L. Zyskind, Appl. Phys. Lett. **48**, 419 (1986).
[3]T. H. Chiu, J. L. Zyskind, and W. T. Tsang, J. Electron. Mater. **16**, 57 (1987).
[4]W. T. Tsang, T. H. Chiu, D. W. Kisker, and J. A. Ditzenberger, Appl. Phys. Lett. **46**, 283 (1985).
[5]J. C. DeWinter, M. A. Pollack, A. K. Srivastava, and J. L. Zyskind, J. Electron. Mater. **14**, 729 (1985).
[6]A. Joullie, F. Jia Hua, F. Karouta, and H. Mani, J. Cryst. Growth **75**, 309 (1986).
[7]M. Astles, H. Hill, A. J. Williams, P. J. Wright, and M. L. Young, J. Electron. Mater. **15**, 41 (1986).
[8]R. Sankaran and G. A. Antypas, J. Cryst. Growth **36**, 198 (1976).
[9]E. R. Gertner, A. M. Andrews, L. O. Bubulac, D. T. Cheung, M. J. Ludowise, and R. A. Riedel, J. Electron. Mater. **8**, 545 (1979).
[10]N. Kobayashi and Y. Horikoshi, Jpn. J. Appl. Phys. **20**, 2253 (1981).
[11]Shanthi N. Iyer, Ali Abul-Fadl, Albert T. Macrander, Jonathan H. Lewis, Ward J. Collis, and James W. Sulhoff, in *Layer Structures: Heteroepitaxy, Superlattices, Strain, and Metastability*, edited by B. W. Dodson, L. K. Schowalter, J. E. Cunningham, and F. H. Pollak, MRS Symposia Proceedings No. 160 (Materials Research Society, Pittsburgh, 1990), p. 445.
[12]A. Okamoto, J. Lagowski, and H. C. Gatos, J. Appl. Phys. **53**, 1706 (1982).
[13]Y. Imamura, L. Jastrzebski, and H. C. Gatos, J. Electrochem. Soc. **125**, 1560 (1978).
[14]J. J. Daniele and A. Lewis, J. Electron. Mater. **12**, 1015 (1983).
[15]J. J. Daniele and A. J. Hebling, J. Appl. Phys. **52**, 4325 (1981).
[16]M. Kumagawa, A. F. Witt, M. Lichtensteiger, and H. C. Gatos, J. Electrochem. Soc. **120**, 583 (1973).
[17]C. Takenaka, T. Kusunoki, and K. Nakajima, J. Cryst. Growth **114**, 293 (1991).
[18]Toshiharu Kawabata and Susumu Koike, Appl. Phys. Lett. **43**, 490 (1983).
[19]S. Iyer, E. K. Stefanakos, A. Abul-Fadl, and W. J. Collis, J. Cryst. Growth **67**, 337 (1984).
[20]A. Abul-Fadl, E. K. Stefanakos, and W. J. Collis, J. Electron. Mater. **11**, 559 (1982).
[21]K. Nakajima and S. Yamazaki, J. Cryst. Growth **74**, 39 (1986).
[22]S. Iyer, E. K. Stefanakos, A. Abul-Fadl, and W. J. Collis, J. Cryst. Growth **70**, 162 (1985).
[23]D. Effer and P. J. Etter, J. Phys. Chem. Solids **25**, 451 (1964).
[24]M. H. van Maaren, J. Phys. Chem. Solids **27**, 472 (1966).
[25]Y. J. Van Der Meulen, J. Phys. Chem. Solids **28**, 25 (1967).
[26]C. Anayama, T. Tanahashi, H. Kuwatsuka, S. Nishiyama, S. Isozumi, and K. Nakajima, Appl. Phys. Lett. **56**, 239 (1990).

[27]C. Benoit a la Guillaume and P. Lavallard, Phys. Rev. B **5**, 4900 (1972).
[28]A. S. Kyuregyan, I. R. Lazareva, V. M. Stuchebnikov, and A. E. Yunovich, Fiz. Tekh. Poluprovodn. **6**, 242 (1972) [Sov. Phys. Semicond. 6, 208 (1972)].
[29]A. A. Kastal'skii, T. Risbaev, I. M. Fishman, and Yu. G. Shreter, Fiz. Tekh. Poluprovodn. **5**, 1596 (1972) [Sov. Phys. Semicond. **5**, 1391 (1972)].
[30]E. J. Johnson and H. Y. Fan, Phys. Rev. **139**, A1991 (1965).
[31]W. Jakowetz, W. Ruhle, K. Breuninger, and M. Pilkuhn, Phys. Status Solidi A **12**, 169 (1972).
[32]W. Ruhle and D. Bimberg, Phys. Rev. B **12**, 2382 (1975).
[33]W. Ruhle, W. Jakowetz, C. Wolk, R. Linnebach, and M. Pilkuhn, Phys. Status Solidi B **73**, 255 (1976).
[34]Fred H. Pollak and R. L. Aggarwal. Phys. Rev. B **4**, 432 (1971).
[35]M. Lee, D. J. Nicholas, K. E. Singer, and B. Hamilton, J. Appl. Phys. **59**, 2895 (1986).
[36]E. T. R. Chidley, S. K. Haywood, A. B. Henriques, N. J. Mason, R. J. Nicholas, and P. J. Walker, Semicond. Sci. Technol. **6**, 45 (1991).
[37]C. Pickering, J. Electron. Mater. **15**, 51 (1986).
[38]S. J. Eglash and H. K. Choi, in *Gallium Arsenide and Related Compounds, 1991*, edited by G. B. Stringfellow (IOP, London, 1992), p. 487.
[39]D. Bimberg, M. Sondergeld, and E. Grobe, Phys. Rev. B **4**, 3451 (1971).
[40]C. Caneau, A. K. Srivastava, J. L. Zyskind, J. W. Sulhoff, A. G. Dentai, and M. A. Pollack, Appl. Phys. Lett. **49**, 55 (1986).
[41]E. W. Williams and H. B. Bebb, in *Semiconductors and Semimetals*, edited by R. K. Willardson and A. C. Beer (Academic, New York, 1972), Vol. 4, Chap. 4.
[42]Ernst O. Gobel, in *GaInAsP Alloy Semiconductors*, edited by T. P. Pearsall (Wiley Interscience, New York, 1982), p. 320.
[43]T. P. Pearsall, L. Eaves, and J. C. Portal, J. Appl. Phys. **54**, 1037 (1983).
[44]H. Kyuragi, A. Suzuki, S. Matsumura, and H. Matsunami, Appl. Phys. Lett. **37**, 723 (1980).

APPENDIX B

J. Appl. Phys. 73, 3958-3961 (1993)

Photoluminescence study of liquid phase electroepitaxially grown GaInAsSb on (100)GaSb

S. Iyer
Department of Electrical Engineering, North Carolina A&T State University, Greensboro, North Carolina 27411

S. Hegde
University of Dayton Research Institute, Dayton, Ohio 45649-0178

K. K. Bajaj
Department of Physics, Emory University, Atlanta, Georgia 30322

Ali Abul-Fadl
Department of Electrical Engineering, North Carolina A&T State University, Greensboro, North Carolina 27411

W. Mitchel
Materials Directorate, Wright Laboratory, Wright Patterson Air Force Base, Ohio 45433-6533

(Received 3 February 1992; accepted for publication 10 December 1992)

Low-temperature (4.5 K) photoluminescence (PL) spectra of liquid phase electroepitaxially grown GaSb and GaInAsSb have been examined. The excitonic transitions observed in GaSb and GaInAsSb layers of compositions close to the GaSb corner of the phase diagram indicate an excellent quality of the grown layers. A systematic trend in the low-temperature PL spectra is observed with the change in the alloy composition. The overall PL emission efficiency decreases and the number of excitonic transitions are fewer with the shift in the composition towards the lower band gap. Shift in the PL peak energy corresponding to the band to band transition with temperature was determined. The linear part of the shift above 100 K exhibits a slope of -0.3 meV/K.

I. INTRODUCTION

Low-temperature photoluminescence (PL) has proven to be an effective method for characterization of the GaSb system, in particular for the layers grown by near equilibrium techniques where the choice of the substrate is severely limited. PL studies of GaSb grown by liquid phase epitaxy (LPE),[1-3] molecular beam epitaxy (MBE),[4,5] and metal-organic chemical-vapor deposition (MOCVD)[6] have been made by a number of workers. The presence of large background concentration of defects/impurities in this material leads to numerous acceptor bound exciton luminescence. Many of these transitions appear to be growth specific. Although there has been several reports on GaSb, there has been no detailed study reported to date on radiative transitions in GaInAsSb.

We have reported earlier[7] the first results on the growth of GaSb and GaInAsSb by the liquid phase electroepitaxial (LPEE) technique. This is a modified version of the LPE technique, where an electric current passing through the substrate-solution interface enables better control of the growth rate[8] and enhances the interface stability,[9] leading to a better compositional homogeneity[10] in the epilayers and significant improvement in the surface morphology.[11]

In this article we report the low-temperature (4.5 K) Fourier transform photoluminescence (PL) study of the LPEE grown epilayers of GaSb and $Ga_{1-x}In_xAs_ySb_{1-y}$. Samples of GaSb and three different compositions of quaternary alloys $Ga_{0.972}In_{0.028}As_{0.016}Sb_{0.984}$, $Ga_{0.912}In_{0.088}As_{0.056}Sb_{0.944}$, and $Ga_{0.83}In_{0.17}As_{0.14}Sb_{0.86}$ labeled as α-23, β-9, and γ-11, respectively, were studied. The layers α-23 and γ-11 were lattice matched to the (100) GaSb substrate while β-9 was mismatched by 0.048%. The room-temperature PL peak wavelengths of band edge related peaks in these samples ranged from 1.7 to 2.28 μm. The results of the variation in the PL spectral characteristics with composition and the temperature dependence of the band edge related transitions are reported.

II. EXPERIMENTAL DETAILS

The details of the growth and characterization of the layers are described elsewhere.[7] Layer compositions were determined using energy dispersive x-ray analysis. Photoluminescence spectra were obtained using a Bomem fourier transform spectrometer and a cooled (77 K) InAs detector. The samples were immersed in a variable temperature continuous flow liquid helium cryostat and were excited with a 514.5 nm line of an Ar-ion laser.

III. RESULTS AND DISCUSSION

Figure 1 illustrates the PL spectra of LPEE grown GaSb and GaInAsSb epilayers. The PL emission intensity has been normalized with respect to the dominant peak present in each of the samples. Integrated intensity, exciton dissociation energy, and assignment of the observed peaks in 4.2 K PL energy spectra of GaSb and GaInAsSb samples are summarized in Tables I and II, respectively. The energy position and full width at half maximum (FWHM)

 0021-8979/93/083958-04$06.00 © 1993 American Institute of Physics

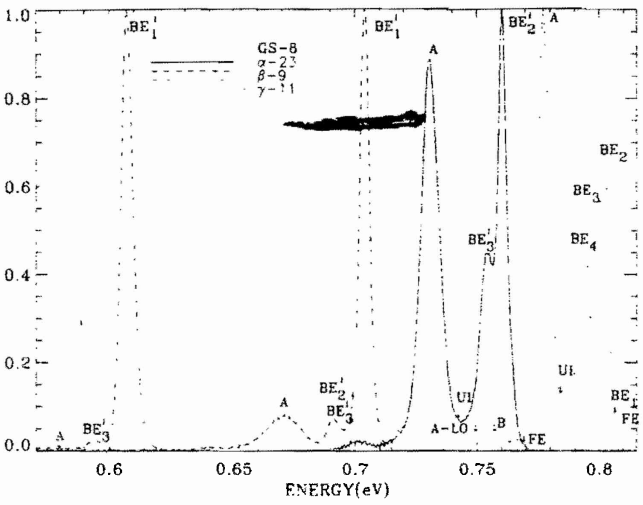

G. 1. Low-temperature (4.5 K) PL spectra of GaSb and GaInAsSb of ree different compositions.

each peak have been determined by a quantitative fit to e experimental PL spectra using the sum of Gaussian line stributions.

As illustrated in Fig. 1, in GaSb (GS-8) five band edge L emission peaks labeled as FE, BE_1, BE_2, BE_3, and BE_4 e observed at 808.5, 805.4, 802.2, 799.1, and 795.8 meV, spectively, as in the LPE grown layers. The presence of a eak broad shoulder at 808.5 meV has been associated ith the free exciton (FE). This indicates the good quality the crystalline LPEE layers. The other lines have been tributed to the decay of excitons bound (BE) to the eutral acceptors. BE_2 has been ascribed[12,13] to the decay an exciton bound to a dominant residual acceptor level, hich has a binding energy of 34 meV. Little is known bout the acceptors corresponding to the two transitions E_1 and BE_3, while there are conflicting reports[2,13–15] as to e origin of the transition BE_4. In the LPEE grown layers nlike LPE, BE_2 is found to be the strongest peak amongst e bound excitons. The band to acceptor transition (A) at 77.5 meV is found to be the dominant peak in the PL ectra and this acceptor with a binding energy of 34 meV as been associated with a complex native defects due to Sb acancies.[16,17] In addition to these, a broadband at a lower

TABLE I. Low-temperature PL features reported in LPE grown GaSb and from current study. A is the band-residual acceptor transition, B is the band-acceptor transition, C is the second ionization level of acceptor A, and ΔE is the exciton dissociation energy.

	Refs. 1, 2	Our Work		
Identity	Energy (meV)	Energy (meV)	ΔE (meV)	Relative intensity
FE	809.9	808.5	0.0	0.05
UI	808.7			
UI	808.0			
BE_1	805.4	805.4	3.1	0.02
BE_2	803.4	802.2	6.3	0.69
BE_3	800.1	799.1	9.4	0.34
BE_4	796.1	795.8	12.7	0.48
UI	795.0			
UI		784.8		0.09
A	777.5	777.5		1.00
BE_4-LO	766.0	765.6		0.03
B	757.0	756.3		0.04
A-LO	748.5	748.2		0.03
B-LO	728.0			
C	710.0			

energy can be resolved to consist of acceptor related transition (B) with a binding energy of 54 meV, phonon replica of A and an unidentified line at 784.8 meV. This unidentified line has also been reported in MBE[4] and MOCVD[6] grown layers. The bound excitons are somewhat broader (with FWHM 1–5 meV) than in the best LPE grown layers with FWHM as low as 0.3 meV for BE_1 reported in the literature.[1] However, it is to be noted that no extensive baking of the melt was carried out prior to the growth of these layers as our primary objective was to use the PL spectral features of GaSb as a reference to get a better understanding of the transitions in the alloy system.

The PL spectra of the quaternary layers exhibit features similar to those described for GaSb layers, however fewer near band edge structures are seen in general. A definite trend in the overall PL spectra is seen with the shift in the composition towards InAs. The overall integrated intensity remains the same for GaSb, α, and β layers, but decreases by almost a factor of 5–10 for γ samples. Free exciton (FE) transition is seen only in the α-23 sample as a weak band on the higher energy spectrum. This feature is seen in both GaSb and quaternary layers under the highest

ABLE II. Low-temperature PL features observed in LPEE grown GaInAsSb layers.

	α-23			β-9			γ-11		
en.	Energy (meV)	Rel. int.	ΔE (meV)	Energy (meV)	Rel. int.	ΔE (meV)	Energy (meV)	Rel. int.	ΔE (meV)
E	765.0		0.00						
E_1'				703.8	1.0	3.0[a]	607.1	1.0	3.0[a]
E_2'	760.5	1.00	4.6	697.9	0.04	8.9[a]			
E_3'	754.3	0.48	10.7	691.1	0.07	15.7[a]	594.1	0.02	16.0[a]
I	742.2	0.07							
	730.6	0.97		670.9	0.08		578.1	0.002	
-LO	702.2	0.03		640.2					

Estimated value of the exciton dissociation energy (ΔE).

excitation level used, typical of a free exciton. In addition, two sharp band edge related transitions (labeled as BE_2' and BE_3') with a FWHM of 4 and 7 meV, respectively, are observed. With the shift in the composition towards higher values of x, the highest energy transition line identified as BE_1' becomes dominant accompanied with a weaker transition BE_3' shifted by 12–13 meV towards the lower energy side. We suggest that these transitions labeled as BE′ are associated with the decay of excitons bound to different neutral acceptors with different concentrations leading to different PL intensities. Our assignment is primarily based on the values of their linewidths and the observed temperature and excitation intensity dependence. First, the spectral distribution of the bound excitons is found to be close to Gaussian with a relatively narrow FWHM in the range of 3–7 meV. Second, the variation of the PL integrated intensity with the excitation intensity revealed a slope of 2 for BE_1' in β and γ layers, 1.4 for BE_2' in α layers, and 1.22 for BE_3' in α and β layers.[18] We have computed the value of this slope using the well-known rate equations. It is found that this value may vary from 1 to 2 depending upon the values used for various recombination parameters, which are highly sample dependent. Third, these transitions are rapidly quenched with increasing temperature by 35–40 K. All these observations are consistent with the expected behavior of the bound excitons.

In addition to the above transitions, we also observe a transition corresponding to free electron to acceptor recombination (A). This transition is very strong in the α sample and becomes weaker in other quaternary alloys. In the γ sample, it is observed only at high sensitivities. This is consistent with the reported observation on alloys grown by nonequilibrium[19,20] techniques where only one peak is seen for layers with compositions closer to or inside the miscibility gap region. The identity of this transition in all the quaternary layers was also further confirmed from the PL intensity dependence with the excitation intensity, which exhibit a perfectly linear variation with a slope of 1.0.

The binding energy of this acceptor can accurately be determined only if the band gaps of the alloys are known. The band gap in the α-23 sample is obtained by adding the free exciton binding energy ($\sim$1.1 meV) to the free exciton transition energy (765.0 meV). The acceptor binding energy obtained in this case is about 35 meV, which is in excellent agreement with the values obtained in GaSb. However, in β and γ layers, due to the absence of the free exciton transition line, the band to band transition can only be estimated. If an exciton dissociation energy of 3 meV for BE_1' with a FE binding energy of 1 meV is assumed, it leads to acceptor binding energies in the range of 33–37 meV, which again agree quite well with that observed in GaSb.

The broad line shifted by 28–30 meV of the A peak seen towards the lower energy side in the quaternary layers has been labeled as the longitudinal optical (LO) phonon replica of A(A-LO), as this energy is very close to the optical phonon energy reported in GaSb.[21] The ratio of the intensity of the A peak and that of the A-LO peak is in the range 32–40 and remains invariant within experimental error with laser power intensity and decreases with increase in temperature. This trend is consistent with the expected behavior of the phonon sideband, further strengthening the assignment of this peak.

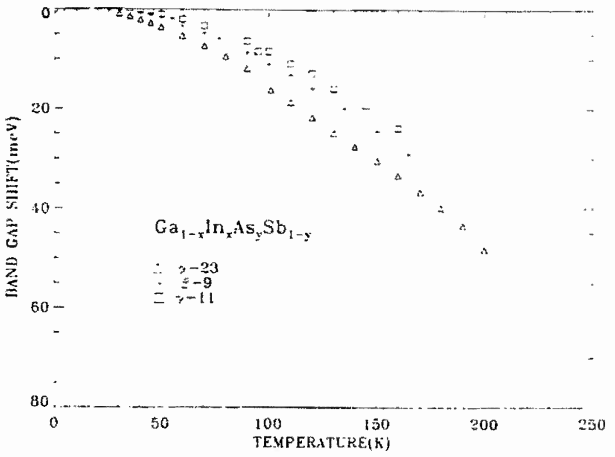

FIG. 2. Temperature dependence of the band-gap shift for GaInAsSb layers of three different compositions.

Temperature dependence of the band to band transition was also examined in the temperature range of 4.5–300 K. The variation of the PL peak energy corresponding to the band to band transition follows the well-known empirical formulation of Varshni,[22] which is given by

$$E_g = E_{g0} - [\alpha T^2/(\beta + T)],$$

where E_{g0} represents the extrapolated value of the band gap at 0 K and α and β are empirical parameters. At low temperatures, the binding energy of the bound exciton was taken into account for the estimation of the band-gap transition as explained earlier. Care was taken that a good fit to data is obtained at higher temperatures ($\geqslant$40 K). Figure 2 shows the temperature dependence of the band-gap shift for the three different alloy layers investigated. The values of α and β that resulted in a best fit to the experimental data is tabulated in Table III. It may be noted that the value of E_{g0} is close to (within 1 meV) our earlier estimation of the band gaps of the alloys. For GaSb, the values of α and β are in excellent agreement with those reported by Camassel *et al.*[23] However, they are considerably larger for the other layers which may be an indication of the presence of a high degree of disorder in these layers. In the temperature range of 100–300 K, the linear portion of the plot exhibited a slope of ≈ -0.31 meV/K for the quater-

TABLE III. Variation of band to band transition in $Ga_{1-x}In_xAs_ySb_{1-y}$ with temperature.

	$E_g = E_{g0} - \alpha T^2/(\beta + T)$			
Sample No.	λ_{PL} (RT) (μm)	E_{g0} (eV)	α (10^{-4} V/K)	β (K)
GS-8	1.70	0.810	3.80	94
α-23	1.81	0.767	6.43	329
β-9	1.96	0.706	5.28	285
γ-11	2.25	0.611	3.36	156

nary layers. This compares well with the value of −0.37 meV/K for GaSb.[23] The implication is that a variation of 7–13 Å/K could be expected in the emission peak wavelength of the lasers and light emitting diodes (LEDs) fabricated from GaSb and its alloy system.

IV. CONCLUSIONS

In conclusion, we have examined the near band edge PL features of LPEE grown GaInAsSb layers on a (100) GaSb substrate. Considering the fact that this is a quaternary alloy system and hence even a small statistical inhomogeneity in the composition could cause sufficient potential fluctuations to result in significant spectral broadening, the values of the FWHM of the bound excitons and the presence of FE attest to the high optical quality of the quaternary layers grown. Temperature dependence of the band to band transition has also been studied.

ACKNOWLEDGMENTS

This work was supported by AFOSR (Contract No. F49620-89-C-004) and USARO (Grant No. DAAL03-89-G-0115). The work of S. H. was supported by the Air Force (Contract No. F33615-88-C-5423).

[1] W. Ruhle, W. Jakowetz, C. Wolk, R. Linnebach, and M. Pilkuhn, Phys. Status Solidi B **73**, 255 (1976).
[2] W. Jakowetz, W. Ruhle, K. Breuninger, and M. Pilkuhn, Phys. Status Solidi A **12**, 169 (1972).
[3] S. C. Chen and Y. K. Su, J. Appl. Phys. **66**, 350 (1989).
[4] M. Lee, D. J. Nicholas, K. E. Singer, and B. Hamilton, J. Appl. Phys. **59**, 2895 (1986).
[5] K. F. Longenbach and W. I. Wang, Appl. Phys. Lett. **59**, 2427 (1991).
[6] E. T. R. Chidley, S. K. Haywood, A. B. Henriques, N. J. Mason, R. J. Nicholas, and P. J. Walker, Semicond. Sci. Technol. **6**, 45 (1991).
[7] S. N. Iyer, A. Abul-Fadl, A. T. Macrander, J. H. Lewis, W. J. Collis, and J. W. Sulhoff, Mater Res. Symp. Proc. **160**, 445 (1990).
[8] C. Takenaka, T. Kusunoki, and K. Nakajima, J. Cryst. Growth **114**, 293 (1991).
[9] A. Okamoto, J. Lagowski, and H. C. Gatos, J. Appl. Phys. **53**, 1706 (1982).
[10] J. J. Daniele and A. Lewis, J. Electron. Mater. **12**, 1015 (1983).
[11] Y. Imamura, L. Jastrzebski, and H. C. Gatos, J. Electrochem. Soc. **125**, 1560 (1978).
[12] E. J. Johnson and H. Y. Fan, Phys. Rev. **139**, A1991 (1965).
[13] C. Benoit a la Guillaume and P. Lavallard, Phys. Rev. B **5**, 4900 (1972).
[14] W. Ruhle and D. Bimberg, Phys. Rev. B **12**, 2382 (1975).
[15] Fred H. Pollack and R. L. Aggarwal, Phys. Rev. B **4**, 432 (1971).
[16] D. Effer and P. J. Etter, J. Phys. Chem. Solids **25**, 451 (1964).
[17] Y. J. Van der Meulen, J. Phys. Chem. Solids **28**, 25 (1967).
[18] S. Iyer, S. Hegde, A. Abul-Fadl, K. K. Bajaj, and W. Mitchel, Phys. Rev. B **47**, 1329 (1993).
[19] S. J. Eglash and H. K. Choi, Inst. Phys. Conf. Ser. **120**, 487 (1992).
[20] T. H. Chiu, J. L. Zyskind, and W. T. Tsang, J. Electron. Mater. **16**, 57 (1987).
[21] C. Pickering, J. Electron. Mater. **15**, 51 (1986).
[22] Y. P. Varshni, Physica **34**, 149 (1967).
[23] J. Camassel and D. Auvergene, Phys. Rev. B **12**, 3258 (1975).

APPENDIX C

MRS Symp. Proc. 299,41-46 (1993)
(In Print)

LOW TEMPERATURE PL CHARACTERIZATION OF LPEE GROWN GaSb AND GaInAsSb EPILAYERS

S. IYER*, S. HEGDE**,K.K. BAJAJ***, ALI ABUL-FADL* AND W. MITCHEL****
*Department of Electrical Engineering, North Carolina A&T State University, Greensboro, NC 27411.
**University of Dayton Research Institute, Dayton, OH 45649-0178.
***Department of Physics,Emory University, Atlanta, GA 30322
****Materials Directorate,Wright Laboratory, Wright Patterson Air Force Base, OH 45433-6533.

ABSTRACT

We have investigated the low temperature (4.5 K) photoluminescence (PL) spectra of GaSb and GaInAsSb layers. The layers were grown by liquid phase electro-epitaxial (LPEE) technique. Several bound excitonic transitions were observed both in GaSb and GaInAsSb layers. Shift in the PL peak energy corresponding to the band to band transition with temperature was determined. The linear part of the shift above 100K, exhibited a slope of -0.3 meV/K.

INTRODUCTION

In recent years, the III-V quaternary alloys GaInAsSb have become an important building block for infrared devices. It is well known that GaSb exhibits p-type conductivity and generally has been accepted to be associated with the native defects due to Sb deficiency [1,2]. These defects and background impurities, which are strongly growth dependent, play an important role in determining the characteristics of these layers. Due to the presence of various residual acceptors, the low temperature PL of GaSb exhibits numerous band edge transitions [3-5]. The nature of these transitions is poorly understood [3,6,7]. Further, the information on the quaternary alloys is very limited. Here we report on our systematic effort to get a better understanding in this area.

The epilayers of GaSb and $Ga_{1-x}In_xAs_ySb_{1-y}$ were grown on GaSb by liquid phase electro-epitaxial (LPEE) technique. The advantages of LPEE over LPE grown layers are well established [8-10]. Samples of GaSb and three different compositions of quaternary alloys $Ga_{0.972}In_{0.028}As_{0.016}Sb_{0.984}$, $Ga_{0.912}In_{0.088}As_{0.056}Sb_{0.944}$ and $Ga_{0.83}In_{0.17}As_{0.14}Sb_{0.86}$ labelled as α-23,β-9 and γ-11, respectively were investigated. The layers α-23 and γ-11 were lattice matched to (100) GaSb substrate while β-9 was mismatched by 0.048%. The room temperature PL peak wavelengths of band edge related peaks in these samples ranged from 1.7 μm to 2.28 μm. The variation in the PL spectral characteristics with composition has been summarized and the temperature dependence of the band edge related transitions is reported.

EXPERIMENTAL DETAILS

The layers were grown by conventional horizontal slider boat system modified for the passage of current through the substrate-melt interface. (100) oriented GaSb substrates of 6mmx6mm area were used. The details of the growth are described elsewhere [11]. Photoluminescence spectra were obtained using a Bomem Fourier transform spectrometer and a cooled (77 K) InAs detector. The samples were immersed in a variable temperature continuous flow liquid helium cryostat and were excited with 514.5 nm line of an Ar-ion laser.

S. Iyer

RESULTS AND DISCUSSION

Figure 1 illustrates the PL spectra of LPEE grown GaSb and GaInAsSb epilayers at 4.5K. The PL emission intensity has been normalized with respect to the dominant peak present in each of the samples. The energy position and the intensity of each peak , as tabulated in Table 1 have been determined by a quantitative fit to the experimental PL spectra using sum of Gaussian line distributions.

As illustrated in Figure 1, in GaSb (GS-8) five band edge PL emission peaks labeled as BE_1, BE_2, BE_3 and BE_4 are observed at 805.4, 802.2, 799.1 and 795.8 meV, respectively as in the LPE grown layers, in addition to free exciton transition at 808.5 meV. The origin of the various bound exciton peaks has been a subject of considerable controversy [3,6,7]. Nevertheless, it has been generally accepted that these excitons are bound to different acceptors. The dominant band to acceptor transition (A) at 777.5 meV commonly observed in LPE layers, along with its phonon replica shifted by 30 meV towards the lower energy have been resolved. Another, relatively weak, deep acceptor related transition (B) is observed at 756.3 meV, which becomes dominant in the Te doped layers. An unidentified line at 784.8 meV reported in MOCVD [3] and MBE [4] grown layers is also present.

The PL spectra of the quaternary layers exhibit features similar to those described for GaSb layers, however a fewer near band edge structures are seen. The overall integrated intensity remains the same for GaSb, α and β layers, but decreases by almost a factor of five to ten for γ samples. Free exciton (FE) transition is seen only in α-23 sample as a weak band on the higher energy spectrum. First few band edge transitions in the quaternary layers have been associated with the bound exciton transitions. Our assignment is based on the narrow linewidths exhibited by these transitions and the observed temperature and excitation intensity dependence of these peaks, which were consistent with that of the bound excitons [12]. The PL line corresponding to the recombination of a free electron to the hole bound to the acceptor (A) was also identified, though the PL integrated intensity significantly decreases with the compositional shift towards the lower gap. The binding energy of this acceptor is in the range of 33-38 meV and is in good agreement with that reported in GaSb. LO phonon replica of A (A-LO) was resolved only in α layers.

The question of course arises as to the presence and dominance of the various bound excitons in the quaternary layers with only one relatively weak band to acceptor recombination. The relatively large binding energies associated with some of the bound excitons in GaSb and the quaternary layers (estimated to be about 6-16 meV) [12,13] are indicative of the presence of deep acceptor centers to which these excitons are bound. Hence, the simple hydrogenic model normally used for shallow centers is not adequate in explaining these observed characteristics. More experimental and theoretical work is needed to get a better insight into the nature of these centers.

Figure 2 depicts the variation of the band to band transition with temperature in the range 4.5K to 300K and was found to follow the well known empirical formulation of Varshni [14] given by

$$E_g = E_{go} - [\alpha T^2/(\beta + T)]$$

E_{go} represents the extrapolated value of the band gap at 0^oK , α and β are empirical parameters. At low temperatures, binding energy of the bound exciton was taken into account for the estimation of the band gap. The values of α and β that resulted in a best fit to the experimental data is tabulated in Table 2. The values of these two parameters are significantly higher in α-23 and β-9 layers than those in GaSb probably indicative of higher disorder in these layers. At temperatures higher than 100K, the band gap decreases linearly with temperature exhibiting a slope of -0.31 meV/K in good agreement with that of GaSb.

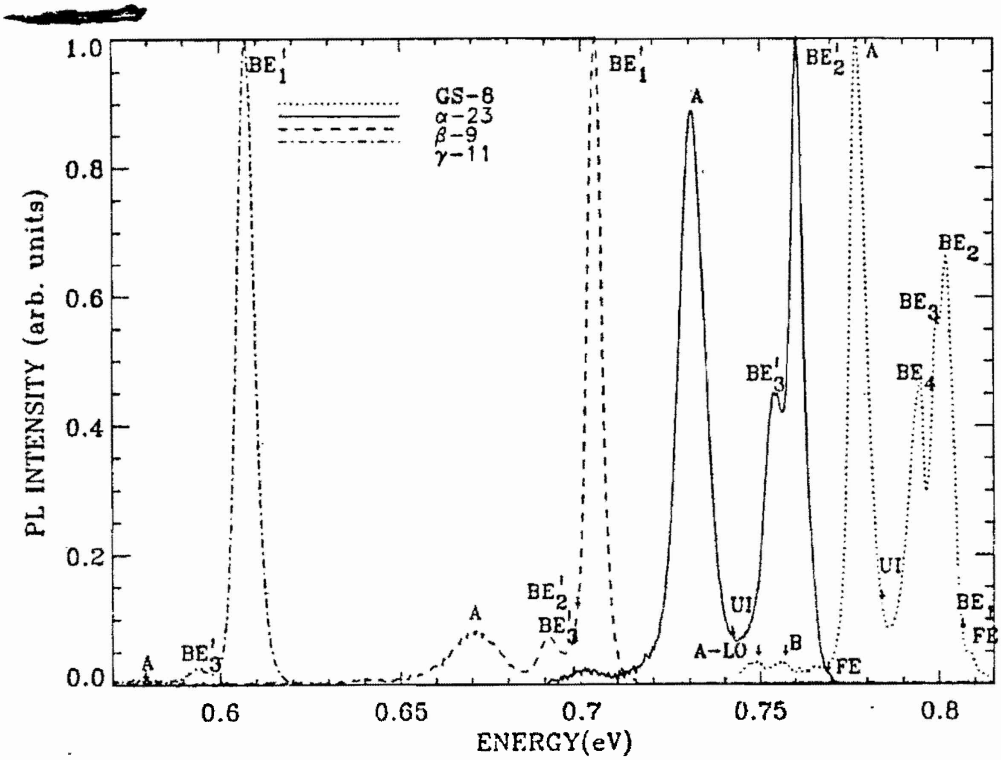

Fig. 1. Low temperature (4.5K) PL spectra of GaSb and GaInAsSb of three different compositions

TABLE I Low temperature PL features observed in LPEE grown GaSb and GaInAsSb layers.

	GaSb			α-23		β-9		γ-11	
Identity	Energy (meV)	Rel. Int.	Iden-tity	Energy (meV)	Rel. Int.	Energy (meV)	Rel. Int.	Energy (meV)	Rel. Int.
FE	808.5	0.05	FE	765.0					
BE_1	805.4	0.02	BE_1'			703.8	1.0	607.1	1.0
BE_2	802.2	0.69	BE_2'	760.5	1.00	697.9	0.04		
BE_3	799.1	0.34	BE_3'	754.3	0.48	691.1	0.07	594.1	0.02
BE_4	795.8	0.48							
UI	784.8	0.09	UI	742.2	0.07				
A	777.5	1.00	A	730.6	0.97	670.9	0.08	578.1	0.002
BE_4-LO	765.6	0.03							
B	756.3	0.04							
A-LO	748.2	0.03	A-LO	702.2	0.03	640.2			

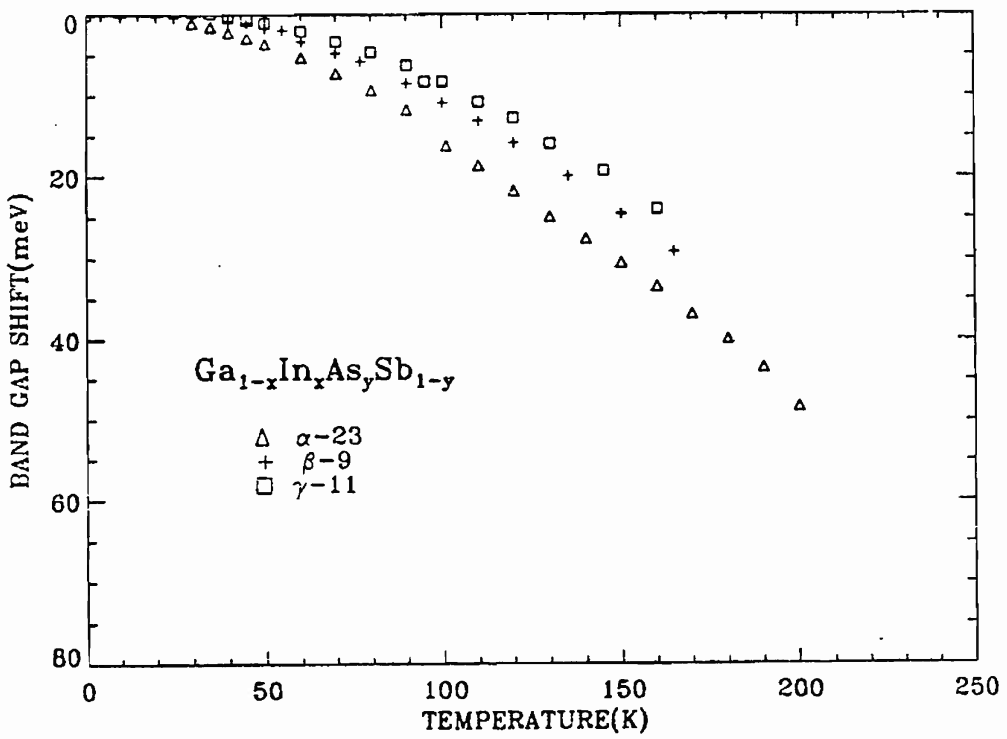

Fig.2. Temperature dependence of the band gap shift for GaInAsSb layers of three different compositions.

TABLE II. Variation of band to band transition in GaInAsSb with temperature.

$E_g=E_{go}-\alpha T^2/(\beta+T)$				
Sample #	λ_{PL} @ RT (μm)	E_{go} (eV)	α (10^{-4}V/°K)	β (°K)
GS-8	1.70	0.810	3.80	94
α-23	1.81	0.767	6.43	329
β-9	1.96	0.706	5.28	285
γ-11	2.25	0.611	3.36	156

This work was supported by AFOSR (Contract No. F49620-89-C-004) and USARO (Grant No. DAAL03-89-G-0115). Work of S.H. was supported by Air Force (Contract No. F33615-88-C-5423).

REFERENCES

1. Y.J.Van Der Meulen, J. Phys. Chem. Solids **28**, 25 (1967).
2. C.Anayama, T.Tanahashi, H.Kuwatsuka, S.Nishiyama, S.Isozumi,and K.Nakajima, Appl. Phys. Lett. **56**, 239 (1990).
3. E.T.R. Chidley, S.K. Haywood, A.B. Henriques, N.J. Mason, R.J. Nicholas and P.J. Walker, Semicond. Sci. Technol. **6**, 45 (1991).
4. M. Lee, D.J. Nicholas, K.E. Singer and B. Hamilton, J. Appl. Phys. **59**, 2895 (1986).
5. W. Ruhle, W. Jakowetz, C. Wolk, R. Linnebach and M. Pilkuhn, Phys. Stat. Sol.(B) **73**, 255 (1976).
6. C. Benoit a la Guillaume and P. Lavallard, Phys. Rev. B **5**, 4900 (1972).
7. E.J. Johnson and H. Y. Fan, Phys. Rev. **139**, A1991 (1965).
8. C.Takenaka,T.Kusunoki and K.Nakajima, J.Cryst.Growth **114** 293(1991)
9. A. Okamoto, J. Lagowski and H.C. Gatos, J. Appl. Phys. **53**, 1706 (1982).
10. J.J. Daniele and A. Lewis, J. Electron. Mater. **12**, 1015 (1983).
11. Shanthi N. Iyer, Ali Abul-Fadl, Albert T. Macrander, Jonathan H. Lewis, Ward J. Collis and James W. Sulhoff, Mat. Res. Symp. Proc. **160**, 445 (1990).
12. S.Iyer, S.Hegde, Ali Abul-Fadl, K.K.Bajaj and W.Mitchel, Phys. Rev. B.**47**, 1329 (1993).
13. S.Iyer, S. Hegde, K.K. Bajaj, A. Abul-Fadl and W. Mitchel, J. Appl. Phys.**73**, 3948 (1993).
14. Y. P. Varshni, Physica **34**, 149 (1967).

APPENDIX D

MRS Symp. Proc. 316,185-190 (1994)

ION IMPLANTATION DAMAGE AND ANNEALING IN GaSb

S. IYER*, R. PARAKKAT*, B.PATNAIK**, N.PARIKH** and S.HEGDE***
* Department of Electrical Engineering, North Carolina A&T State University, Greensboro, NC 27411
** Department of Physics and Astronomy, University of North Carolina, Chapel Hill, NC 27599
*** University of Dayton Research Institute, Dayton, OH 45649-0178

Ion implantation technique is being investigated as an alternate technique for doping GaSb. Hence an understanding of the production and removal of the damage is essential. In this paper, we report on the damages produced by implantation of Te, Er, Hg and Pb ions into undoped (100) GaSb single crystals and their recovery by Rutherford backscattering (RBS)/channeling. The implantations of 10^{13} to 10^{15} ions/cm^2 in GaSb were done at liquid nitrogen temperature at energies corresponding to the same projected range of 447Å. A comparison of the damage produced by the different ions and their recovery was made by RBS/channeling along <100> axis of GaSb. Near surface damage equivalent to that of an amorphous layer was observed even at lower doses. Upon annealing at 600°C for 30 sec., the Te implanted samples showed best recovery compared to others (χ_{min} = 11%), the value of χ_{min} being better than those normally observed in unimplanted Te-doped substrates.

INTRODUCTION

Ion-implantation has been used in III-V semiconductors as an important doping technique. It has the advantage of being a low temperature process that allows accurate control of the dopant profile with good reproducibility. The application to optoelectronic devices has made GaSb particularly attractive for research. To date there has been only limited study on the ion implanted GaSb materials. The damage removal process in GaSb seems to be more complex in comparison to other III-V compounds. Pearton et al.[1] and Von Neida et al. [2] have assessed the disorder produced in GaSb implanted with Si and Mg., using Rutherford backscattering (RBS). Rapid thermal annealing (RTA) is found to recover the crystalline quality of the damaged layer much more effectively than furnace annealing [3]. In Si implanted layers, the best results on the recovery of layers have been found on samples rapid thermal annealed at 600° C for 30 s [3]. Remnant damages were observed to be in the form of dislocation loops and microtwins [1]. Higher annealing times and temperatures resulted in surface degradation of the samples [3]. In Mg implanted GaSb [2], though RTA did not result in any significant redistribution on the substrate side of the implant profile, a significant loss of Mg to the surface and gettering to regions of maximum disorder was observed.

Anomalous elevations up to 6μm in the surface region of GaSb [4] and large incorporation of oxygen in ion-implanted GaSb have been reported [2,4] which is similar to the behavior observed in heavily damaged InSb[5]. However, swelling phenomenon has

Mat. Res. Soc. Symp. Proc. Vol. 316. ©1994 Materials Research Society

been attributed to the formation of a porous layer, unlike in InSb [5-7] where the surface expansion phenomenon has been correlated to the enhanced oxygen absorption at the surface.

To date, all the published reports have been on room temperature implanted GaSb samples and the regrowth process of the implanted layer was found to be unsuccessful for the cases when the near surface regions were amorphized [1]. In this paper, we report on the mechanism of production and removal of damages in 77 K implanted GaSb samples. We have attempted to compare quantitatively by RBS/channeling, the amount of damage produced in the form of atoms displaced from their normal sites in the as implanted samples and after rapid thermal annealing, thereby estimate the percentage of damage recovery. Dependance of damages on atomic weight and dosages of the implanted species on (100) GaSb was investigated , with an emphasis on annealing dependance of the Te implanted samples. All the implanted samples were amorphized in the near surface region for the doses of implants examined and the extent of recovery of the lattice is found to be functions of both the atomic weights and dosages of the implanted species.

EXPERIMENTAL

Undoped (100) GaSb were implanted with Te, Er, Hg and Pb at liquid nitrogen temperature for three different fluences in the range of 10^{13}, 10^{14} and 10^{15} /cm^2 at 146 KeV, 180 KeV, 200 KeV and 206 KeV, respectively. The dosages and the implantation energies were chosen so that the same amounts of energy were deposited by nuclear collisions on the substrate in roughly the same volume. TRIM calculations indicated the projected range to be ~ 447Å . The damage distribution was determined by 2 MeV He^+ Rutherford backscattering/channeling along <100> axis with the detector kept at 170°. It was also possible to detect the heavier implanted atomic species especially for higher doses. In contrast, Te could not be distinguished from Sb in the RBS spectra, because of its proximity in mass. Rapid thermal annealing was performed in nitrogen ambient by placing the samples face down on top of a similar material to minimize the loss of the volatile constituents. Annealing was carried out at 600°C in all cases except the samples with Hg , where annealing was done at 300°C to avoid preferential evaporation of the implant. Surface morphology was examined using field emission scanning electron microscope. A few of the Te doped samples were characterized by Secondary Ion Mass Spectroscopy (SIMS) using Cs^+ ion beam in a Perkin Elmer 6300 system to study the redistribution of the implanted ions on annealing. Step height measurements were carried out by Tencor Profiler.

RESULTS AND DISCUSSION

Fig.1 shows the RBS spectra of 2 MeV He^+ ions scattered at 170^0 from a GaSb sample, aligned along <100>, as implanted with 10^{13} Te ions/cm^2 and after annealing at 600°C for 60 s. Also shown is a spectrum of the same sample in random orientation. The peaks at the highest channel numbers of the aligned spectra represent the yield of He^+ ions scattered from the Ga and Sb atoms displaced from their normal lattice sites. The area under the peaks

gives a measure of the damage of the GaSb substrate. As can be seen in Fig.1, the height of the damage peak of the as implanted sample reaches that of the random orientation, indicative of an amorphized surface layer. This was indeed observed for all the as implanted samples. The scattering yields immediately to the left of the peaks in the aligned spectra correspond to the substrate depths just beyond the damaged layer. The ratio of this yield to the yield at the same depth for random orientation is denoted by χ_{min}. Upon annealing at 600°C, the area under the damaged peak as well as χ_{min}, decrease, showing partial recovery of the damage. Comparing the areas of the residual damage peaks after annealing with that of the as implanted samples, we obtain the fractional residual damages for different annealing times. These, along with the values of the χ_{min} are shown in Table I.

As Te implanted GaSb has a potential application for devices, the study was mostly focussed on these samples. The results of RBS/channeling spectra of the GaSb samples implanted with 10^{13} Te ions/cm^2, before and after annealing at 600°C for 30,60,90 and 120 s are tabulated in Table 1. Durations of 30- 60 s appear to be the optimum annealing time for achieving low χ_{min} and low residual damage. For longer annealing, χ_{min} either degrades or remains the same. Examination of surface morphology by SEM revealed significant degradation of the surface for annealing durations beyond 90 s. The lowest residual disorder and χ_{min} is obtained at lower implantation doses as expected. The samples with 10^{13} Te ions/cm^2 annealed for 30 s had a backscattering yield as low as 11% , which is better than the yield normally observed in unimplanted Te-doped GaSb substrates. These unimplanted substrates also showed an improvement in the crystalline quality on annealing. Presumably the Te-doped (unimplanted) substrates have inherent defects which anneal out under annealing.

In the samples implanted with 10^{15} ions/cm^2, a considerable deficit in the backscattering yield from Sb atoms near the surface was noticed (see Fig.2), when annealed at 600°C beyond 60 s. There are evidences of preferential evaporation of Sb at the surface and of enhanced oxygen incorporation in these samples from SIMS data.

SIMS depth profile of the Te implanted samples did not indicate any significant redistribution of the dopant on annealing . Surface morphology of these layers exhibited systematic change from smooth to sponge like appearance with increasing dosages. In addition anomalous expansion from 30-40 Å to 600Å of the implanted surface region was also observed with increasing dopant dosages. This is consistent with the observations reported in room temperature implanted GaSb where swellings up to 6μm were observed for Ar^+ implantations of similar energies and dosages [4]. The swelling phenomenon was attributed to the formation of a porous layer and was found to be a function of the atomic mass of the dopant, energy of implantation and the dosage of implanted ions [4].

RBS/channeling analysis of the samples implanted with Er, Pb and Hg all showed that the scattering yield from the damaged layer reached the random level. In general, at high influences of 10^{15} ions/cm^2, χ_{min} for the as implanted samples showed an increasing trend with the atomic weight of the implanted species. This result is in accordance with the observations in other III-V semiconductors, where heavier ions were found to produce more damage on implantation. On Pb-implanted samples at this high fluence, the damage was extensive enough to preclude channeling of the He^+ ions past this layer. However, at low dosage, the χ_{min} appears to be in the range of 34 to 54% and no definite trend was observed. Considerable scatter in these data could be attributed to the variation in the χ_{min} (4 to 10%) observed for the starting GaSb wafers. After implantation and annealing at 600°C for 30 to 120 s duration, all but the Hg-implanted samples exhibited significant recovery, with the best results achieved in the Te-implanted samples. In general, the recovery of the

Table I

Implantation parameters and RBS data on the annealing behavior of different elements in undoped (100) GaSb

ELEMENT	DOSAGE (/cm²)	FRACTION OF DAMAGE (%) AFTER ANNEALING DURATION (SEC)				χ_{min} (%)			
		30	60	90	120	AI	ANNEALING DURATION (SEC) 30	60	90
Te	$1.2X10^{13}$	12	5	6	4	50	11	12	13
	$1.2X10^{14}$	13	12	16	13	54	17	12	
	$1.2X10^{15}$	25	18	--	--	54	33	26	27
Er	$1.1X10^{13}$					54	17		
	$1.1X10^{14}$					49	18		
	$1.1X10^{15}$					48	25		
Hg	$1.1X10^{13}$					34			
	$1.1X10^{14}$					46			
	$1.1X10^{15}$					84			
Pb	$1.1X10^{13}$					52	26		
	$1.1X10^{14}$					60	52		
	$1.1X10^{15}$								
MSTe55W						16	8		

MSTe55W - Te doped substrate
AI - As implanted sample

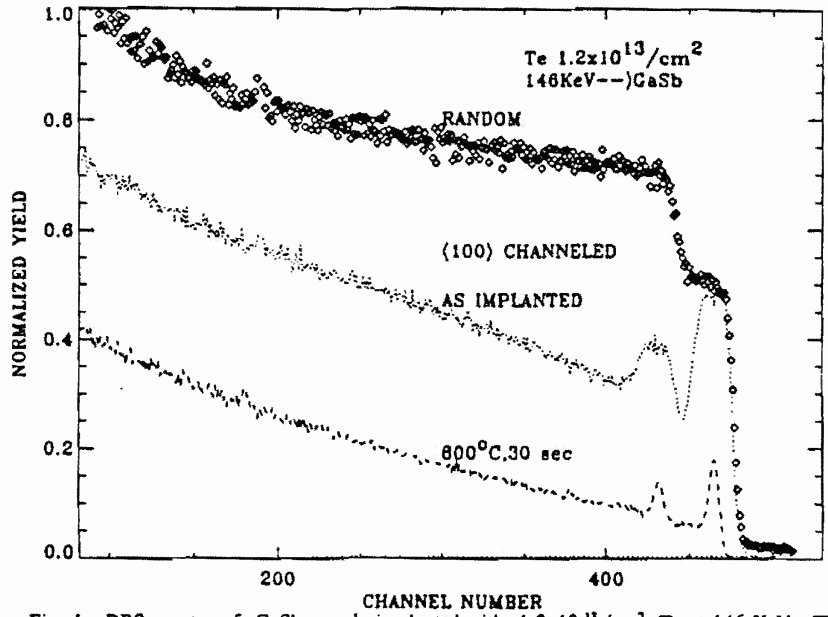

Fig. 1. RBS spectra of GaSb sample implanted with 1.2x10 ^{13} /cm^2 Te at 146 KeV. The yields for the as implanted GaSb sample and of the sample rapid thermal annealed at 600 °C for 30 s are shown.

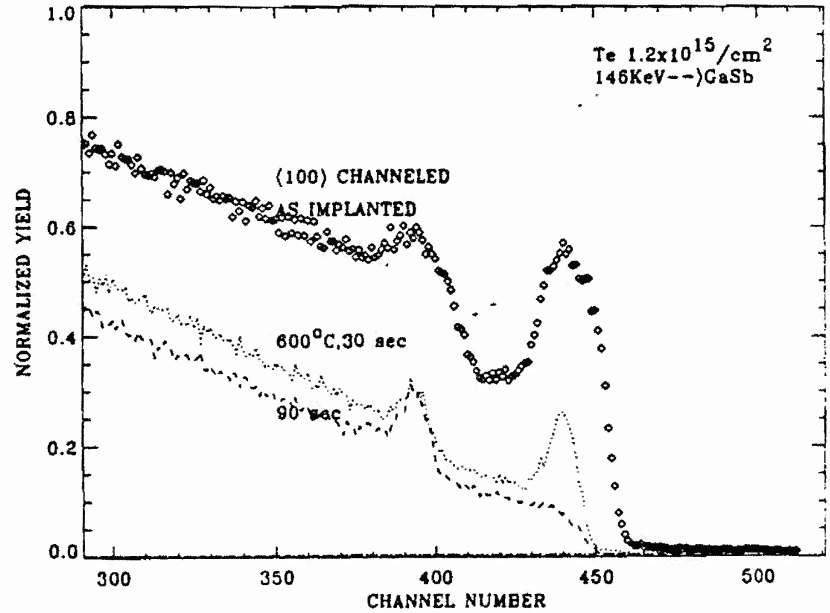

Fig. 2. Partial <100> aligned spectra of the 1.2x10 ^{15} /cm^2 Te implanted GaSb sample and of the samples rapid thermal annealed at 600 °C for the durations of 30 and 90 s. The backscattering yield has been normalized with respect to the random spectra of the as-implanted sample.

lattice on annealing, as determined by χ_{min}, seems to be relatively poor for the samples implanted with the heavier atomic species. The Hg implanted samples were annealed at 300°C to minimize the evaporation of Hg from the surface. Due to the low annealing temperature these samples did not exhibit any appreciable recovery of damage.

In conclusion, we have shown that a good lattice recovery of the implanted layer could be achieved in GaSb with the near surface region of the implanted layer being amorphous. Excellent recovery was obtained in Te implanted samples annealed at 600°C for 30 - 60 s with χ_{min} somewhat lower than in the Te-doped substrate. For higher dosages of implanted ions the extent of damage\ production and removal appears to be dependent on the mass of the implanted ions.

ACKNOWLEDGEMENTS

The authors are grateful to Mr. Badri Mangalam for data processing, and Dr. Mark Ray and Mr. Mark Denker from Microelectronics Center of North Carolina for their assistance with the SIMS. This work was supported by AFOSR (Contract No. F49620-93-1-0111DEF) and USARO (Grant No. DAAL03-89-G-0115).

REFERENCES

1. S. J. Pearton,A. R. Von Neida, J. M. Brown, K. T. Short, L. J. Oster and U. K. Chakrabarti, J. Appl. Phys. 64, 629 (1988).
2. A. R. Von Neida, K. T. Short, J. M. Brown and S. J. Pearton, Mat. Res. Soc. Symp. Proc. 100, 689 (1988).
3. Y. K. Su, K. J. Gan, J. S. Hwang and S. L. Tyan, J. Appl. Phys. 68, 5584 (1990).
4. R. Callec, P. N. Favennec, M. Salvi, H.L'Haridon and M. Gauneau, Appl. Phys. Lett. 59, 1872 (1991).
5. M. Shaanan,R. Kalish and V. Richter, Nucl. Instr. and Meth. Phys. Res. B7/8, 443 (1985).
6. G. L. Destafanis and J. P. Gailliard, Appl. Phys. Lett. 36, 401 (1980).
7. P. Martin, E. Ligeon and J.P. Gailliard, Nucl. Instr. and Meth. 197, 47 (1982).